Development of FSW for composite materials

Flávio André Teixeira Vilhena

Master's Thesis

Supervisor: Dr. Pedro Moreira

Cossupervisor: Prof. Torres Marques

Integrated Master in Mechanical Engineering

12 March 2020

To my family

Abstract

With the rise in usage of thermoplastic matrix composites, the development of new and better ways to join this kind of materials becomes more interesting. Friction stir welding is a technology, that initially was developed to weld hardly weldable metals. There are some studies made regarding the utilization of friction stir welding in thermoplastic, but little attention was given to the usage of this technology in the welding of composites.

The work developed in the frame of this thesis are focused on the development of a technological solution to apply Friction Stir Welding (FSW) to join composites, in particular in a butt joint configuration. Different tools, rotating shoulder, hybrid and stationary shoulder, were developed to weld a short fibre reinforced composite, PA6 GF30, in a butt joint configuration. The analysis is made qualitatively when regarding the weld appearance and quantitively regarding the forces present during welding and the tool's temperature.

A design of experiment using a L_4 orthogonal matrix was made in order to study which welding parameters were more influential in the weld strength when using the static shoulder tool.

With this work, it was verified that the presence of a static shoulder produced welds with better appearance. The hybrid tool preheated to 269 ºC produced the highest tensile strength specimen with a value of 88.2 MPa, which corresponds to 58.7% of the base materials strength. The static shoulder tool produced the best appearance welds and the best specimen had a tensile strength of 64.1 MPa which corresponds to 42.7% of the base material's strength.

Desenvolvimento de ligações em FSW para materiais compósitos

Resumo

O aumento de utilização de compósitos de matriz termoplástica, torna interessante o desenvolvimento de novas e melhores formas de união deste tipo de materiais. Soldadura por fricção linear é uma tecnologia inicialmente desenvolvida para soldar metais dificilmente soldáveis. Existem alguns estudos relativos à utilização de *friction stir welding* (FSW) em termoplásticos, mas pouca atenção foi dada à utilização desta tecnologia em compósitos.

Esta tese dedica-se ao estudo de diferentes tipos de ferramentas, de ombro rotativos, híbrido e estático, na soldadura por fricção linear de compósito de fibras curtas, PA6 GF30, numa configuração topo a topo. A análise é feita qualitativamente em relação ao aspeto visual das soldaduras obtidas e quantitativamente no tocante às forças presentes durante a soldadura, assim como a temperatura da ferramenta.

Um DOE foi feito usando uma matriz ortogonal L_4 de forma a avaliar quais os parâmetros mais influentes na tensão de rutura das soldas obtidas utilizando a ferramenta de ombro estático.

Com este trabalho ficou evidente que presença de um ombro estático produz soldas com melhor aspeto. A ferramenta híbrida pré-aquecida a 269 °C produziu o provete com maior tensão de rutura, 88.2 MPa, que corresponde 58.7% do material base. A ferramenta com ombro estático produziu as soldas com melhore aspeto visual, o melhor provete produzido com esta ferramenta teve uma tensão de rutura de 64.1 MPa que corresponde a 42.7% do material base.

Acknowledgements

I would like to thank my supervisor Dr. Pedro Moreira for his guidance during this thesis. I am also thankfull for the opportunity of working at LOME. I would like to thank Prof. Torres Marques for his time and availability. I thank Lanxess for donating the Durethan PA 6 GF30 plates used in this thesis. I would like to thank Prof. Miguel Figueiredo and Rui Silva for their assistance with the tensile tests. I would like to thank Mr. Domingos Carvalho for producing the composite welding tool.

Finally, I would like to thank my family for their patience and support through all my education years. Without them none of this would be possible.

Contents

Abbreviations

CFR	Carbon Fibre Reinforced
DOE	Design of Experiment
FRP	Fibre Reinforced Plastic
FSpW	Friction Spot Welding
FSRW	Friction Self-Riveting Welding
FSSW	Friction Stir Spot Welding
FSW	Friction Stir Welding
GFR	Glass Fibre Reinforced
GMT	Glass Mat Thermoplastic
HDPE	High Density Polyethylene
HMW-PE	High Molecular Weight Polyethylene
HNT	Halloysite nanotubes
MFI	Melt Flow Index
NBR	Nitrile Butadiene Rubber
OMC	Organic Matrix Composites
PA6	Polyamide 6
PA6-GF30	Polyamide 6 reinforced with 30% glass fibre
PEEK	Polyether ether ketone
PEO	Plasma Electrolytic Oxidation
PLA	Polylactic acid
PMC	Polymeric matrix composites
PMMA	Polymethyl methacrylate
PP	Polypropylene
PTFE	Polytetrafluoroethylene
RTM	Resin Transfer Moulding
S/N	Signal to Noise
SiC	Silicon Carbide
SSFSW	Stationary Shoulder Friction Stir Welding
TWI	The Welding Institute
UTS	Ultimate Tensile Strength

List of figures

List of tables

1 Introduction

Organic matrix composites originated in the World War II as a way to produce materials with higher specific strength and stiffness for aerospace application and, in more recent years, they have expanded to diverse areas. In the sports and recreation market, composites are used in golf clubs, tennis rackets, bicycles and so on. In the automobile industry, the utilization of composites makes it possible to achieve more energy-efficient vehicles through weight reduction [1].

Polymer composites offer a wider design freedom than traditional materials, such as metal or wood. Parts can be made larger, permitting the reduction of joints and consequently reduction of assemblage costs. Aesthetically polymers are very versatile, being able to resemble other materials, also they can be transparent or opaque, coloured and decorated [2].

Thermoplastics have lower density and lower energy consumption during processing, compared to metals. When compared to thermosets, thermoplastics have shorter processing times, higher toughness, the ability to be welded and are easier to recycle [3].

Thermoplastic composites have been used in aeronautical applications, some of them include the wing leading edge of the Airbus A380, the horizontal tail plane of the Leonardo AW169 helicopter and the rudders and elevators of the Gulfstream and Dassault business jets [4]. It is an interesting material group for space structures because of their low moisture absorption and low outgassing which reduce problems related to moisture swelling [5]. According to Effing [6], short fibre reinforced thermoplastics represent the 48% of the European composite market, making it the largest market segment, as can be seen in Figure 1.

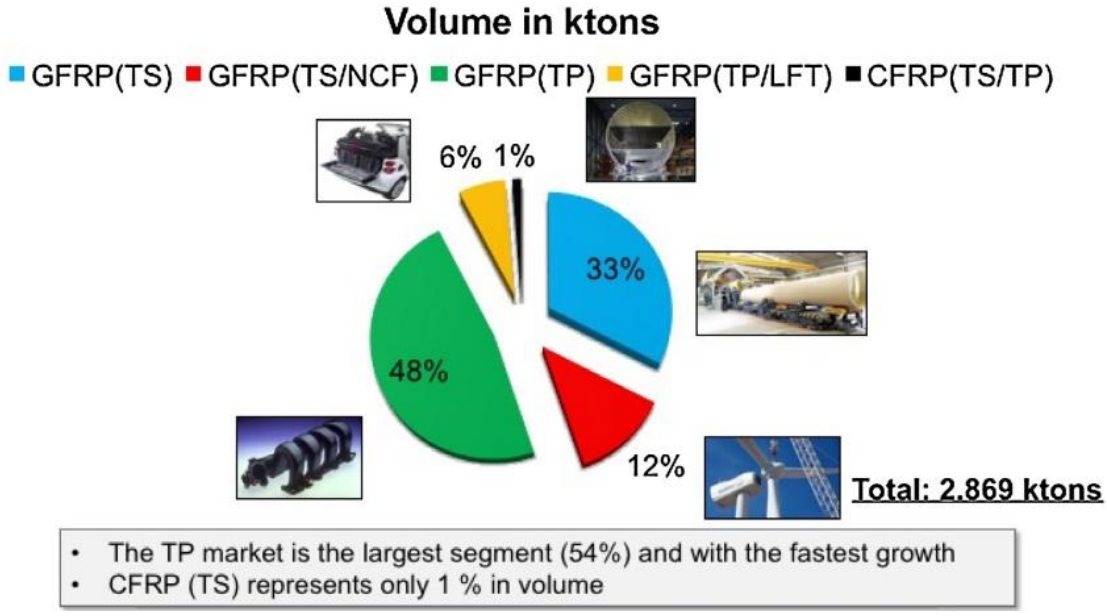

Figure 1 - European Composites market volume in 2016 [6]

Friction stir welding (FSW) has been used in several industrial applications, for example in the welding of the Audi R8 Spyder B pillar [7]. Initially developed to weld hardly weldable metal alloys like 2000- and 7000-series aluminium alloys, FSW presents several advantages [8, 9]:

- Lower energy consumption than other welding processes;
- Absence of filler materials;
- Absence of toxic fumes;
- Ability to weld dissimilar material;
- Ability to be used in different joint configurations.

More recently, it has been investigated its usage when welding polymers, but there are still few studies about friction stir welding of composites.

The demand for lightweight structures and vehicles, as well as a higher awareness about environmental issues make the usage of FSW and thermoplastic matrix composites an attractive option to achieve more environmentally friendly and energy efficient solutions. The increase in usage of thermoplastic composites demands the development of joining techniques that provide better efficiency, fast joining times and easy automation. Friction stir welding may be an alternative to achieve these goals.

The welding of composites in this thesis was executed in INEGI's Optics and Experimental Mechanics Laboratory (LOME).

1.1 Project goals

The goal of this thesis is to study the weldability of composites by friction stir welding. For this purpose, a literature review was made in order to identify the type of composites with wide industry usage more suitable for friction stir welding and to identify the main features necessary to design a suitable tool for composites welding.

1.2 Structure of the thesis

The structure of the thesis is presented below and is constituted by 6 different chapters.

Chapter 1 - Introduction to the thesis, presenting the motivation for the work and the topics discussed in the present work.

Chapter 2 - Literature review about composites and composite joining. First, an introduction to composites is given, followed by a description of alternatives to join thermoplastic composites.

Chapter 3 - Literature review on FSW of composites regarding different materials, tool designs and most influential parameters.

Chapter 4 - Experimental details, such as the material used, tools used, design of experiments and testing procedures are described in this chapter.

Chapter 5 - This chapter regards the experimental results of the temperatures and forces during welding when using different weld tools, different preheating temperatures and the results of design of experiment using an L_4 matrix being the response the UTS of the specimens obtain through tensile tests.

Chapter 6 - The conclusions from the experimental work are presented in this chapter.

2 Thermoplastic Composites

According to Bootle, et al. [10] composite materials are the combination of two or more distinct materials at a macroscopic level having a recognizable interface between them, usually they consist of a reinforcement material such as fibres or particles supported by a binder (matrix) material. In the automotive industry thermoplastic matrix reinforced with randomly oriented short (typically less than 1 mm long) E-glass fibres are used in parts like air intake manifolds, water pump housings and gears in the door window mechanism, while thermoplastics reinforced with unidirectional or bi-directional continuous fibres can be found in seat structures, bumper beams and cross members [3].

Composite materials are becoming more prominent due to their low weight and other unique features, an example of this is that the Boeing aircraft, 777 Dreamliner had 12% components manufactured from composite while the more recent aircraft, 787 Dreamliner contains 50% components manufactured from composites [11]. Composites are commonly classified at two distinct levels: the matrix constituent and the reinforcement form [1].

2.1 Matrix

The major composite matrix classes are metal matrix, ceramic matrix and organic matrix. This last one can be further divided into polymer matrix and carbon matrix [1]. In this work an emphasis will be given to polymer matrix composites, in particular thermoplastic composites.

According to the Oxford Dictionary of Biochemistry and Molecular Biology (2nd Edition) [12] a polymer is “any substance that is composed of molecules containing a large number of constitutional units (or ‘mers’) that are in repetitive covalent linkage and that maybe of one or more than one species. Polymers are generally considered to comprise at least ten mers, although sometimes the term is taken to imply simply ‘more than one’ mer.”

In terms of polymers these can be divided in to thermoplastic and thermosetting. Thermoset plastics are network polymers, they have covalent crosslinks between adjacent molecular chains, whereas thermoplastic the adjacent molecules are affected mainly by secondary forces [13].

The advantage of thermoplastics over thermosetting polymer is that latter one resists deformation and heat softening and thus cannot be reprocessed. To join thermosetting polymers it must be used either mechanical fastening or adhesive bonding since welding methods cannot be applied [11]. Thermoplastics are high-molecular weight polymers that can be reheated, which causes a weakening of secondary van der Waals or hydrogen bonding forces enabling welding operations, also their processing time is significantly lower than thermosets [3, 14]. Although they can be processed repeatedly, this will cause deterioration of some of their properties [3].

Polymers can be categorized in relation to their crystallinity. Crystallinity refers to the molecular arrangement which produces an ordered atomic array, if there is no repeating structure then the polymer is amorphous. As a result of their size and complexity polymers are

usually semi-crystalline, this is, they have crystalline regions disperse in an amorphous region, as can be seen in Figure 2 [13].

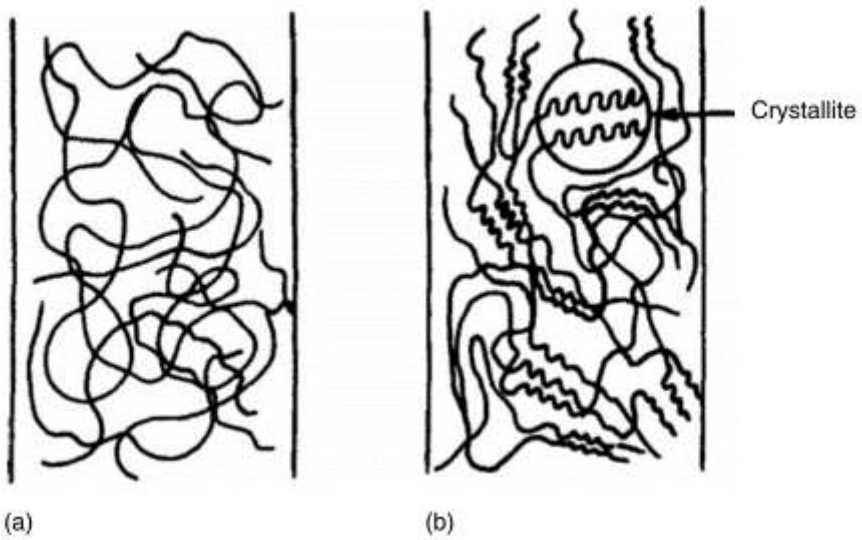

Figure 2 - Arrangement of molecules in (a) amorphous polymers and (b) semi crystalline polymers [15].

Crystalline thermoplastics are tough, soft and translucent to opaque, they are used in structural applications, compared to amorphous thermoplastics they have good wear resistance, high chemical resistance, high coefficient of thermal expansion and low coefficient of friction, but low impact resistance. Some of these polymers are polyethylene and polypropylene [11]. To be welded they have to be heated above their melting temperature [16].

Amorphous thermoplastics are hard, rigid and clear, they soften over a range of temperature and are easy to thermoform. They have good impact resistance and their structure consists of randomly oriented and tangled molecules. Some of these polymers are polycarbonate and acrylonitrile butadiene styrene [11]. To be welded they must be heated above their glass transition temperature [16].

Semi crystalline uncross-linked polymers behaviour depends on how they are solicitated, higher rate of deformation reduces the loading time, causing stress increment to reach higher levels, also the relaxation of molecular chains makes the deformation time dependent [17].

The incorporation of fibres into a thermoplastic resin is much harder than in a thermosetting resin, because of their higher viscosity, making it difficult to get good fibre wet-out, although Arkema provides a liquid thermoplastic, Elium®, that can be processed like a thermoset and is suitable to be used with RTM, a technology normally only appropriate for thermosetting resins [18]. Thermoplastic prepregs can be stored for unlimited time without any special storage facility, and are produced by hot melt impregnation, solution impregnation, liquid impregnation, film staking, fibre mixing and dry powder coating [15].

2.2 Reinforcement

The reinforcements can be particulates, whiskers, continuous fibres and woven composites, they are classified in Table 1. In order to provide a useful increment in proprieties, usually 10% or more volume of reinforcement is required. There are materials that contain particles, not for the purpose of reinforcements, but for cost reduction they are generally referred as “filled” systems rather than composites [1].

Table 1 - Reinforcement classification [1]

Reinforcement	Description	Type
Particle	All dimensions are roughly the same	Discontinuous
Whisker	Aspect ratios between 20 to 100	Discontinuous
Short fibre	Have length much greater than their cross-sectional dimensions An increment in fibre length translates in an increment of the composite proprieties	Discontinuous
Continuous fibre	Have lengths much greater than their cross-sectional dimensions An increment in fibre length doesn´t translates in an increment of the composite proprieties	Continuous
Woven	Interlocking fibres that have orientations slightly or fully in an orientation orthogonal to the primary structural plane	Continuous

The most common fibre reinforcements are glass fibres, aramid fibres and carbon fibres. Glass fibres represent an estimated 95% of consumption while the remaining 5% is mostly accounted by carbon and aramid fibres. The practical goals of fibre reinforcement are to increase modulus and strength, improve heat deflection temperature, reduce tendency to creep and in some cases to save costs [19].

The most common types of Glass fibres are E-glass and S-glass. They are used due to their low cost, high tensile strength, high chemical resistance and insulating properties, but suffer from low tensile modulus, high density, sensitivity to abrasion during handling, low fatigue resistance and higher tool wear. Carbon fibres have exceptionally high tensile strength, high tensile modulus, low coefficient of linear thermal expansion, high fatigue strength, high thermal conductivity, but they have high cost, low strain to failure and low impact resistance. Aramid fibres are highly crystalline aromatic polyamide fibres that have the highest tensile strength to weight ratio, are resistant to impact damage and have low coefficient of thermal expansion, but they are difficult to cut or machine and have the lowest compressive strength [15]. Table 2 compares the mechanical properties of the three previously mentioned fibres.

Table 2 - Mechanical properties of different fibres [19]

Fibre Properties	E-glass	Aramid	Carbon
Density [g/cm^3]	2.6	1.44	1.7-2
Tensile strength [MPa]	2000-3500	2900-3000	2000-6400
Tensile Modulus [GPa]	70-73	70-130	200-590
Elongation at break [%]	3-5	2-4	0.5-2

2.3 Fabrication processes

The incorporation of fibres into the matrix can be divided into two separate groups: one in which the fibres and the matrix are processed simultaneously into the finished product and the other where fibres are incorporated into the matrix to prepare ready-to-mould sheets [15].

2.3.1 Injection moulding

Parts made of thermoplastic composite reinforced with short fibres up to 10 mm may be produced through conventional injection moulding, that consists in forcing melted thermoplastic into a mould cavity and then cooling it down under pressure. The injection machine comprises of an extruder with heating device, a ram system, to allow filling of the mould cavity and application of pressure, and a cooling device to cool down the mould and the part allowing to a faster solidification and release of the part, an can be seen in Figure 3 [20].

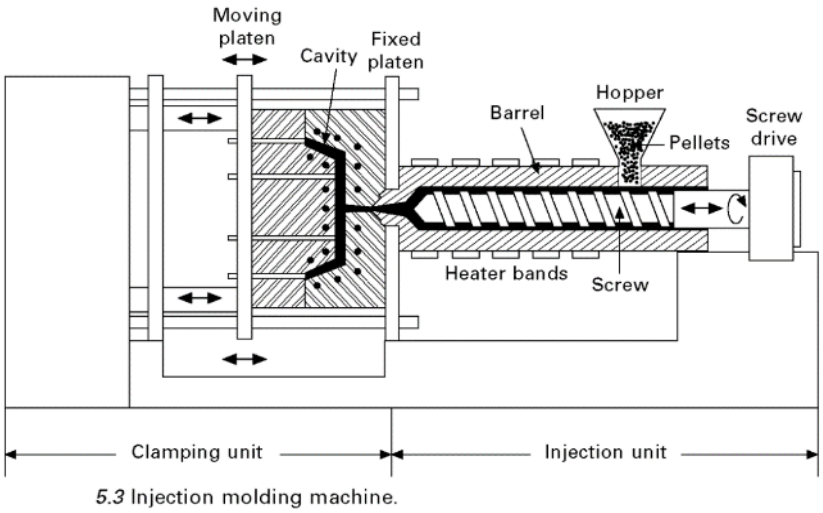

Figure 3 - Injection moulding machine [3]

Parts with fibres longer than 20 mm cannot be processed on conventional injection, but they may be processed with compression moulding or extrusion-compression technique. Compression moulding consist in using composite sheets or chopped unidirectional tapes that are compressed by a hot mould and when the composite is softened and shaped the mould is cooled and the part demoulded. Extrusion-compression consists in heating the composite and extruding it with a screw extruding machine that feeds a compression mould, the composite is then compressed and the part is obtained [20].

2.3.2 Prepreg

A prepreg is a fibre layer pre-impregnated with a polymer, these layers can be stacked to produce a laminated composite [3]. Prepregs of thermoplastic can be produced by[15].

- Hot melting process: mainly used for semi crystalline thermoplastics and consists in pulling collimated fibre tows through a die that delivers a fine sheet of hot polymer melt under high pressure.
- Solution impregnation: only suitable for polymers that can be dissolved in an adequate solvent and consists in dissolving the polymer in the solvent and using the mixture to impregnate the fibres, afterwards the material is heated to remove the solvent, for this reason low boiling point solvents are preferred.

- Film stacking: consists in using woven fabrics or random fibre mats between sheets of unreinforced thermoplastic polymer, the layers are pressed together and heated to force the thermoplastic into the reinforcement layer.
- Fibre mixing: a process where fibres of reinforcement and filaments of thermoplastic are mixed by commingling, wrapping or co-weaving. During the moulding stage the thermoplastic fibres are melted and spread to wet the reinforcement fibres.
- Dry powder coating: a process that charges and fluidizes thermoplastic powder in order to coat the reinforcement fibres. The fibres are then heated, and the polymer coating is melted on the fibre surface.

To produce a laminated thermoplastic composite, stacks of several layers of continuous fibre prepregs or bi-directional fabric prepregs are heated and then pressed. The fibre orientation can be different in each layer, as can be seen in Figure 4, giving more design flexibility [3].

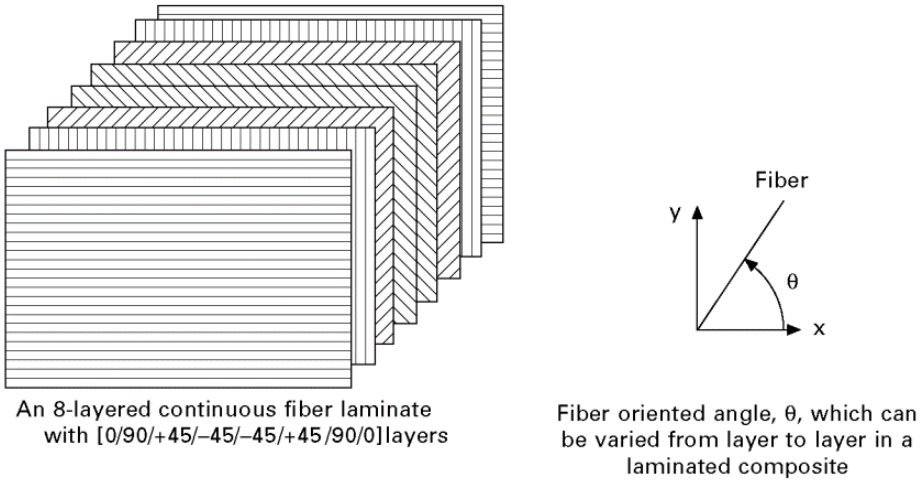

Figure 4 - Example of laminate made from differently oriented layers [3]

Most laminated composites are orthotropic. They have properties that are different in three mutually perpendicular directions. a load applied parallel to these axes produces only normal strains and loads not parallel to the axes produce normal and shear strains [21].

2.4 Joining

In plastic product design, as well as in composite materials, the ideal situation is to a have one piece item, but manufacturing limitation may make necessary to use joining operations [14].

Plastic joining can be categorized as fastening, bonding and welding procedures. Fastening uses an external body to produce the joint, bonding uses a solvent or an adhesive to join the parts and welding is a procedure where the parts are fused together. Figure 5 displays and categorizes different plastic joining procedures.

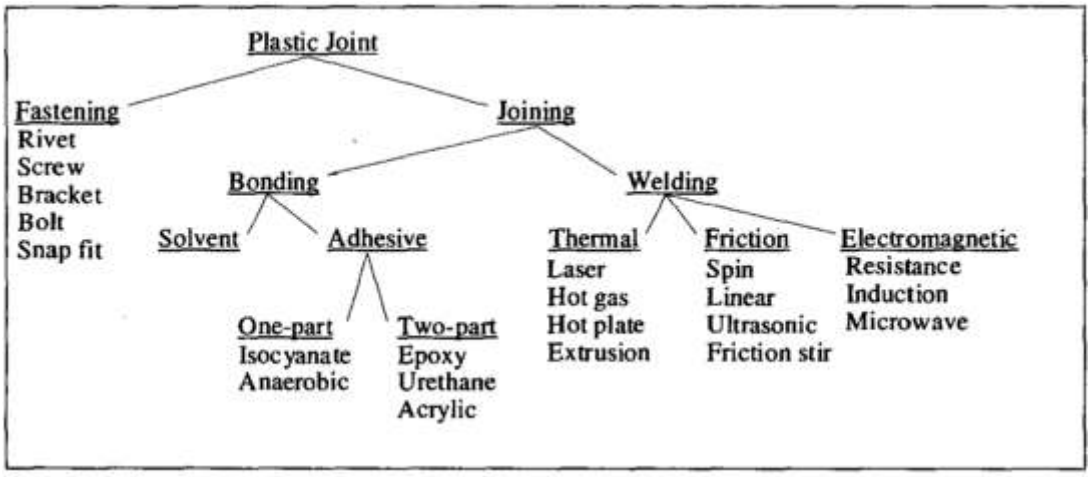

Figure 5 - Various plastic joining processes [22]

2.4.1 Adhesive bonding

In a general way, adhesive bonding consists in the application of an adhesive (usually a polymeric material) to a substrate and holding the components together while the adhesive cures. The main mechanisms which allow the joining to occur are: adsorptive, electrostatic and diffusive [23].

Adsorptive forces result from intimate interaction between particles at the joint surface. The attachment can be through weak, dipolar or van der Waals interactions or through chemical bonds. Electrostatic forces are a result of ionic bonds between oppositely charged species or molecules. Diffusive forces are consequence of molecular chain entanglement between the substrate and the adhesive as they diffuse through the joint interface [23].

Adhesives can be classified as a one-part system or two-part system. One-part systems don't require mixing or stirring before usage, with the curing times ranging from seconds to hours depending on the adhesive. Two-part adhesives rely in the mixing of two components in specific proportions [22].

There is a limit to how long an adhesive can be stored, this limit is denominated as shelf life and can varies from a few days to over a year depending on storage conditions and adhesive. In general, two-part adhesive systems have longer shelf life, but after mixed they have a limited time to be applied, this time is the pot life. After the joint has been made, there is a cure time required to achieve the best mechanical properties of the joint, this time depends on the ambient conditions and the adhesive [24].

Structural adhesives are adhesives that can support high proportion of its maximum failing load for long periods without failure. The most used adhesive groups are epoxies, polyurethanes, modified acrylics, cyanoacrylates and anaerobics [24].

Adhesive bonding of thermoplastics usually results in lower bond strengths when compared to thermosets. Thermoplastics have inert, nonpolar surfaces that make it difficult for the adhesive

to wet the surface and thus surface preparations such as sodium hydroxide etching, grit blasting, acid etching, plasma treatments, silane coupling agents, corona discharge or aramid peel plies must be employed to improve adhesion [14].

Joint design is important to ensure that the adhesive is loaded in shear, since bonded joint that are subjected to peel or cleavage are less efficient. If peel forces cannot be avoided, a ductile adhesive should be used. Double strap joints and scarf joints may perform better than single lap joints, but they are more time consuming and difficult to produce, so single lap joints remain one of the most used configurations for adhesive bonding [24]. Different joint designs can be seen in Figure 6.

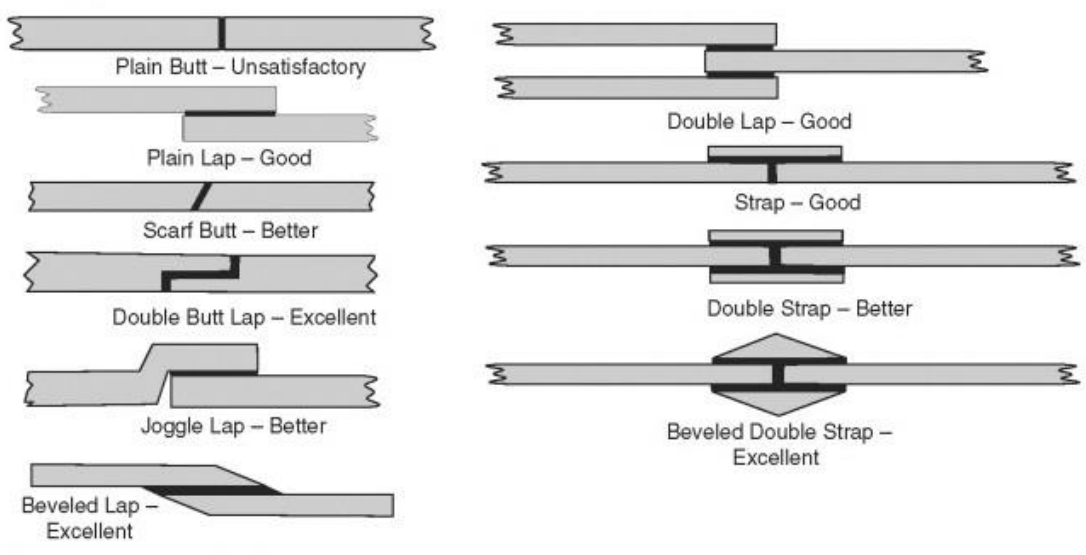

Figure 6 - Joint designs for adhesive bonding adapted from [23]

Adhesive bonding is a common procedure when regarding composite joining. It allows for a continuous connection avoiding large stress concentrations when compared to mechanical fastening, bonded joints are usually lighter than mechanically fastened joints and, in some applications, less expensive, also dissimilar material can be joined together.

However there are disadvantages when using adhesives which are the necessity of a clean surface, the application of a surface treatment in order to increase surface energy and thus wetting, the requirement of long curing times, the strength of the bond is highly affected by the physical and chemical actions of the environment, thermosetting adhesive bonding is harder to recycle, it is difficult to assess the joint strength without destructive tests and joints are permanent [24, 25].

2.4.2 Mechanical fastening

Fastening refers to the introduction of a foreign body to join mechanically two different parts. This process is suitable for joining similar and dissimilar materials. Some examples of fasteners are screws, rivets, bolts, snap-fits, brackets, clamps and staples. It's one of the simplest solutions for joining different components and can be divided into two categories: permanent fasteners and non-permanent fasteners. Permanent fasteners are more robust and economical but non-permanent fasteners are easier to disassemble and replace [16, 22]. Figure 7 shows some of the fasteners available for thermoplastics.

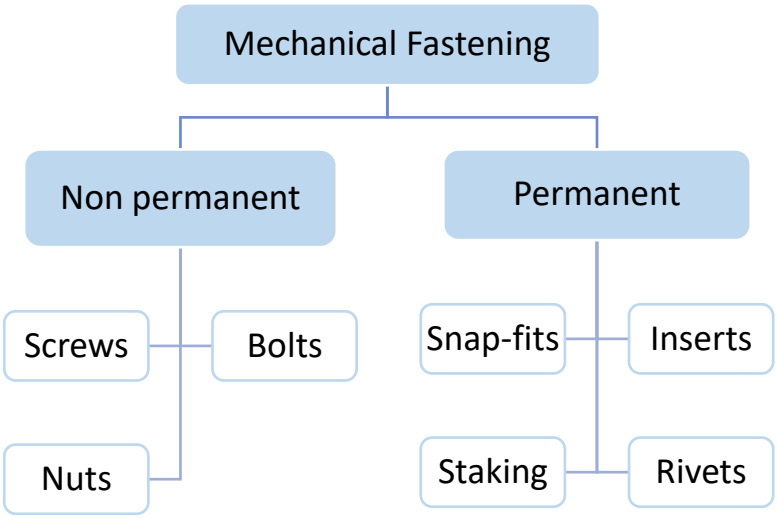

Figure 7 - Different mechanical fasteners for thermoplastics

Mechanical fastening is an option when regarding the joining of composite materials. However, some typical problems from fastening are stress concentration due to the presence of holes and cut-outs, delamination originating from the localized wear occurring during drilling, also the hole drilling process is time consuming, differential thermal expansion of the fasteners relative to the base material, possible galvanic corrosion at fastened joints, additional weight to the structure, development of stresses with the passage of time and difficulty in having a leak proof seal [11, 25].

Friction riveting

Friction riveting is a relatively new variant of mechanical fastening technique suitable for joining polymers to metals, or polymers to polymers, patented by Amancio Filho, et al. [26].

It consists in the insertion of a metallic rivet that deforms inside the polymeric material to be joined. Firstly, the material to be welded is firmly fixed. Then, a rotating rivet descends into the material to be joined generating heat through friction, and when pre-set friction time is reached the rotation stops and forging pressure is applied up to the end of the joining time. Figure 8 exemplifies the process [27].

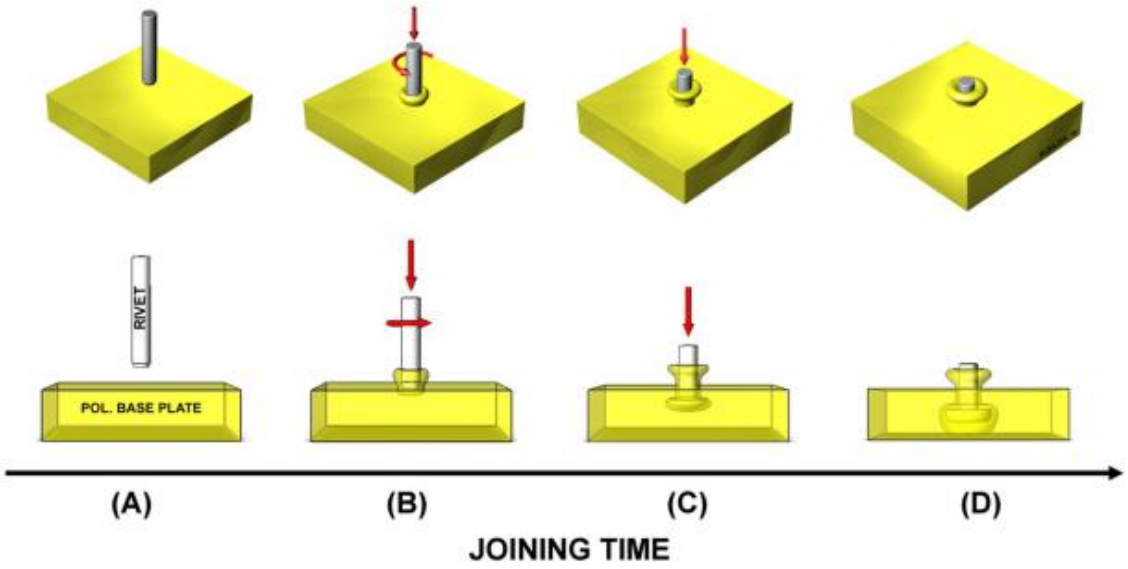

Figure 8 - Schematic of friction riveting process A) Positioning and clamping of joining partners, B) Insertion of rotating rivet into the polymeric base plate, C) Rotation braking and subsequently rivet forging, D) Cooling and joint consolidation. [27]

The rivet deforms inside the polymer due to the low thermal conductivity of the polymer which makes possible to achieve temperatures high enough to plasticize the rivet and soften the tip. The process can be decomposed into distinct phases.

Firstly, the friction regime is solid state, but when the polymers achieves the softening point (for amorphous polymers it's when the glass transition temperature is reached and for semi-crystalline it's when the melting point is reached), the friction regime changes to molten state beginning an unsteady state of viscous dissipation.

Another phase is after it reaches a steady state of viscous dissipation, then starts the phase where the rivet is forged. This is when the rotation is stopped, and it is pushed into the material which causes a deformation that results in a paraboloidal shape of the rivet and produces flash from the squeezed polymer.

Finally, the joint cools down under constant pressure, this is the consolidation phase, the molten polymer consolidates around the rivet creating a joint obtained by mechanical interference and enhanced by polymer-metal adhesion [27].

Gagliardi, et al. [28] studied friction riveting of two PA6 plates with and without glass fibre reinforcement and concluded that the strength of the joint was very dependent of the spindle speed. The reinforced polymer formed a stronger joint compared to the unreinforced polymer. The forging pressure is mainly dependent on the rivet stroke, if the rivet stroke increases the forging pressure increases. The temperature is affected mainly by the linear velocity during plunging of the rivet during the friction phase.

The advantages of this procedure is the ability to join dissimilar materials, such as plastic to metal, no surface treatment is required, disassembly of components for inspection and repair is relatively simple, and the integrity of the joint can be predicted [11, 14].

2.4.3 Welding

Welding is an establish technology in the thermoplastic industry where the welded joint can approach the properties of the bulk material. It has reduced processing times and less surface preparation compared to other methods, but it may induce residual stresses, the presence of carbon fibres imposes difficulties such as uneven heating, delamination and distortion of the laminates due to the increase of thermal and electric conductivity. Moreover, a high percentage of fibre reinforcement makes it more difficult to weld because of the reduction of matrix available to melt and reconsolidate [25].

Kiss, et al. [29] studied the welding of neat PLA and basalt fibre-reinforced PLA by laser, ultrasonic, hot gas and friction stir welding and concluded that, even though the joint efficiency on the composite was much lower, the joined material with fibres had higher strength than the joined material without fibres for all welding methods.

Fiebig and Schoeppner [30] analysed the influence of the initial fibre orientation when welding by hot plate and vibration. They concluded that for short fibres there is no advantage in orientating the fibres since the squeeze flow has too much influence in the final orientation of the fibres of the welded specimens. In contrast for long fibres, having more fibres initially orientated perpendicular to the weld seam results in better results when using hot plate welding, but not with vibration welding. Further studies need to be made in other to assess if these conclusions are applicable to FSW.

It is possible to join different polymeric material if their viscosity and their melt flow index (MFI) are similar enough. This condition makes it possible for strong mixing between the two. In order to approximate the MFI of the materials, particle reinforcements may be added to the polymers [31].

Compared to metals, the heat requirement of thermoplastics is less, but they are more sensitive to it, making the welding temperature range more restrictive. Excessive heat input will cause material degradation and insufficient heat input will produce defective joints [31].

Hot Tool Welding

Hot tool welding or hot plate welding consists in putting the parts to be welded in contact with a heated tool until a soften layer is created. The tool is removed, and the parts are pressed together until the molten layers consolidate, as schematically shown in Figure 9. The main parameters of this process are the tool temperature, the pieces preparation, the welding time, the thickness of the molten material and the weld penetration. The shorter the welding penetration, the higher is the weld strength for different meltdown thicknesses [32, 33].

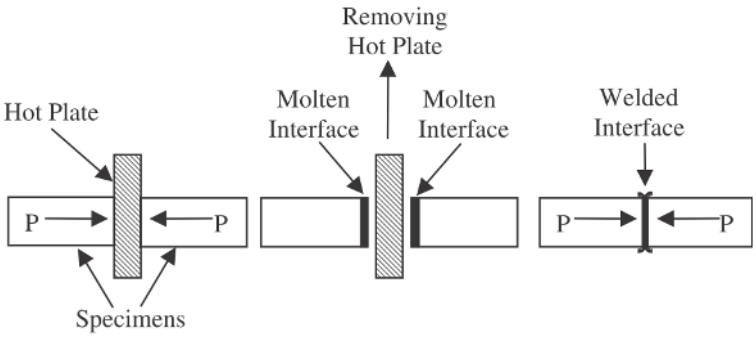

Figure 9 - Schematic of the hot-tool welding [33]

The advantages of this process are ease of assembly, no need for filler materials, ability to embed parts between the two joining pieces, freedom of shape, high production rates and the ability to produce hermetic seals. The disadvantages are the high energy consumption, expensive tool equipment, required cleaning of the welding tool, presence of residual stresses and a slow start up, this is, the required time to heat up the tool is high [32].

Gehde, et al. [34] studied hot tool welding of glass mat reinforced thermoplastic (GMT) of polypropylene and polyamide matrices, glass fibre reinforced with average fibre length of 30 mm and with fibre mass content of 25% for the PP and 35% for the PA The molten layer does not affect much the strength of the weld, but the weld penetration does. Higher weld penetration (joining length) translates into lower weld strength. A thicker molten layer makes it easier to get good results for different joining lengths. The joint efficiency was of 0.42 for the PP GMT and 0.4 for the PA GMT and the highest weld strength was similar to the strength of unreinforced base material.

Kagan [35] studied several materials and welding methods, one of which was PA 6 reinforced with 33% short glass fibres welded using hot plate welding. The joint efficiency obtained was 48%, corresponding to a strength increment of 12% relative to the unreinforced base material.

Induction Welding

Induction welding consists in the utilization of an induction coil that when passed with alternating current creates a time variable magnetic field that induces eddy currents in the electrically conductive material in the vicinities. The induced currents are met with resistance from the material and energy is lost in the form of heat, for this to work the material must be electrically conductive or have a susceptor between the parts [36].

The equipment consists in a radio frequency power generator, a heat station which includes the induction coil, the material to be welded and secondary equipment such as cooling system. It is important that the distance between the coil and the part is as small as possible in order to assure maximum energy transfer, also the coil needs to be designed to avoid magnetic field cancellation. The main parameters of this process are the current frequency, input power, pressure between the parts, welding time and cooling time [36].

There are different geometries for induction coils, some of them are single turn, solenoid coil and pancake, illustrated in Figure 10. Single turn coils concentrate the magnetic field around the diameter and is used mainly in circular areas. Solenoid coils are bigger versions of single turn ones and are able to heat larger cylindrical areas within its centre. Pancake coils can heat large flat areas and using then in both sides of the welding zone creates more uniform heating and thus better results [36].

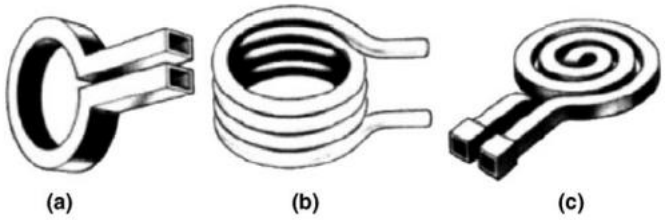

Figure 10 -Different types of coils, (a) single turn (b) solenoid (C) pancake [36]

If the fibres are not electrically conductive, for example aramid and glass fibres, then an insert must be used as a magnetic susceptor. The advantages of using a susceptor are a more precise location of the heat and the ability to weld nonconductive composites, but the addition of an insert raises weight, requires good bonding between it and the composite and it could act as a contaminate inducing residual stresses or causing stress concentration [23, 36].

The advantages of this process are high production rates, hermetic seals, joints with high strength, precise heating control, welding of large parts with bond lines up to 6 m, welding of joints with complex three-dimensional shapes and no surface treatment is needed. The disadvantages are complicated assembly operations, expensive machinery, the magnetic field may heat unintended elements around it that are not insulated and the edge effect, which causes uneven heating [23, 32, 36].

Resistance Welding

Resistance welding consists in using a metallic heating element between the parts that will be welded, it will remain embedded in the joint after welding is finished, Figure 11 exemplifies the process, also it's one of the most utilized welding techniques for composites.

The metallic insert is heated through the Joule heating affect and currents as high as 150 A may be applied, in order to achieve temperatures higher than the materials melting point. It is important to maintain pressure between the parts during welding and cooldown, in order to prevent deconsolidation due to fibre bed relaxation [14, 32]. The Airbus A380 has the ribs welded to the skin of the wings leading edge through this method, another application is in the joining of car bumpers and panels [14, 26].

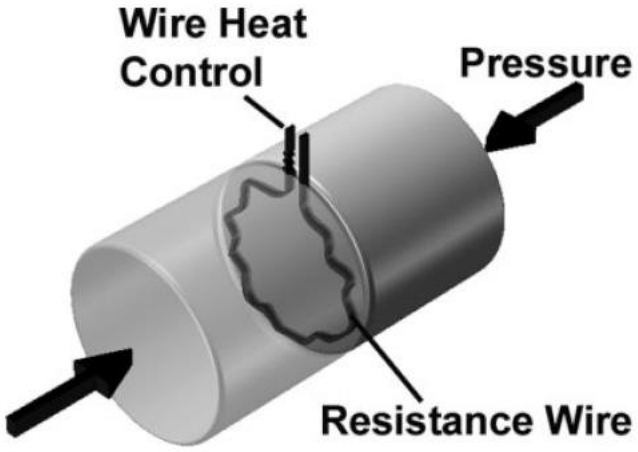

Figure 11 - Schematic of resistance welding [32]

The advantages of this technique are easy workability, joint design flexibility, ability to disassemble through the heating of the insert, reduced risk of air contamination and inexpensive equipment. The disadvantages of this procedure are the high skill required from the operator, long welding times, the mandatory use of a resistance element, which also results in harder recycling of the component and the resistance must be insulated from any conductive constituents making the introduction of a neat resin film as an interlayer beneficial due to better thermal and electrical isolation and helping the diffusion process by creating a resin rich region [25, 32].

Ultrasonic Welding

Ultrasonic welding produces good results in the joining of composites. It consists in subjecting the workpiece to ultrasonic vibrations (usually from 20 to 40 kHz) using a sonotrode which produces heat that can be selectively generated at the joint interface. For this to happen, the surface should have asperities that concentrate and dissipate heat, Figure 12 exemplifies the equipment [25]. The weldability is basically determined by the rigidity of the material, the greater the stiffness the better the weldability will be [32].

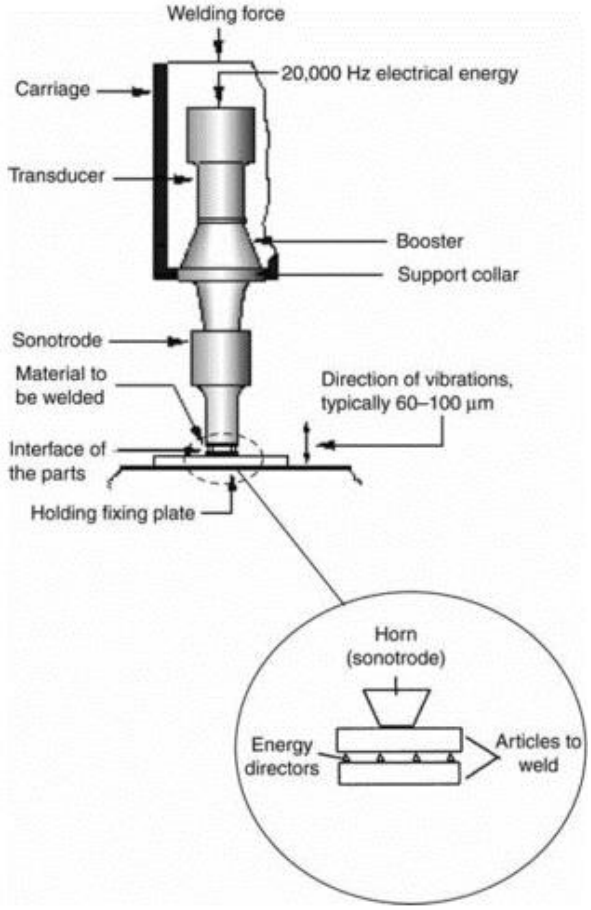

Figure 12 - Schematic of ultrasonic welding [37]

The advantages are that it is easily automated, fast, economical, consistent, absence of filler material and energy efficient [23, 25, 32].

The disadvantages of ultrasonic welding are the introduction energy directors (man-made asperities) and consequent fibre disruption at the interface, the impossibility to weld large joints in a single operation. Tooling costs for fixtures can be high, specifically designed details are required, noise concerns, at 40% filler content, fibres accumulate at the joint interface, and insufficient thermoplastic material is present to form a strong bond, highly plasticized materials such as vinyl are poor conductors of ultrasonic energy making them very hard to weld and it may cause damage to electrical components [23, 25].

Laser Welding

This welding process consists in the application of a laser beam to heat and melt the joint area. It's well suited to deliver controlled amounts of energy to a precise location due to the ease of controlling the laser beam size and the available range of methods for positioning and moving the beam. When the laser strikes the polymer it may be transmitted, reflected or absorbed. The type of material, additive content, surface coatings, laser wavelength, intensity and movement affect the radiation absorption [23].

There are two types of laser welding: absorptive and transmitted. Absorptive uses a CO_2 laser, but due to the limited radiation penetration it is limited to thin sections. Transmitted laser welding, exemplified in Figure 13, uses YAG laser and it requires that one of the welding pieces is transparent to the laser radiation while the other piece observes it. This technique allows for thicker pieces to be welded [23, 32].

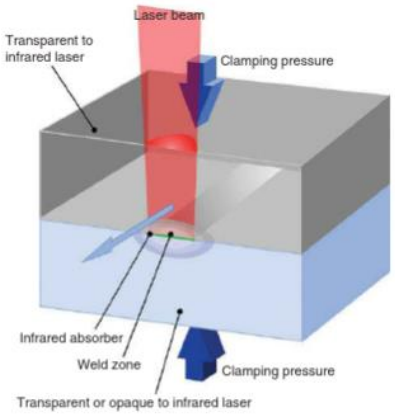

Figure 13 - Transmission laser welding [23]

Laser welding has the advantage of the absence of generated particulates, smooth flash, fast weld cycles, low amount of residual stress, well defined heat affected zone, possible to automate, no vibrations, suitable for high melting point polymers and no contact with heated tools. However it suffers from high equipment cost, limited weldable materials and geometries, joint surfaces must be of good quality, part clamping is necessary to ensure contact during welding and thickness limitations especially in highly crystalline materials [23, 32].

3 Friction Stir Welding

Friction stir welding, invented at The Welding Institute (TWI) of UK in 1991, is a solid-state joining technique initially applied to difficult to weld aluminium alloys [38, 39]. Although it is a solid-state welding technique (welding occurs below the materials melting point) in the case of metallic material, it's not fully solid-state in the case of polymers, due to the different molecular weights, they don't have a particular melting point, but a melting range [40].

FSW consists in a non-consumable rotating tool that generates heat through friction with the material being welded. The tool can be decomposed into two main parts, the probe and the shoulder. The combination of the localized heating around the probe, the tool's rotation and translation plasticizes and transports the parent material in the nugget zone. The material in the weld nugget moves from the front of the pin to the back of the pin, due to the rotation of the pin [16, 38]. Figure 14 exemplifies the FSW process. The weld can be divided into two sides: one in which the rotational direction matches the welding direction (advancing side), and one in which the rotational direction is opposite to the welding direction (retreating side) [9].

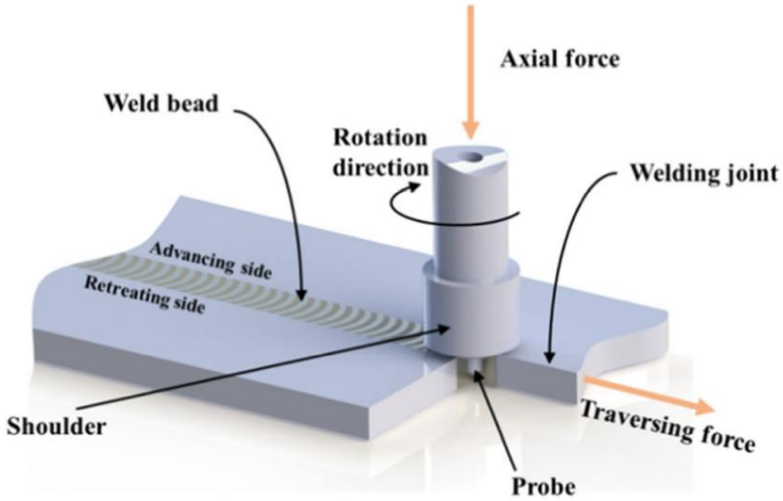

Figure 14 - Schematic of conventional FSW process [41]

The welding technique can be decomposed into tree distinct stages, plunging, traversing, and retracting as seen in Figure 15 [11].

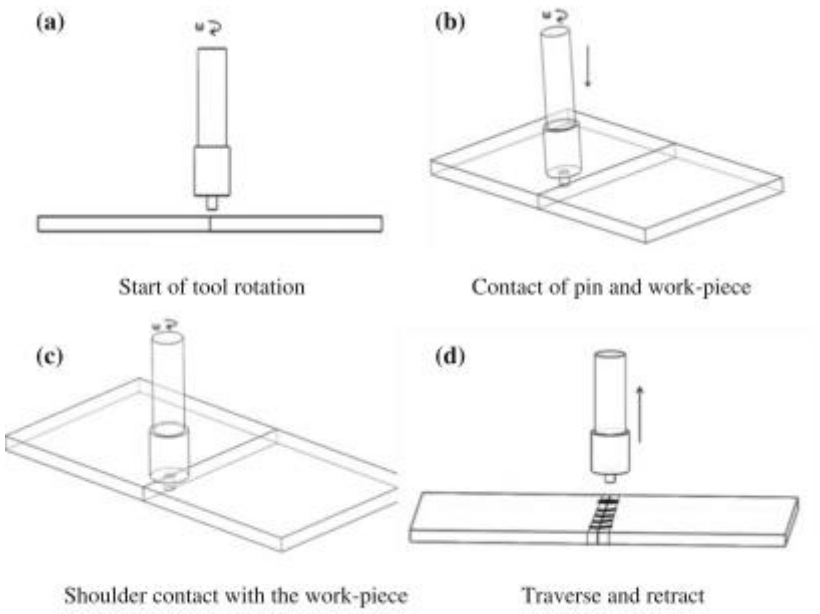

Figure 15 - Stages during welding [11]

The process can be used in many joint configurations for metallic materials, as can be observed in Figure 16, but has been mostly used in the butt and lap configuration since its invention [11]. Most studies of FSW of polymers tend to use either the butt or lap configuration and only a few analyse the T lap joint configuration.

The butt joint configuration is more challenging to weld due to the torque of the tool, which causes lateral movement of the plates during the plunging stage, resulting in defects. To avoid this, careful clamping setup is required [9].

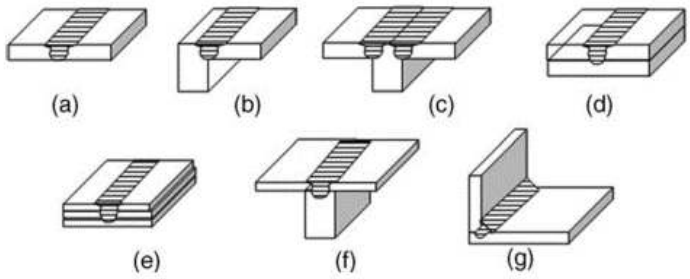

Figure 16 - Joint configurations for friction stir welding: (a) square butt, (b) edge butt, (c) T butt joint, (d) lap joint, (e) multiple lap joint, (f) T lap joint, and (g) fillet joint [38]

The advantages of this technique are its simplicity and energy efficiency when compared to ultrasonic wielding and laser welding, non-addition of weight during the welding process, the ability to join dissimilar materials, consistent weld quality and high productivity can be achieved through proper combination of materials, parameters and tool design [11].

FSW process variables can be divided into three groups, machine parameters, welding tool parameters and material properties. They are as followed [23, 42]:

- Machine parameters;
    - Axial force;
    - Dwell time;
    - Plunge depth;
    - Rotation speed (ω);
    - Tilt angle (α);
    - Travel speed (ν);
- Welding tool parameters;
    - Pin diameter;
    - Pin length;
    - Pin topology;
    - Shoulder design;
- Material Properties;
    - Mechanical;
    - Thermal.

Some of the difficulties present in FSW are the high reactive forces required to keep the tool in the joint line, the necessity of a rigid clamping system and finding which parameters are better suited to weld the material. Some of the defects that may occur from this process are: keyhole defect, tunnel defect, flash defect, lack of filling, lack of mixing, root defect, voids in the retreating side, kissing bonds and material degradation [11, 42].

Flash defect occurs when soft material is overflows from the weld seam, accumulating at the top surface of the workpiece [42]. An example of flash defect is present in Figure 17.

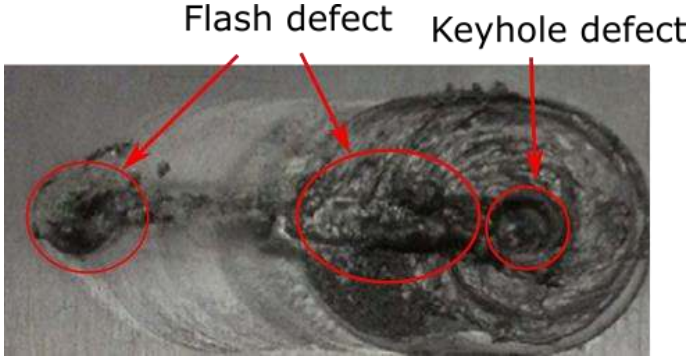

Figure 17 - Example of flash defect and keyhole defect [40]

Tunnel defect is a result of improper mixing due to the material not reaching the plastic stage and, thus cannot be stirred causing a through inside cavity along the welding direction. It usually happens when the traverse rate is too high [11, 42]. This defect may also result from high rotational speeds due to excessive turbulence [43]. Increasing the plunge depth may help eliminate this problem [44]. An example is shown in Figure 18.

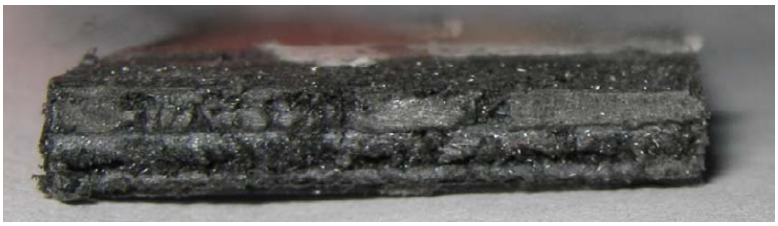

Figure 18 - Tunnel defect in stir zone [43]

Weld seam quality in the advancing side is better than on the retreating side, this may result from the lower temperature on the retreating side causing voids to form and poor material mixture [44, 45]. Simões and Rodrigues [46] FS welded PMMA and observed that the lack of transparency of the material was due to the formation of voids of its deeply non-homogeneous structure. This effect was more drastic in the retreating side of the weld as Figure 19 shows.

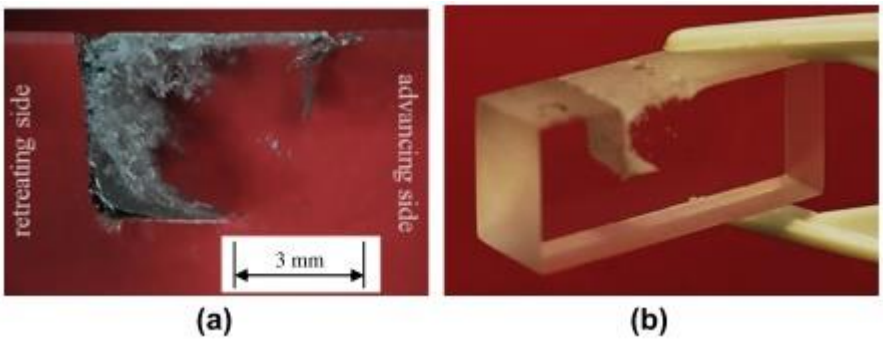

Figure 19 - Two (a) and three (b) dimensional images of PMMA weld [46].

The lack of length of the pin will result in lack of penetration and consequently the root side will not be bonded (root defect), as can be seen in Figure 20. On the other hand, if the pin is too long it will make the material from the root stick to the anvil [11]. The thickness of the root defect is roughly the difference between the probe length and the plate thickness, this can be eliminated using a double pass method [41].

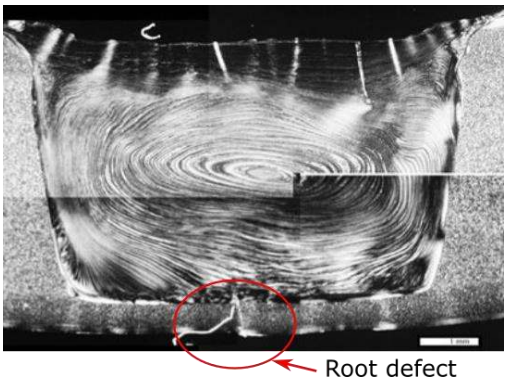

Figure 20 - Root defect in weld [47]

The probe geometry in the FS welding of polymers needs to be threaded, otherwise proper mixing will not be achieved, visible in Figure 21, which results in lower strength of the welded joint [40].

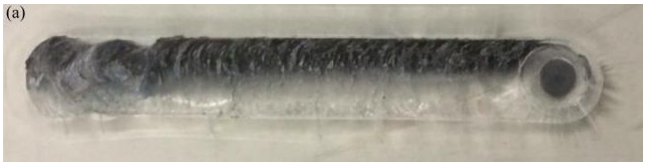

Figure 21 - Weld seam obtained using nonthreaded probe [40]

One of the most important aspects in welding polymers is the heat input and temperature during the process. Banjare, et al. [48] obtained better surface quality and mechanical properties when FS welding PP with an external heat source and Vijendra and Sharma [49], got better results using an induction heated tool when welding HDPE.

3.1 Conventional Friction Stir Welding

Joining FRP using conventional welding processes causes the fibres to align parallel to the seam due to squeeze flow which results in reduced strength and introduces weak spots, but FSW causes material flow around the pin, this may have positive effect over the fibre orientation in the seam [45]. When using FSW, welding in the same direction as the fibre orientation may produce higher joint efficiency than welding in a perpendicular direction to the fibre orientation.

It has been studied that the tool design has a big influence in the quality of the weld both in thermoplastics and composites with thermoplastic matrix. Ahmadi, et al. [50] concluded that the pin design has an important role in creating friction, heat and material flow, having obtained better results with a threaded cylindrical-conical pin, Figure 22, when lap welding two PP composites with 20% CF.

In another paper Ahmadi, et al. [51] studied the influence of welding speed, tilt angle and rotation speed of the pin, in the same material and configuration, having concluded that the most significant parameter was the travel speed and the least significant was the tilt angle. It should be noted that the tool used had a rotating shoulder.

Kumar, et al. [52] also studied the influence of tool rotation, travel speed and tilt angle, having concluded that the most significant parameter was tool rotation, followed by travel speed and tilt angle. The welded material was 30wt% glass filled Nylon 6 in a butt joint configuration. It was noted the highest tensile strength specimens presented a uniform microstructure at the weld and failed on the advancing side instead of the retreating side.

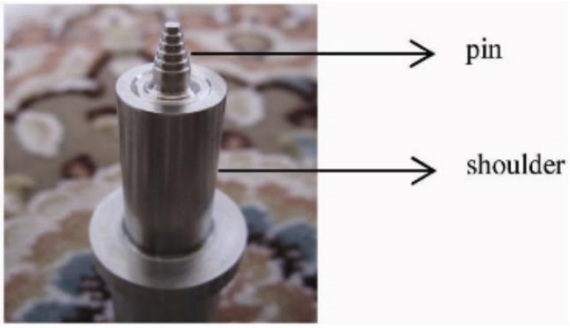

Figure 22 - Conventional FSW tool used by Ahmadi, et al. [51]

Kordestani, et al. [53] evaluated the effect of the pin design when FS welding two types of composites: PP composite plates reinforced with 30% GFs, with fibre lengths of 0.2-0.3 mm and PP composite plates reinforced with 30% CFs, with fibre lengths of 0.2-0.3 mm. The best results were achieved using a threaded tapered pin with a chamfer which resulted in a tensile strength of 30% relative to the base material in the case of the GF and 34% tensile strength relative to the base material for the CF composite.

Raza, et al. [17] studied the tool profile and particulate ceramic reinforcements in the FS welding of HDPE. He concluded that conical grooved pin with a concave shoulder gives better results compared with an unthreaded pin and to a plane shoulder. All of the reinforced material had a lower joint efficiency and ultimate strength than the welded plain HDPE, being SiC the particle reinforcement that provided best joint efficiency and graphite the most ductile behaviour. The SiC reinforced composite had the least variation of hardness across the weld nugget. The welding of composite via conventional FSW are summarized in Table 3.

Table 3 - Conventional FS welding of composites

Base material	Tool design	ω [rpm]	v [mm/min]	α [º]	Efficiency factor [%]	Ref.
30 wt.% glass filled Nylon 6 5 mm	shoulder Ø18 mm cylindrical pin Ø6 mm stand-off 0.2 mm	600	12	2	42	[52]
30 wt.% CFR PP 5 mm	shoulder Ø25 mm threaded-tapered pin with a chamfer Ø5 mm	2000	8	5	34	[53]
30 wt.% GFR PP 5 mm	shoulder Ø25 mm threaded-tapered pin with a chamfer Ø5 mm	2000	8	5	30	[53]
30 wt.% GFR PP 5 mm	shoulder Ø15 mm Taper pin with groove Ø5 mm	630	8	2	25	[43]

Depending on the base material and tool design, the most influential parameter is either the rotation speed or the travel speed, but the tilt angle is consistently the less influential for every tool and material. The effect of the axial force in the welding of composites lack study.

3.2 Stationary Shoulder Friction Stir Welding

The presence of a rotating shoulder in FS welding of thermoplastic and thermoplastic matrix composites results in bad surface quality and mechanical properties, due to the pushing of soft material out of the weld seam (flash defect). It causes material loss and, thus, poor joining, mainly in the retreating side of the weld [9, 54]. Stationary shoulder friction stir welding (SSFSW) was developed to weld low heat conductivity materials, where a more uniform heat input is beneficial [55].

A design that better suits the welding of polymers is the “hot shoe” design, shown in Figure 23. It consists in a static shoulder made of aluminium coated at the bottom with PTFE, in order to produce a smooth weld seam and preventing the sticking of the base material to the tool. The shoe is mainly responsible for trapping the soft material inside the weld bead and holding the weld under axial force while it cools down [9]. The primary source of heat is the friction between the rotating pin and the workpiece, but because many polymers tend to be self-lubricating at elevated temperatures and have low heat conduction, it may be required to provide external heat. This can be done by applying a thermocouple and heater to the shoe, or by using a hot backplate to heat the base material. This last method, although capable of creating very strong welds, has problems with repeatability [22, 41].

In order to reduce joint defects, it’s important to have a uniform cooling rate throughout the weld volume. If the outer material cools quicker than the inner material, a hard shell is formed and as the inner material cools down it contracts and pulls down from the shell causing the formation of voids [22].

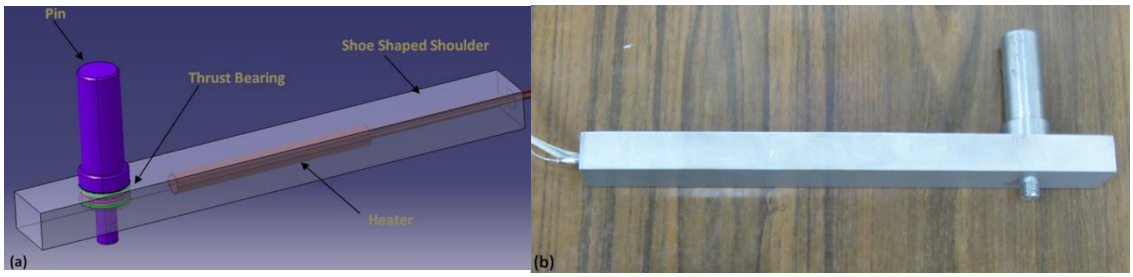

Figure 23 - Hot shoe schematic (left) and picture (right) [56]

To avoid using external heating elements, Eslami [9] developed a tool consisting of a high performing thermoplastic material static shoulder, a rotating steel probe and a copper sleeve. The frictional heat generated between the copper sleeve and the rotating probe is enough to achieve quality welds with 97% strength of the base material, HMW-PE, in a butt joint configuration. Using this tool, rotational and traversing speeds are the most effective parameters regarding tensile strength of the welds, and it has good axial force stability when using position control.

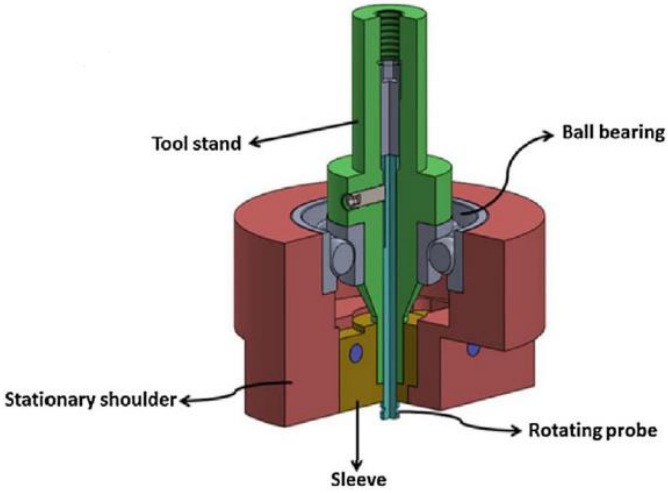

Figure 24 - Static shoulder tool developed by Eslami [9]

Using a static shoe made of PTFE instead of a rotating shoulder, Czigány and Kiss [54] were able to produce butt welds with an efficiency factor of about 64% on a PP sheet reinforced with 30% glass fibres. The fibres in the seam were on average shorter than in the base material, this is due to the shearing forces evolving during the rotation of the tool. The FS welded glass fibre reinforced PP, when compared to FS welded PP sheets with no reinforcement, was found to have higher flexural strength which can be explained by the presence of the fibres in the seam.

Laieghi, et al. [44] welded the polymeric nanocomposite composing of the combination of 80wt% polyamide 6 grafted with various percentages of halloysite nanotubes with 20% nitrile butadiene rubber. The tool used was a heated shoe design with the highest tensile strength being of 61 MPa, which is over 91% of the base materials strength. It was noted that insufficient heat resulted in rough surface as well as chip formation, material loss and fast solidification. In contrast by increasing the rotation of the pin and thus the thermal input, thermal degradation occurred due to polymer burning in the welding area which translates to a reduced weld strength.

Meyer, et al. [45], when welding polyamide 6 with 30% glass fibre in a butt joint configuration with a patented DeltaN tool that has a stationary shoulder, were able to obtain a tensile strength of 50 % the base material. A smaller shoulder diameter in combination with small tilt angles, low feed rates and high contact forces produced the best results. Lower feed rates lead to a higher energy input which lower the material viscosity and benefits the dynamics of the material

flow also improving the fibre presence and orientation in the seam. The fibre length in the seam was analysed, being observed that their size was reduced in 10 to 20%, but no correlation was found between the process parameters and fibre shortening, so the tensile strength was mainly influenced by processes parameters. The comparison of results for welding different composites using a stationary shoulder is shown in Table 4.

Table 4 - Stationary shoulder FS welding of composites

Base material	Tool design	ω [rpm]	v [mm/min]	α [º]	Efficiency factor [%]	Ref.
80wt%PA6/HNT 20wt%NBR 5 mm	hot shoe 30x160 mm threaded pin Ø5 mm	900	14	-	91	[44]
30wt% GFR PP 10 mm	Static PTFE shoulder 4-tooth milling cutter Ø8 mm	2100	-	-	64	[54]
PA6-GF30 5.3 mm	Shoulder Ø20 mm threaded conical pin Ø6 mm	2000	25	2	50	[45]

3.3 Friction Stir Spot Welding

It is like FSW, but without the linear motion. The welding tool plunges into the base material under an axial force and after the desired temperature is achieved, by dwelling, it retracts as can be seen in Figure 25. The tool usually has a concave shoulder and a threaded pin. The anvil or backplate is used below the materials to be welded to counteract the axial force of the tool.

The contact between the tool and the material produces heat by friction. When softened, the material is stirred and flows along the vertical direction along the pin's threads. The tool displacement is continued until either a predetermined level of displacement or axial force is achieved, depending of the control mode of operation, after this, the rotation is kept for a specific dwell time and then retracted. This method was used in the welding of the Mazda RX-8 aluminium rear doors and hood [8].

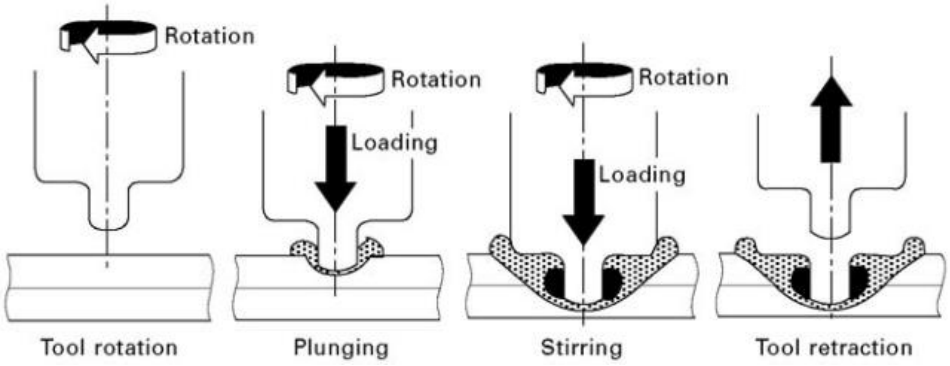

Figure 25 - Friction Stir Spot Welding process [8]

The advantages of this method are low energy consumption, cost efficiency and environmentally friendliness. Friction stir spot welding (FSSW) is limited to specific applications and geometries, also it requires an overlapped positioning of the joint [9].

3.3.1 Friction Spot Welding

There are some papers about a variant of FSSW, friction spot welding (FSpW), developed and patented by the Helmholtz Zentrum Geesthacht (HZG) research centre in Germany, used in composites [57]. Gonçalves, et al. [58] used friction spot welding to weld 2-mm-thick carbon fibre-reinforced polyamide 66 laminate with 49 vol% of fibres.

Friction spot welding distinguishes itself from friction stir spot welding, because it can avoid the formation of a keyhole defect by using a tool that consists of three distinct coaxial pieces: the clamping ring, the pin and the sleeve. The process can be seen in Figure 26 and consists in the fixation of the overlapped specimens by the clamping ring and the backing bar under constant pressure, after this the pin and sleeve rotate in the same direction at a pre-set speed and during a given friction time, followed by the plunging of the sleeve in to the specimen generating enough heat to soften or melt the polymer, simultaneously the pin retracts, creating a gap that is filled by the softened material, in the end the pin and sleeve return to their original positioning, by doing this the entrapped material in the gap is forced by the pin to refill the void left by the sleeve, after the weld cools down the tool can be retracted [58].

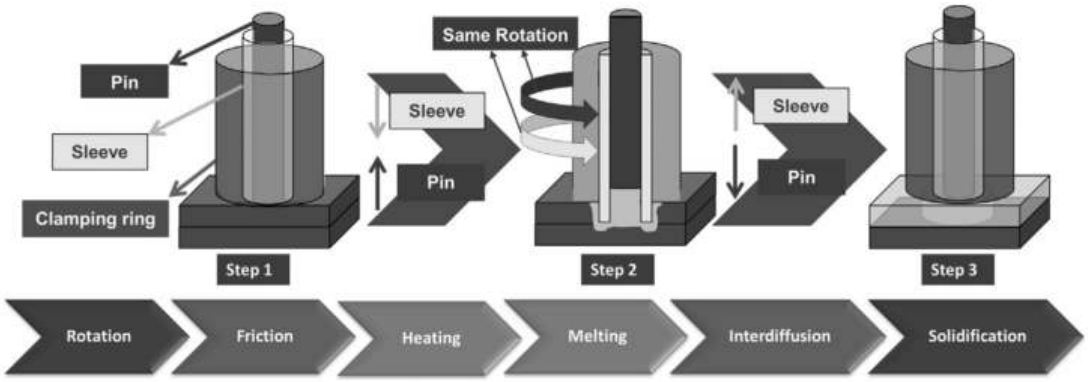

Figure 26 - Illustration of the FSpW process, showing the tool and the main steps [58]

3.4 Vertical reciprocating FSW

Vertical reciprocating FSW consists in a blade that reciprocates in the vertical direction, generating heat between the blade and the plastic material. The problem with this process is that there is no shoulder to maintain the molten material in the joint, as a result voids are created in the weld and strength is reduced. Viblade^{TM} welding is a variant of the vertical reciprocating FSW, in which the blade remains fully in the joint making it easier to contain the melt in the weld. The tool can be seen in Figure 27 and consists of a blade and a shoulder, that run along thermoplastic with a downward force, almost all the heat input is generated by the blade, since the top shoulder only melts material on top of the joint [23, 59].

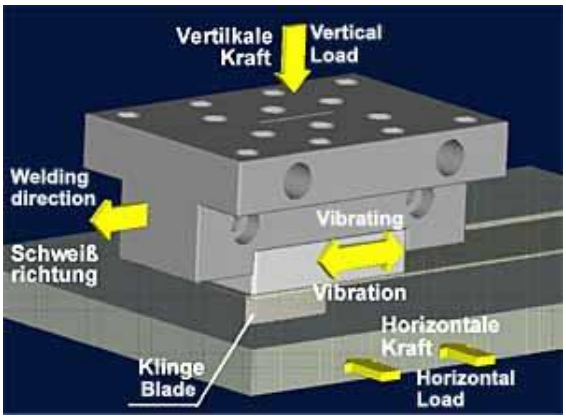

Figure 27 - A schematic illustration of Viblade^{TM} welding [59]

3.5 Friction self-riveting welding

Friction self-riveting is different to FSW. This technique is studied in the joining of metals to thermoplastic composites and the tool used consists in a rotating shoulder without a pin, so there is no mixing between the joined materials. The metal to be joined has pre-drilled holes and the frictional heat generated by the upper metal plate and the rotating tool allows for the softening and squeezing of the bottom thermoplastic composite into the pre-drilled holes of the upper metal plate, as illustrated in Figure 28 [60].

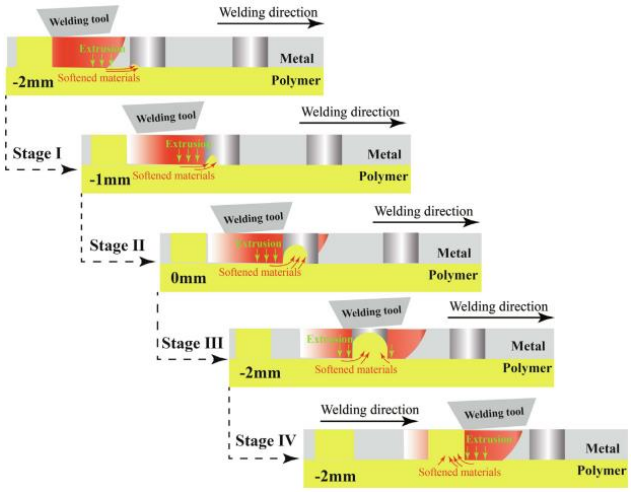

Figure 28 - Schematic of Friction self-riveting welding [60]

The joining of AA6082-T6 aluminium and self-reinforced polypropylene was studied by Baffari, et al. [61]. The tool used was a pinless rotating shoulder with a diameter of 29mm. Different kinds of hole geometries were drilled and investigated. It was concluded that counterbore holes with a chamfer at the base of the hole resulted in the best results.

Meng, et al. [60] friction self-riveted glass fibre reinforced polyphenylene sulphide (GFR-PPS) and AA2060-T8 aluminium. Different hole sizes were tested, and the results were compared with other joining techniques. The metal sheet was submitted to a plasma electrolytic oxidation (PEO) treatment in order to create a porous oxide structure at the surface and increased the strength of the joint. The best tensile shear stress results were achieved by FSRW with 2mm holes and with POE treatment, surpassing FSW with POE treatment.

FSW is able to weld composite and to join composites to metals, but the present state of the technology is unable to achieve high joint efficiency. Due to its simplicity and ease of automation, it's a technology worth studying and developing. To further the state-of-art of FSW experimental work was done.

4 Experimental procedure

4.1 Base Material

The materials to be welded are 4 mm thick plates of Durethan BKV 30 H2.0 901510 (PA 6 reinforced with 30% short glass fibres) supplied by Lanxess, with properties, according to the suppliers material sheet, presented in Table 5.

Table 5 - Selected properties of Durethan BKV 30 H2.0 901510 [62]

Density [kg/m^3]	**Tensile Modulus [MPa]**		**Tensile stress at break [MPa]**		**Tensile strain at break [%]**		**Melting temperature [ºC]**
	Dry	Cond.	Dry	Cond.	Dry	Cond.	
1360	9500	5900	170	100	3	6	222

Polyamides are synthetic polymers that contain multiple amide -CONH- groups as a recurring part of the chain, they are also designated as nylons. The most used polyamides are the semicrystalline, accounting for 90% of global usage. In general, polyamides are prepared directly from dicarboxylic acids and diamines and are identified by numbers that corresponds to the number of carbon atoms in the monomer [63].

Some properties of polyamides are [63]:

- Resistance to oils and solvents;
- Toughness;
- Low friction;
- Abrasion and fatigue resistance;
- Stability at high temperatures;
- Good processability;
- High strength;
- Fire resistance;
- Can be modified in order to achieve desired properties and processing behaviour.

4.1.1 Tensile test

The base material tensile strength was determined in two orthogonal directions in order to study the anisotropy of the material. Specimens were machined along the fibre direction and perpendicular to the fibre direction, as can be seen in Figure 29.

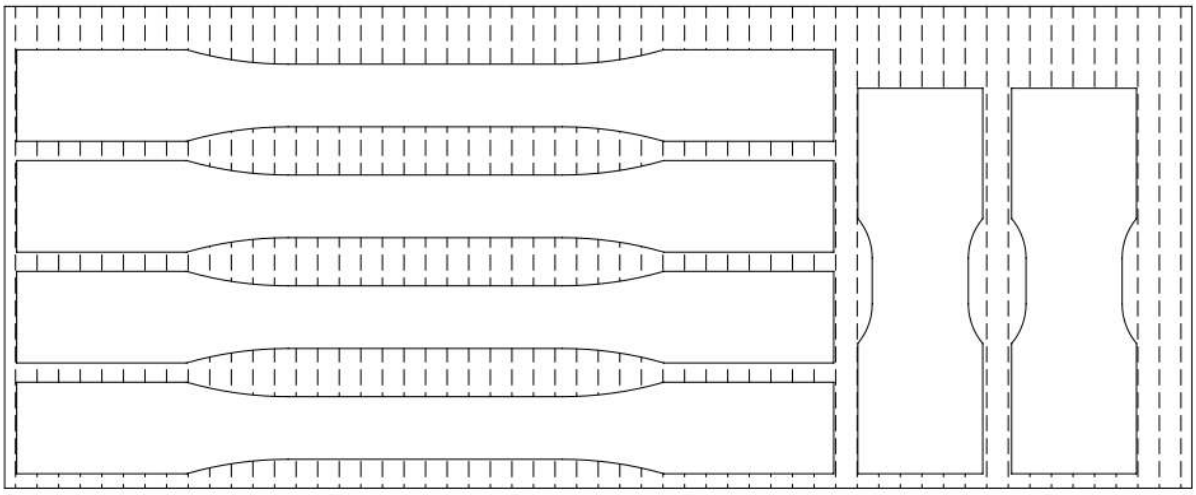

Figure 29 - Specimens machined in perpendicular directions

Five specimens with dimension according to ASTM D638 - 14 [64], as can be seen in Figure 30, were machined perpendicular to the fibre direction.

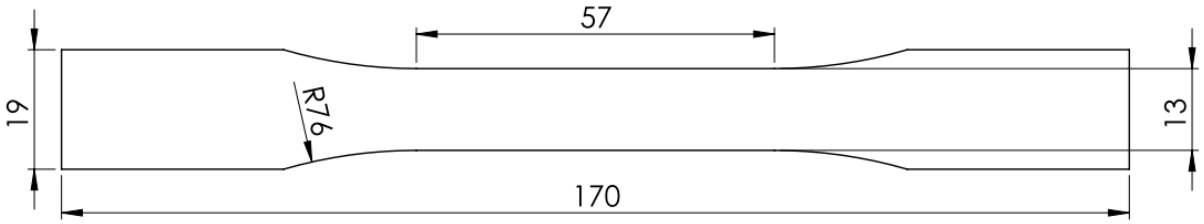

Figure 30 - Type I specimen according to ASTM D638 - 14

The crosshead speed used was 2 mm/min and each specimen cross section was measured three times along the gauge length. The strain was measured using an extensometer. The average area was used to calculate the UTS of the specimens which can be seen in Table 6.

Table 6 - UTS of the base material

	B1	B2	B3	B4	B5	Average	Standard Deviation
UTS [MPa]	78,0	79,4	82,1	83,0	84,2	81,35	2,59
ε_u [%]	3,75	4,01	4,94	5,58	5,11	4,68	0,77
E [MPa]	4458	5267	4314	4823	4413	4655	392

From Figure 31 it's possible to see that the maximum tensile strength obtained from specimens B1 to B5 did not fall in the range of the supplier's datasheet, neither did the average tensile modulus, which was 4655 MPa. The only parameter that fell under the expected range was the strain at rupture, which was on average 4.68. This discrepancy in values may be a consequence of high levels of moisture or anisotropy of the material.

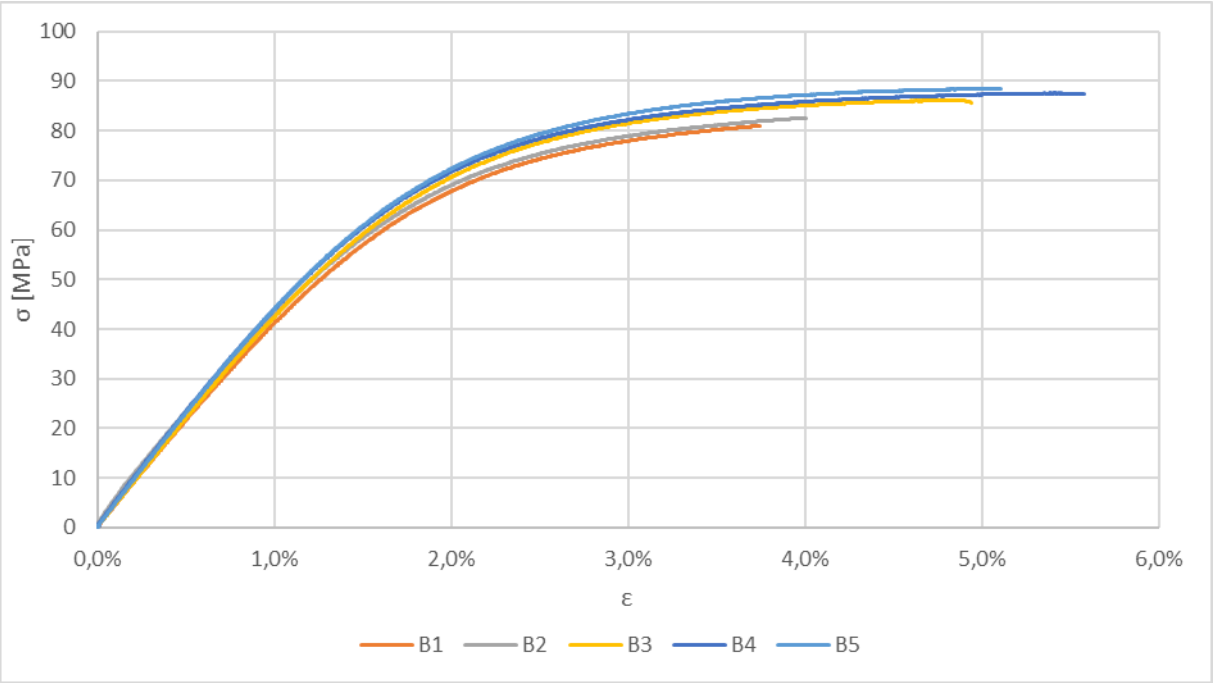

Figure 31 - True stress-strain curves for specimens B1 to B5.

Only Three specimens were machined along the fibre direction and with unorthodox dimensions due to limitations on the amount of base material available. The dimensions of the specimens are shown in Figure 32.

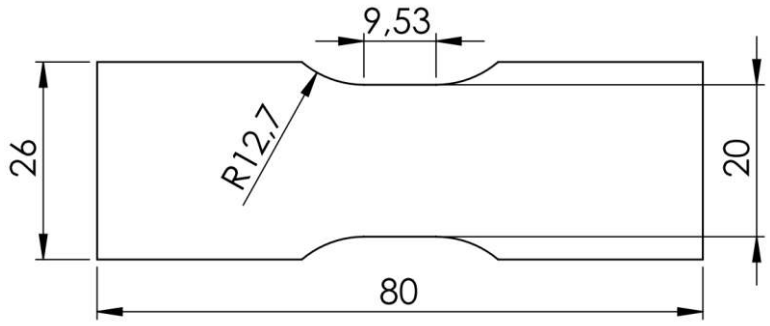

Figure 32 - Small specimens

The crosshead speed was 2 mm/min and each specimens thickness and width were measured three times in the gauge length. The UTS are presented in Table 7.

Table 7 - UTS of the base material

	Bs1	Bs2	Bs3	Average	Standard Deviation
UTS [MPa]	-	151,4	149,1	150,27	1,65

Specimen Bs1 broke outside the gauge length, Figure 33, because of that the value obtained was discarded. The values obtained in Table 7 are within the values from the material datasheet. The average value of Bs2 and Bs3 will be used as the comparison for the rest of this work. This is not ideal since the specimens used do not follow a standard and the number of specimens was less than 5.

Figure 33 - Specimen P1 broken outside the gauge length

4.1.2 Material dimensions for welding

The supplied plates were dimensions 400x250x4 mm^3 and were cut into plates of size 247x100x4 mm^3 as exemplified in Figure 34.

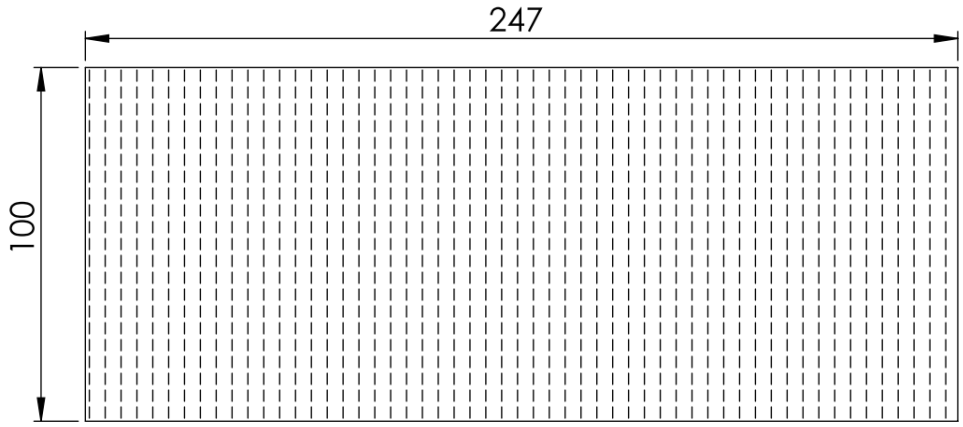

Figure 34 - Dimensions of individual plates used for welding in a butt joint configuration

After being cut, the plate edges were machined, Figure 35, in order to assure good contact between the abutted joint and thus prevent the existence of gaps when fixing the plates for welding in a butt joint configuration.

Figure 35 - Machining of the edges of 4 plates

The plates were clamped with the edges in contact in order to weld in a butt joint configuration. The welds were performed perpendicular relative to the fibre direction material strength, this is demonstrated in Figure 36.

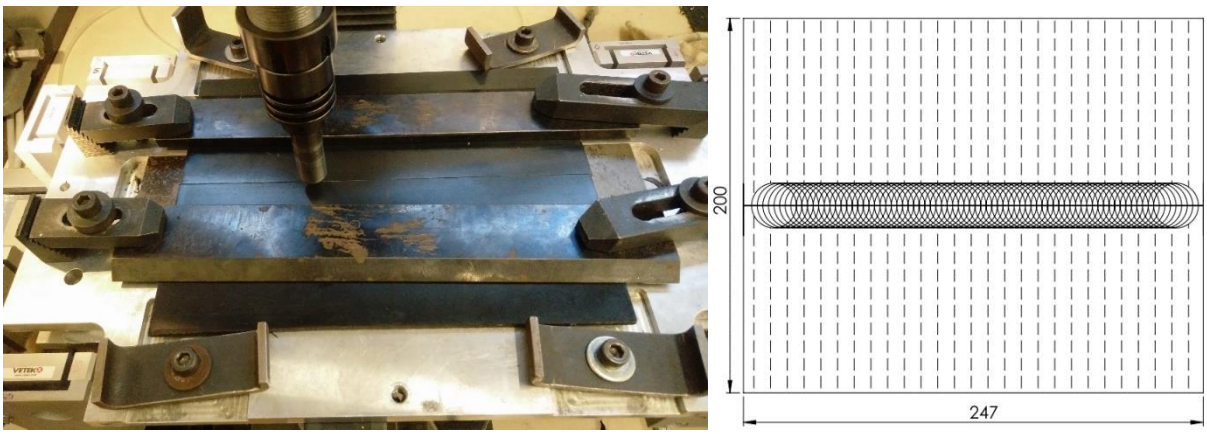

Figure 36 - Setup used for welding plates in a butt joint configuration (left) and schematic of welded plates (right).

4.2 Data acquisition

4.2.1 Sensitized clamping system

During friction stir welding different forces are applied to the material by the tool, which affect the quality of the weld. The axial force is, in general, the highest and most influential on the weld quality when compared to the lateral and traversing forces. The lateral force is caused by the tool rotation and the traverse force results of the linear movement of the tool, as can be seen in Figure 37. To measure the forces during welding, a sensitized clamping system, with the ability to acquire the generated forces in three different directions, is required [9, 16].

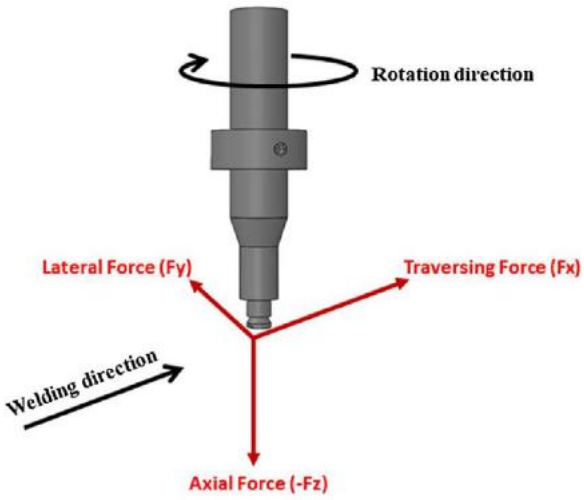

Figure 37 - Schematic of the forces directions during FSW process [65]

The force platform used consists of 3 parallel plates and 12 load cells (four for each axis) and is connected to a data acquisition system with a dedicated LabView code. The load cells are Vetek planar load cells (202WA) with a maximum capacity of 2940 N each and the system is able to measure axial force (F_z), lateral force (F_y) and traverse force (F_x) [9, 16]. The top plate is connected to the floating plate through four load cells with M4 bolts, these load cells are the ones that measure axial force. The floating plate is connected to the bottom plate through 4 rod-end spherical bearings that allow movement in both the x and y direction, but not in the z

direction. The floating plate is in contact with the lateral load cells through the use of spherical pins and half sphere holes, allowing to eliminate the influence of the vertical force on the x and y direction load cells. Figure 38 shows the measuring device without the top plate making the axial load cells visible [65].

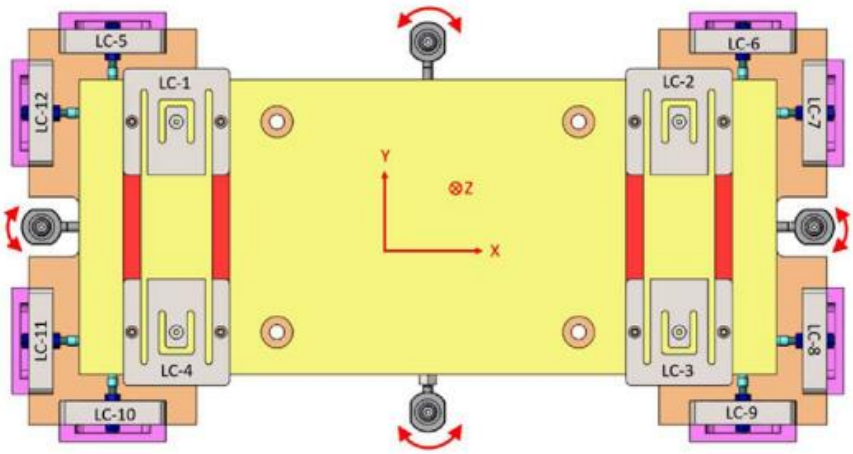

Figure 38 - Schematic of floating plate [65]

It was studied by Eslami, et al. [65] that by using this system it is possible to consider the axial force as a welding parameter when using position control, since the tool's vertical position is responsible for the axial force during welding. It should be noted that this applies to static shoulder tools, because the axial force tends to stabilize, in contrast rotating shoulder tools result in unstable loading when using position control [66].

To setup the desired force, shims with known thickness and bigger than the height of the pin are placed beneath the shoulder, after this the head is moved downwards until the axial force measured is the desired. This position is recorded by the control software of the machine as a zero for the z axis. The tool is then raised enough so that the probe does not touch the material and the shims are able to be removed, this will become the new zero of the machine, so it's best that the raised height is a round number. By programming the machine tool to go downwards the thickness of the shims and the height required to remove the shims, the welding process will have predeterminate axial force during the welding stage. It should be noted that during the plunging and dwelling stages the force is not the desired and usually in the beginning of the dwelling stage the force measured is the highest, surpassing the desired force. Figure 39 illustrates the process.

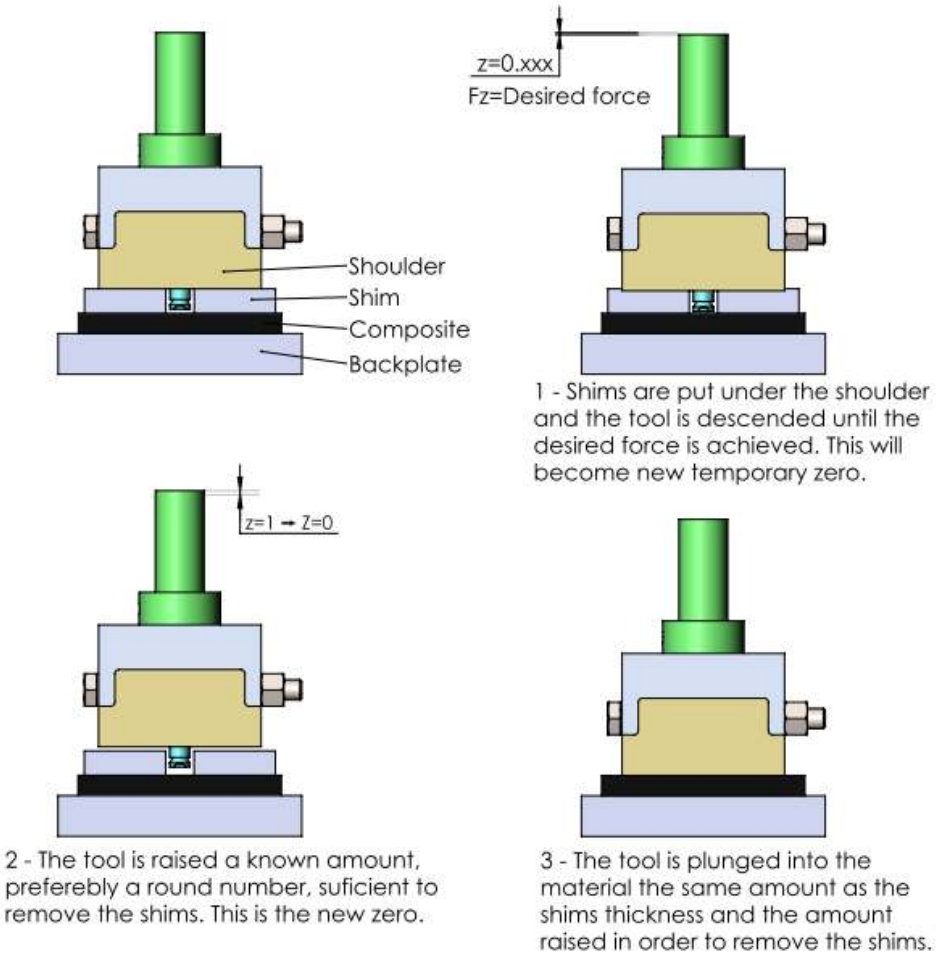

Figure 39 - Schematic procedure to use a specific axial force

The plates where clamped to the force plate platform using two different clamp types. Four clamps were used to prevent lateral motion and two metal bars to prevent vertical motion of the plates and to guide the welding tool, this is exemplified in Figure 40.

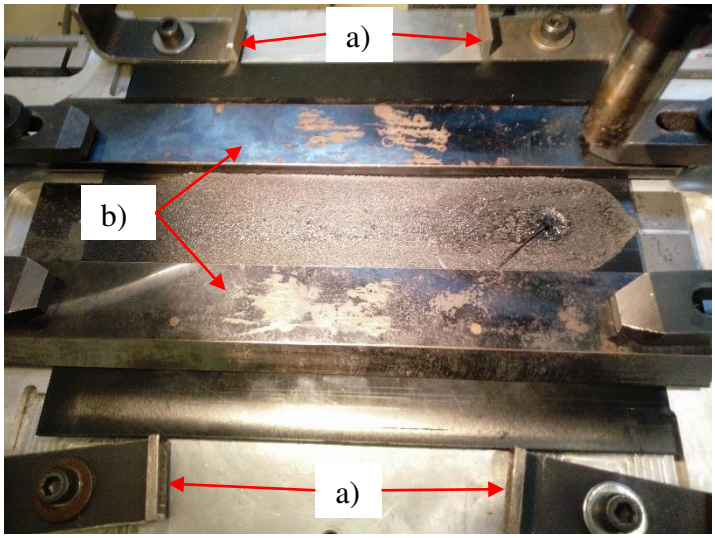

Figure 40 - Clamping system used, a) four clamps for lateral movement and b) two metal bars

4.2.2 Temperature acquisition

The tool's temperature was obtained using a K-type thermocouple and the device seen in Figure 41, which uses a Maxim Integrated MAX31855 cold junction compensated thermocouple-to-digital converter. The MAX31855 outputs data in a signed 14-bit, SPI-compatible, read-only format, allows reads from -270 ºC to 1800 ºC, with a resolution of 0.25ºC and an accuracy of ±2 ºC, for K-type thermocouples in a range of -200 ºC to 700 ºC. The device was connected to a computer via USB and the data was recorded to a text file using Free Serial Port Monitor software.

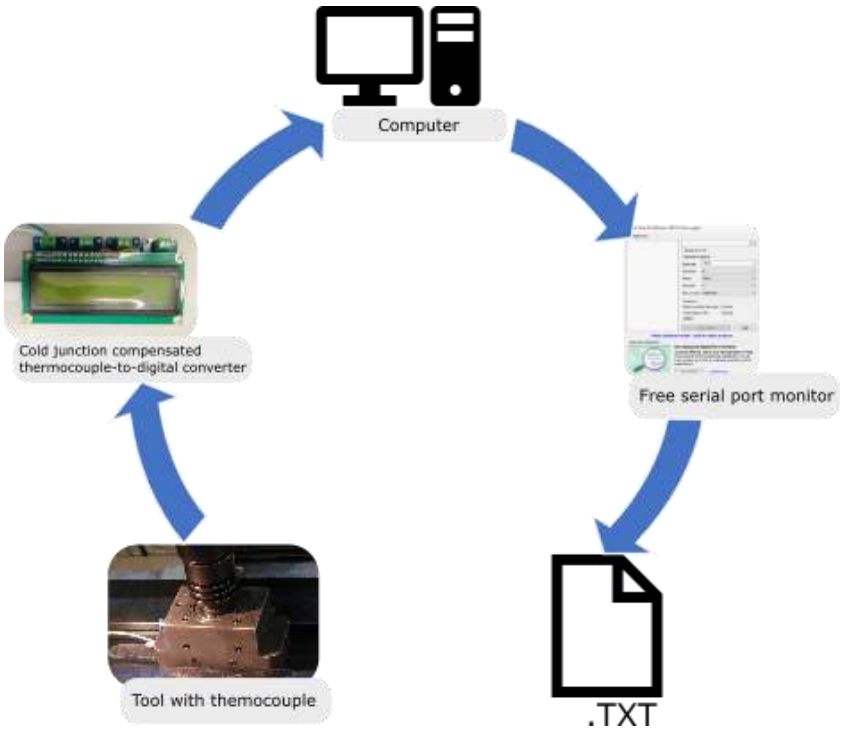

Figure 41 - Temperature measurement system.

4.3 Tool design and machinery

The machine used as the friction stir welder is an adapted Optimum BF20 3 axis CNC milling machine, Figure 42, controlled with G/M codes using Mach3 software.

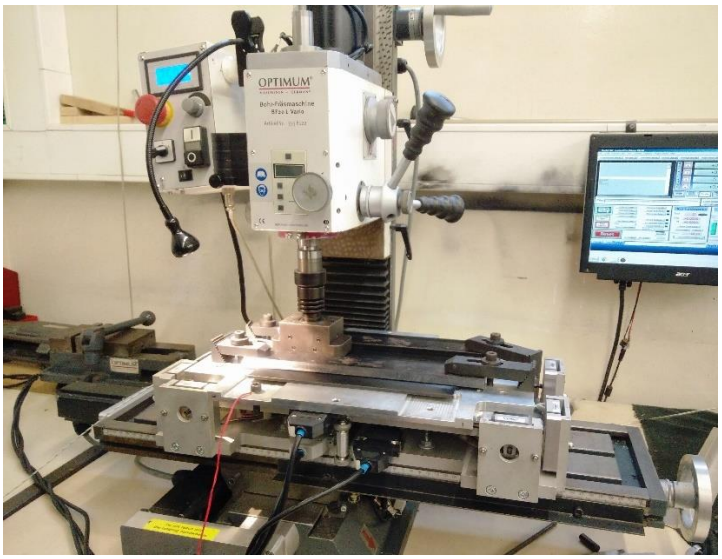

Figure 42 - Machine used for FSW.

Two different tools were used. A hybrid tool originally designed for joining aluminium to polymeric material which consisted of a steel stationary shoulder, a copper sleeve, a rotating steel shoulder and a steel probe. The steel shoulder has holes to make possible to air cool it if necessary. The tool is shown in Figure 43.

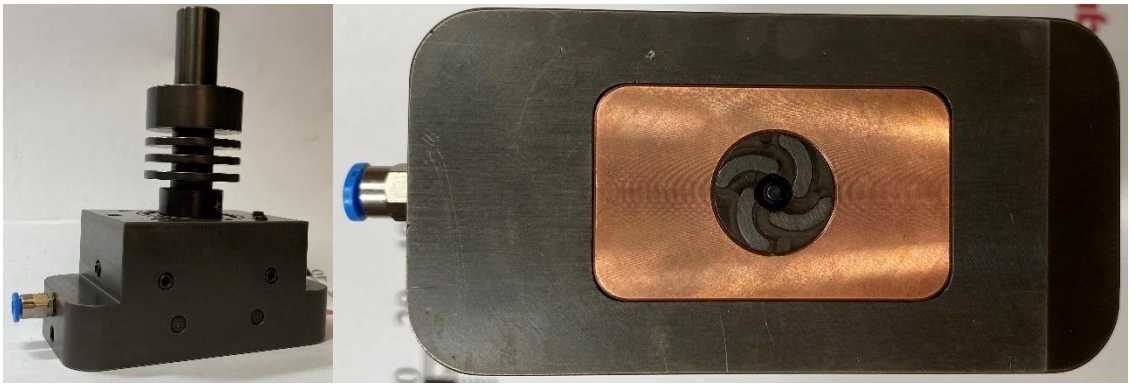

Figure 43 - Hybrid welding tool

The main dimensions of the hybrid tool are in Table 8

Table 8 - Main dimensions of the hybrid tool

	Width [mm]	**Length [mm]**
Static Shoulder	50	100
Sleeve	30	50
	Diameter [mm]	**Length [mm]**
Rotating shoulder	17	0.3
Probe	5	3.9

The other tool is a stationary shoulder tool, designed to weld polymers, that is composed by a stationary shoulder made of PEEK, a copper sleeve and a steel probe, as can be seen in Figure 44.

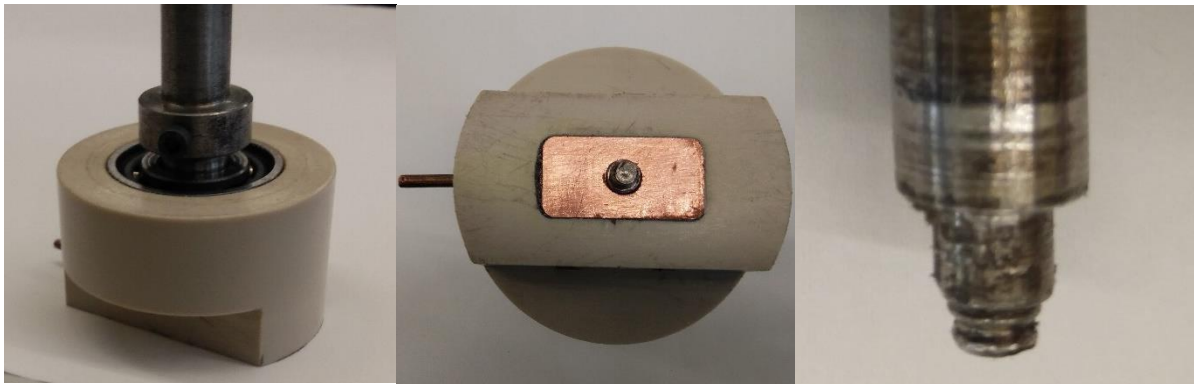

Figure 44 - Stationary PEEK tool designed to weld polymers

The main dimensions of the polymer welding tool are in Table 9.

Table 9 - Main dimensions for polymer welding tool

	Width [mm]	**Length [mm]**
Static Shoulder	26	50
Sleeve	12	24
	Diameter [mm]	**Length [mm]**
Probe	5	3.9

The tool designed for welding the composite material is the tool based on the one developed by Eslami [9] to weld polymers. It consists of a tool stand, a steel probe, a copper sleeve, an insulation layer, a polymeric shoulder, an aluminium upper shoulder, a bearing, two locking shafts, two bolts and two nuts. The tool stand rotates and is mounted to the stationary shoulder through an angular contact bearing, allowing for the axial force to be transferred to the shoulder and not the probe. The probe rotates with the tool stand, using a screw to secure then, and can have its height adjusted relative to it, using another screw. The sleeve's vertical positioning is fixed relative to the shoulder by two locking pins [9]. Figure 45 displays the components of the tool.

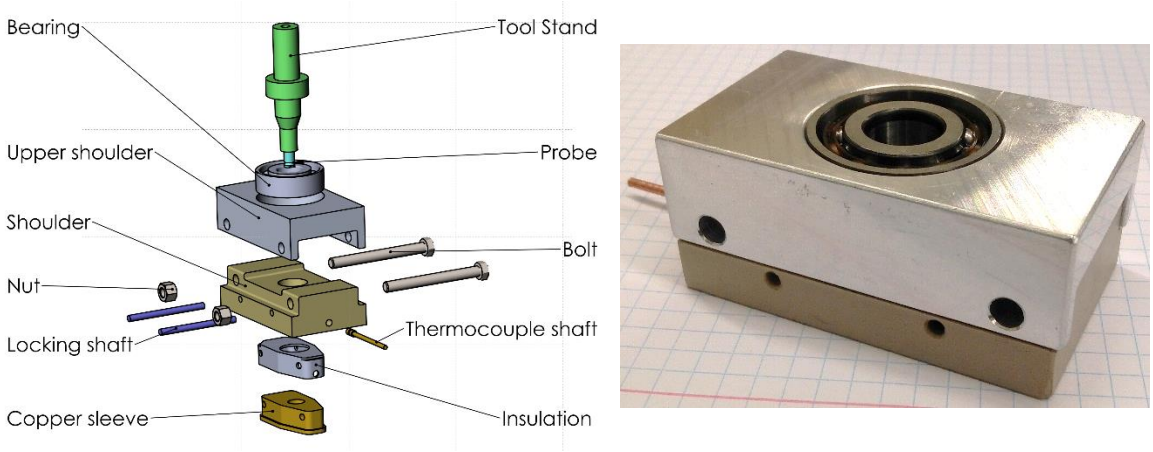

Figure 45 - Components of the welding tool (left) and image of welding tool (right).

The heat is generated through friction between the rotating probe and the stationary copper sleeve and, not only heats up the probe, but also the base material creating a "sleeve layer" that is the same width of the copper sleeve. This tool may achieve temperatures in the order of 400 ºC in the copper sleeve. The stationary shoulder serves to keep the soften material in the weld bead, to make the material cool down under pressure and to help insulate the copper sleeve so that as much heat is transferred to the material being welded [9].

The main differences between this tool and the one used by Eslami [9] is the presence of an insulation layer between the copper sleeve and the polymeric shoulder, the different geometry of the sleeve and polymeric shoulder and the presence of an upper shoulder.

4.3.1 Shoulder material

The shoulder is an important component when regarding the weld quality. As it has been previously discussed in chapter 3, a stationary shoulder provides better weld surface quality than a rotating one. The shoulder material has also influence in the surface quality of the weld, polymers or polymer coated tools are the ones that present best results [40]. A specific requirement of this tool is that the shoulder should have a high service temperature since the

copper sleeve may achieve temperatures up to 400ºC, also the sleeve should be insulated in order to transfer most of its heat to the material being welded and not the shoulder [67]. Figure 46, shows the maximum service temperatures and thermal conductivity of different bulk materials and it can be seen that non-technical ceramics present a similar thermal conductivity to plastics but a much higher working temperature. The problem with most ceramics is their brittleness and difficulty in machining.

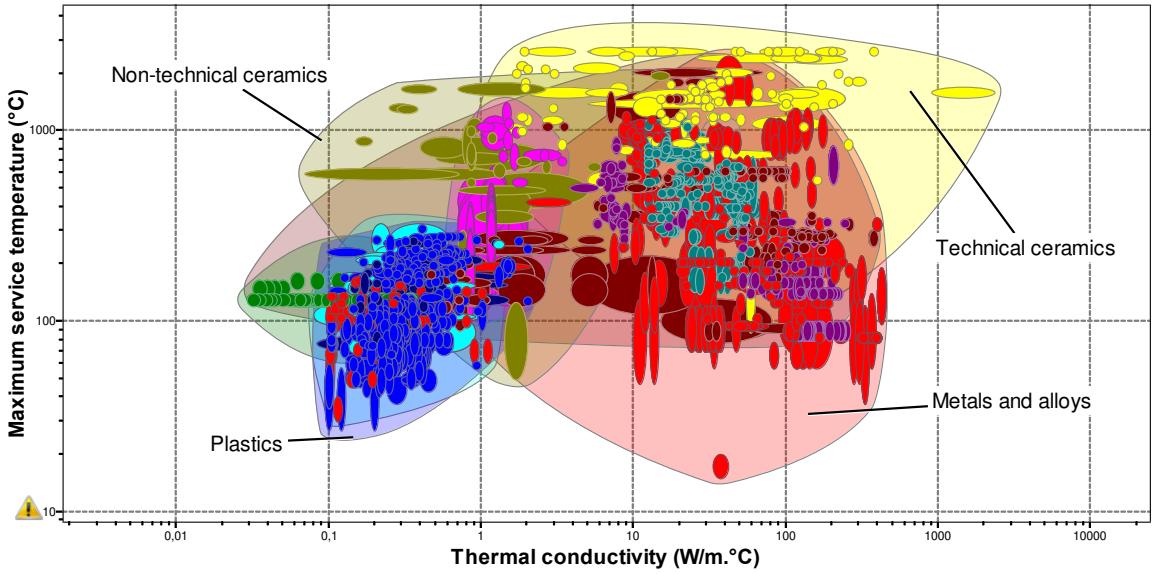

Figure 46 - Maximum service temperature and thermal conductivity of different material groups [68].

Figure 47 shows the maximum service temperature and thermal conductivity of different plastics and non-technical ceramics with service temperature above 250ºC and with less than 1 W/mºC of thermal conductivity. The plastic that presents the highest service temperature is PBI, but the plastic that presents the highest insulation is PEEK reinforced with 30% glass fibres. The only materials which have service temperatures above 400ºC and thermal conductivity similar to the aforementioned plastics are non-technical ceramics. Cements and concretes are part of this group of materials and can be easily moulded into complex shapes when newly mixed making then an interesting material to use between the plastic shoulder and the copper sleeve.

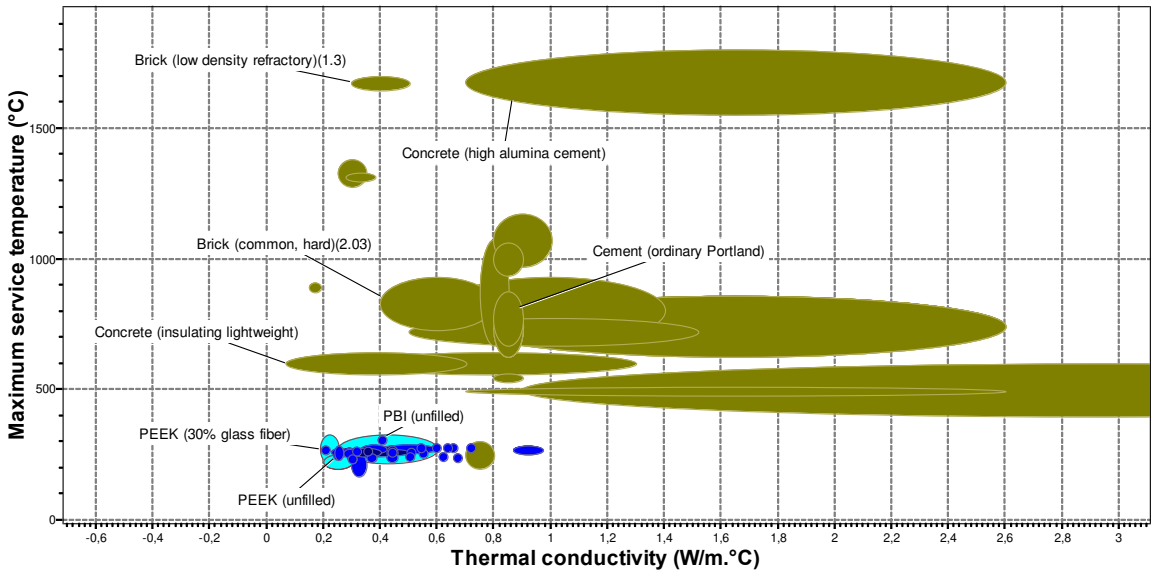

Figure 47 - Maximum service temperature and thermal conductivity of different plastics and non-technical ceramics with service temperature above 250ºC and with less than 1 W/mºC of thermal conductivity [68].

4.4 Design of Experiment

To study the influence of the welding parameters in the strength of the joint a Taguchi design of experiment (DOE) was employed. The advantage of Taguchi design is that it allows to reduce the number of experimental procedures and thus reducing time and cost. A full factorial design consists in analysing each possible combination of parameters, although it may be more correct to assess the influence of the parameters studied, in most cases it's too unpractical due to the sheer amount of trials.

Using a Taguchi DOE, the selected array will not have all the possible parameter combinations and there will be confounding between then, this is, the interactions of parameters may be mixed with the effect of another parameter and therefore an additional uncertainty is introduced to the analysis. It is important to set up the array to minimize the potential for confounding between factors and interactions. The resolution of an experimental design is a rating for the effectiveness of isolating factors from low-order interactions. They can be describes as [69]:

- Resolution III - There is no confounding between factors, but at least one factor is confounded with a two-factor interaction;
- Resolution IV - There is no confounding between main factors or between a main factor and a two-factor interaction, but here is at least one two-factor interaction confounded with another two-factor interaction;
- Resolution V - There is confounding between a two-factor and a three-factor interaction, but no confounding with lower order interaction.

This logic continues, at the extreme there is no confounding and that represents a full factorial design. In the Taguchi DOE interactions of order higher than 2 are considered non-existent.

By rewriting the quadratic loss function, it is possible to obtain Taguchi's signal to loss (S/N) ratios, which don't always involve a ratio of signal to noise. The most common categories of S/N ratio are smaller-the-better, larger-the-better and nominal-the-best [69].

When the ideal value of the response is zero and the response cannot have negative values, the smaller-the-better S/N ratio is employed and corresponds to Equation (4.1).

$$(S/N)_i = -10 \log_{10} \left(\frac{1}{N} \sum_{n=1}^{N} y_{i,n}^2 \right) \tag{4.1}$$

When the ideal value of the response is infinity and the response cannot have negative values, the larger-the-better S/N ratio is employed and corresponds to Equation (4.2).

$$(S/N)_i = -10 \log_{10} \left(\frac{1}{N} \sum_{n=1}^{N} \frac{1}{y_{i,n}^2} \right) \tag{4.2}$$

When the ideal value of the response has an intermediate value and the average can be adjusted by applying a adjustment factor with no effect on the coefficient of variance then the nominal-the-best S/N ratio is applied and corresponds to Equation (4.3)

$$(S/N)_i = 10\log_{10}\left(\frac{\mu_i}{\sigma_i}\right)^2 \quad (4.3)$$

Where:

(S/N) is the signal to noise ratio
N represents the total number of replicates
y is the experimental value obtained
μ represents the average response
σ represents the standard deviation
i designates the treatment conditions
n denotes the replicate number

For the analysis of the results from the experiment the analysis of variance (ANOVA) is used. For that the sum of squares (SS), the mean squares (MS), the F test, the p-value and the percentage contributions are calculated [70].

The total sum of squares (SS_T) can be calculated using equations (4.4) or equation (4.5).

$$SS_T = \sum_{i=1}^{A}\sum_{n=1}^{N}(y_{in} - \bar{y})^2 \quad (4.4)$$

$$SS_T = \sum_{i=1}^{A}\sum_{n=1}^{N}(y_{in}^2) - \frac{Y^2}{AN} \quad (4.5)$$

Where:

y is the experimental value obtained
$\bar{y}$ is the average of all experimental values
Y is the sum of all the experimental values
i represents the experimental treatment conditions
A represents the total of different treatment conditions
n represents the replicant
N represent the total number of replicants

The total sum of squares (SS_T) can be decomposed as observed in equation (4.6)

$$SS_T = \sum_{p=1}^{P} SS_p + SS_E \quad (4.6)$$

Where:

SS_p is the sum of squares for factor p
P is the total number of factors
SS_E is the sum of squares of the error

The sum of squares for a main factor can be calculated using equation (4.7).

$$SS_p = \sum_{l=1}^{L}\frac{(Y_{pl})^2}{T_{pl}} - \frac{Y^2}{AN} \quad (4.7)$$

Where:

Y_{pl} is the sum of experimental results for level l of factor p
T_{pl} is the total number of experimental results for level l of factor p
L is the total number of levels for factor p

The mean squares (MS) is the division of the sum of squares of a factor by its corresponding degree of freedom (DOF) as can be observed in equation (4.8).

$$MS_p = \frac{SS_p}{DOF_p} \tag{4.8}$$

Where:

MS_p is the mean square of factor p
SS_p is the sum of squares of factor p
DOF_p is the degrees of freedom of factor p

The F-test is simply dividing the mean square of a factor by the mean square of the error and then comparing it to the critical F value for the corresponding degrees of freedom. Equation (4.9)

$$F_p = \frac{MS_p}{MS_E} \tag{4.9}$$

The degree of contribution (ρ) can be obtained by using equation (4.10)

$$\rho_p = \frac{SS_p}{SS_T} \tag{4.10}$$

4.4.1 Parameters and Orthogonal matrix

The experimental tests to evaluate the effect of the parameters in the ultimate tensile strength were performed using the Taguchi design of experiments using an L_4 orthogonal array. The tool used was the stationary shoulder tool designed to weld polymers.

The parameters to be evaluated are the rotation speed of the probe, the Traversing speed and the axial force with values showed in Table 10. For all tests the dwell time, the plunge speed, the pin length, the pin geometry and the pin diameter are constant and are shown in Table 11, the values were selected due to primary experimental tests.

Table 10 - Level values for welding parameters

Level	Rotation speed [rpm]	Traversing speed [mm/min]	Axial force [N]
1	2000	20	800
2	2800	40	1000

Table 11 - Constant parameters

Dwell time [s]	Plunge speed [mm/min]	Pin length [mm]	Pin diameter [mm]
40	5	3.9	5

The two level three factor design can be seen in Table 12. Each of the treatment conditions was repeated 5 times. To identify the samples, the nomenclature Sij was used, where i represents the treatment condition and j represent the repetition number.

Table 12 - L_4 orthogonal array for three parameters with two levels each

Experiment	Rotation speed [rpm]	Traversing speed [mm/min]	Axial force [N]
S1	2000	20	800
S2	2000	40	1000
S3	2800	20	1000
S4	2800	40	800

The specimens were made according to ASTM D3039/D3039M-00 [71] with the dimensions seen in Figure 48.

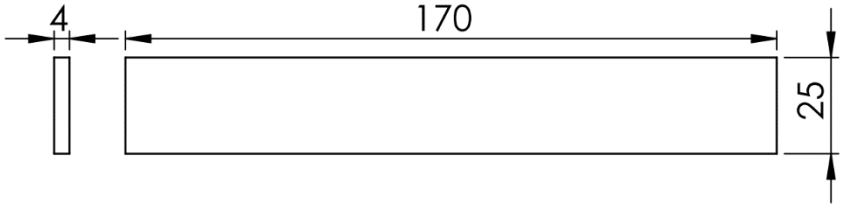

Figure 48 - Specimens dimensions.

A total of 20 specimens were made. Firstly, they were cut with a band saw to a width of 30 mm and a length of 170 mm, after this, four samples were firmly clamped down and machined using an Optimum BF20 3 axis CNC milling machine with a 6 mm diameter end mill. The welded plate, the milling procedure and the final specimens can be seen in Figure 49.

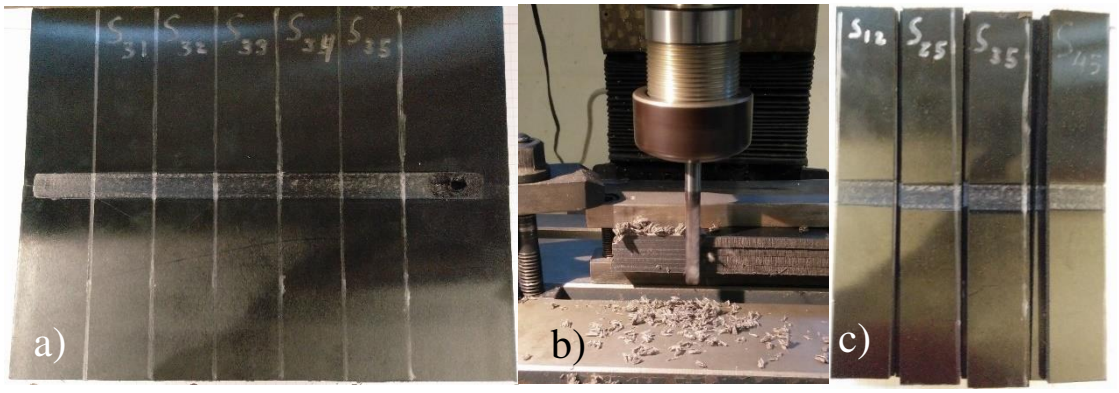

Figure 49 - a) Plates with markings b) machining of the specimens and b) final specimens

After machining the specimens, the weld became visible from the sides and is shown in Figure 50.

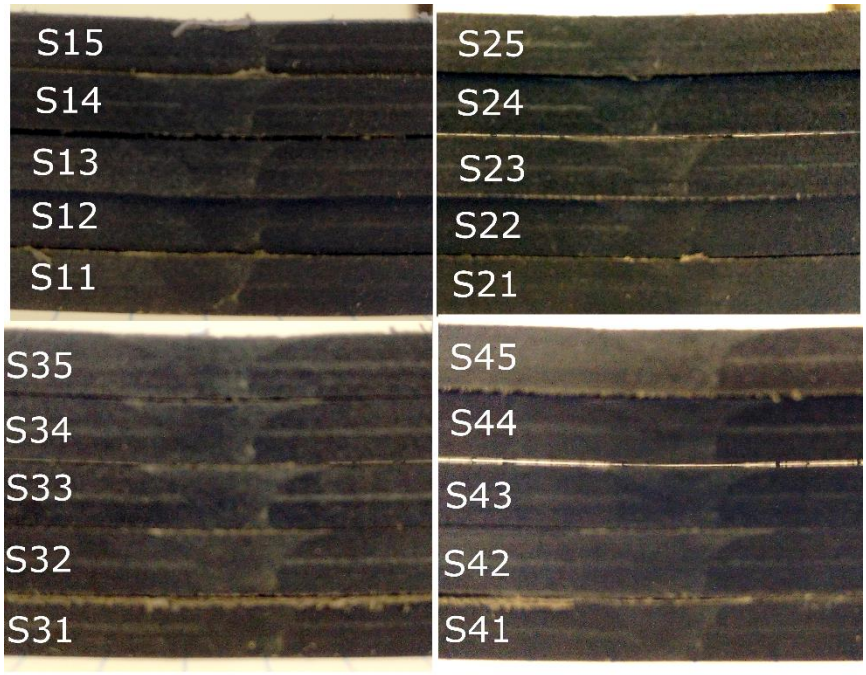

Figure 50 - Specimens weld view from the side

The tensile tests were performed using a speed of 2 mm/min with a distance between grips of 100 mm. No extensometer was used for these tests. The tensile test setup is shown in Figure 51.

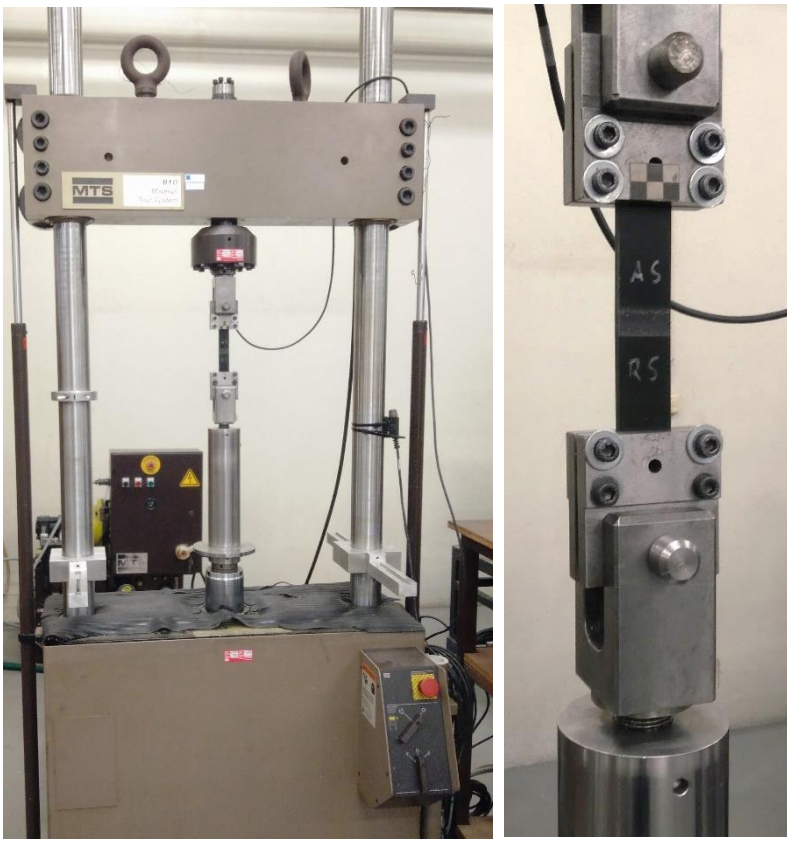

Figure 51 - Tensile test of specimen

The ultimate tensile strength was calculated using (4.11).

$$UTS = \frac{F_{max}}{A} \tag{4.11}$$

Where:

UTS is the ultimate tensile strength [MPa]
F_{max} is the maximum load before failure [N]
A is the average cross-sectional area [mm^2]

5 Experimental Results

5.1 Welding with hybrid tool

A tool originally designed for joining polymers to aluminium was used to weld plates of PA6 GF30. The tool consists of a hybrid between a stationary shoulder tool and a rotating shoulder tool. The bottom of the tool is visible in Figure 52.

Figure 52 - Bottom view of hybrid tool

5.1.1 Welding without preheating

Using the hybrid tool, composed of a steel static shoulder, a copper sleeve and a probe with a rotating shoulder, some test were made in the PA6 30GF plates. The parameters used are present in Table 13.

Table 13 - Parameters used for FSW with non-heated hybrid tool.

Rotating speed [RPM]	Traversing speed [mm/min]	Axial force [N]	Dwell Time [s]
2800	40	1000	60

Firstly, it was noted that the plates to be welded did not contact evenly through all their extension, leading to the presence of gaps. This affects negatively the quality of the weld. The clamping system used was insufficient, this resulted in the plates moving laterally, the formation of gaps, that can be seen in Figure 53, and in abrupt variations in the axial force during welding. The weld was made, but it's possible to note that the heat produced by the sleeve wasn´t enough, resulting in the absence of the sleeve layer. The weld was done only where the rotating shoulder entered in contact with the material.

The weld presented some defects in the beginning, but at the end of the weld it became smoother. This behaviour can be due to the tool being hotter at the end of the weld, meaning that a higher heat output may be required.

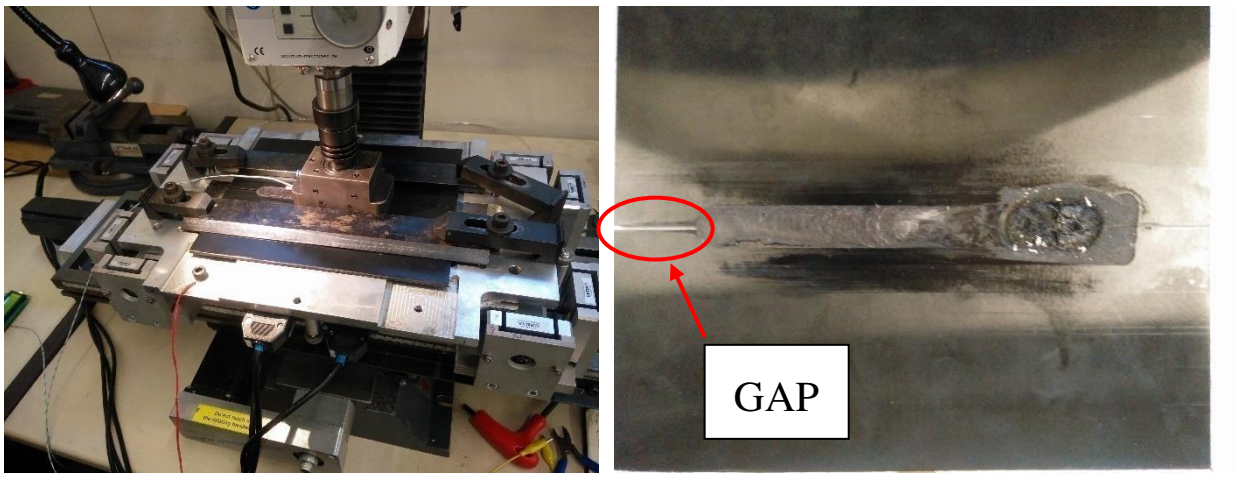

Figure 53 - Welding with hybrid FSW tool (left) and resulting weld (right)

Some composite material from the weld got stuck inside the tool and on the surfaces of the tool that entered in contact with the weld. This led to a loss of material from the plates and required to clean the tool between welds. Figure 54 exemplifies this problem. A polymeric or ceramic coating may be applied in order to prevent the material from sticking form the bottom. To prevent the material from getting inside the tool, tighter tolerances may be used, but this solution wont last long due to tool wear

Figure 54 - Weld material stuck inside the tool, on the probe and on the shoulder face

Since most of the heat was being produced by the rotating shoulder of the tool, a test with only the rotating part of the tool was made with the parameters present in Table 14.

Table 14 - Welding parameters for non-heated rotating shoulder tool.

Rotating speed [RPM]	**Traversing speed [mm/min]**	**Axial force [N]**
1800	20 in the first half 40 in the second half	400

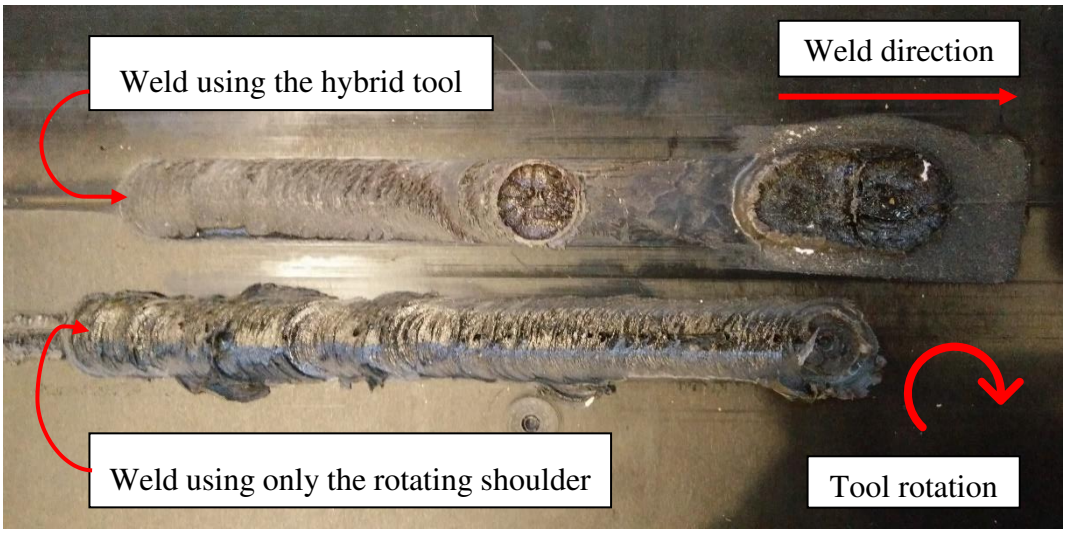

Figure 55 - Welds obtained from hybrid tool (top) and weld from rotating shoulder tool (bottom)

The comparison between the welds can be seen in Figure 55, and it is visible that the static shoulder helps to obtain a smoother weld and with less flash. The shoulder contains the material in the weld, which is important to produce strong welds. Although the hybrid tool produced better results there was significant defect on the retreating side, evidenced in Figure 56, also in the beginning it's possible to see an onion ring defect on the surface of the weld. A higher heat output and optimized parameters are required in order to produce an acceptable weld.

Figure 56 - Defect in the retreating side and onion ring defect of the surface of weld.

Another attempt was made to weld the composite plates with the hybrid using a rotational speed of 1800 rpm, Traversing speed of 20 mm/min, axial force of 400 N and a dwell time of 80 s, but it was not possible to finish it due to failure of the machine's electric motor. Due to this setback, the tool was preheated in the posterior tests.

5.1.2 Welding with preheating

To determine the dwell time the temperature of the tool was recorded in two different setups. In one setup the tool was plunged into the composite material and remained stationary. The axial force used was 600 N with a rotation of 2000 rpm. Figure 57 shows the temperature values obtained.

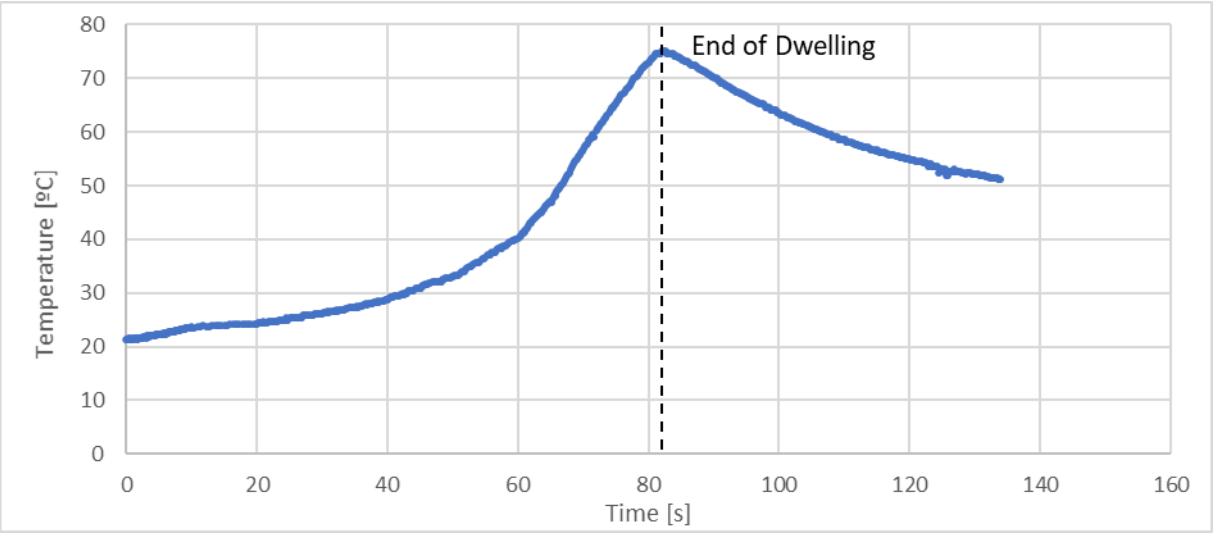

Figure 57 - Temperature measurement for dwell time of 82 s with an axial force of 600 N and a rotation of 2000 rpm.

The problem with such a long dwell time is that, in this period, the composite becomes viscous causing excessive torque to be applied to the milling machine. The molten composite sticks to the surfaces of tool and impregnates the tool through its gaps, making it a necessity to dissemble the tool in other to clean it after a weld.

To measure the full capability of the tool without having to clean it afterwards and to prevent possible damage of the milling machine, a test was made in which the tool was fixed with wooden blocks and the axial force was set to zero. The axial force was increased a small amount by manually pushing the milling machine spindle downwards into the tool. This made it possible to approximate the dwell time needed without using the base material. In this test the axial force was controlled manually, and the results obtained are displayed in Figure 58.

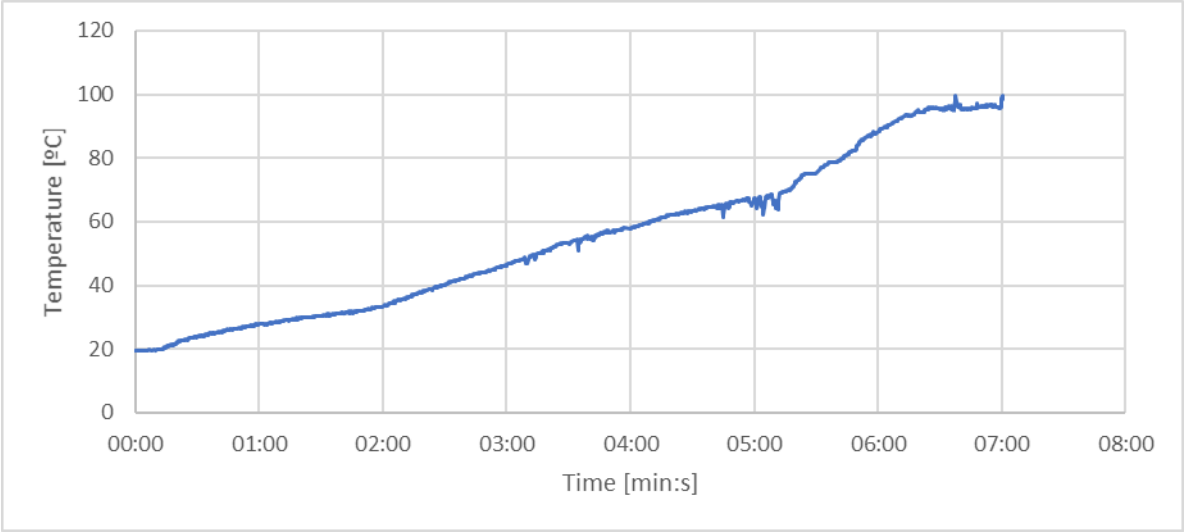

Figure 58 - Temperature measurement during dwell time without using composite material.

With this method the temperature in the tool reached a maximum of 99.7 ºC, but it took 7 minutes to reach that temperature. This dwell time duration is not acceptable for the tool, since the longer the dwell time the more composite material gets inside the tool. The melting temperature of PA6 30GF being welded is around 222 ºC, which means that 99.7 ºC is a temperature not high enough to weld the material.

As an alternative to preheat the tool, for this it was attempted to use soldering irons and a heat gun. The soldering irons were unable to heat up the tool within a reasonable time frame, as visualized by Figure 59, were as the heat gun was able to heat up the tool much more quickly.

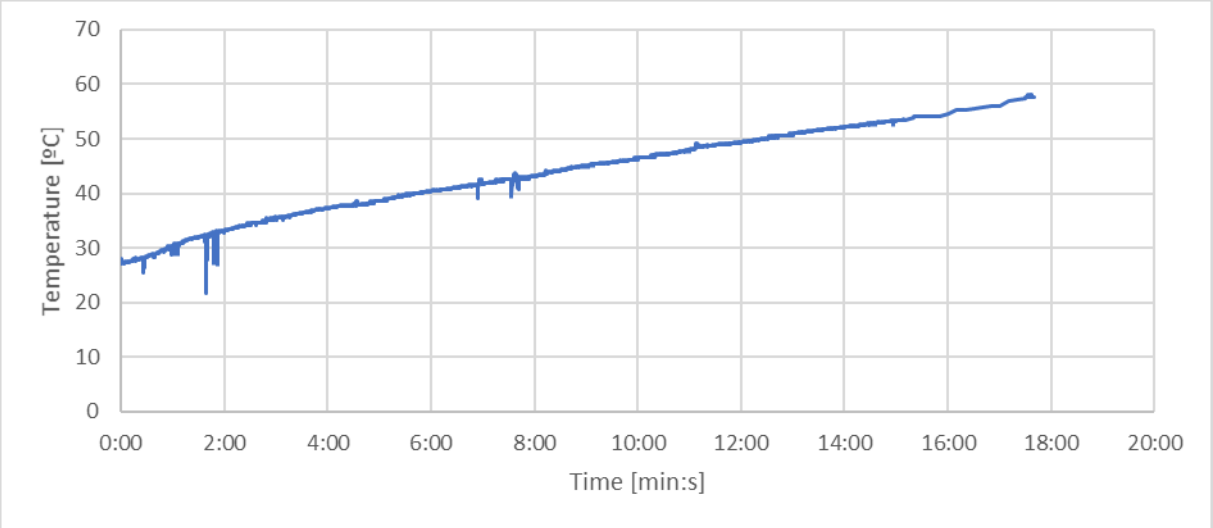

Figure 59 - Temperature measurement for tool heated with two soldering irons.

The heat gun was able to heat up the tool to 150 ºC in about 16 minutes and 30 seconds, making it a more viable option, compared to the soldering irons, for heating the tool body. Figure 60 shows the temperature measurement taken while heating the tool with a heat gun.

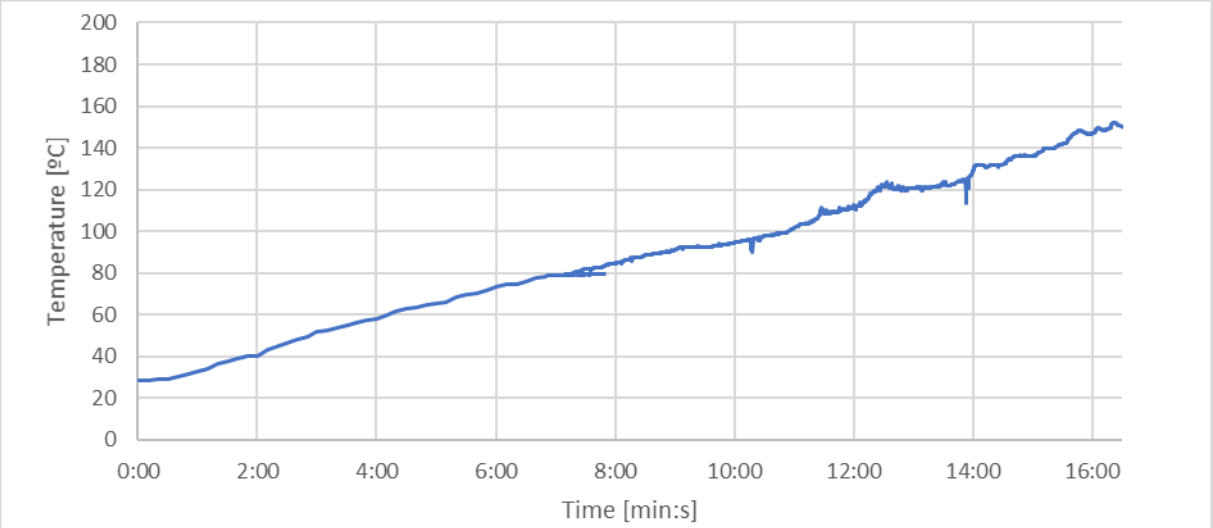

Figure 60 - Temperature measurement for tool heat with heat gun

Figure 61 Compares the different heating methods and makes it visible that the fastest way to heat the copper sleeve, which is where the thermocouple is located, is using friction, the second-best option is the utilization of the heat gun and the worst option is to use soldering irons to heat the tool.

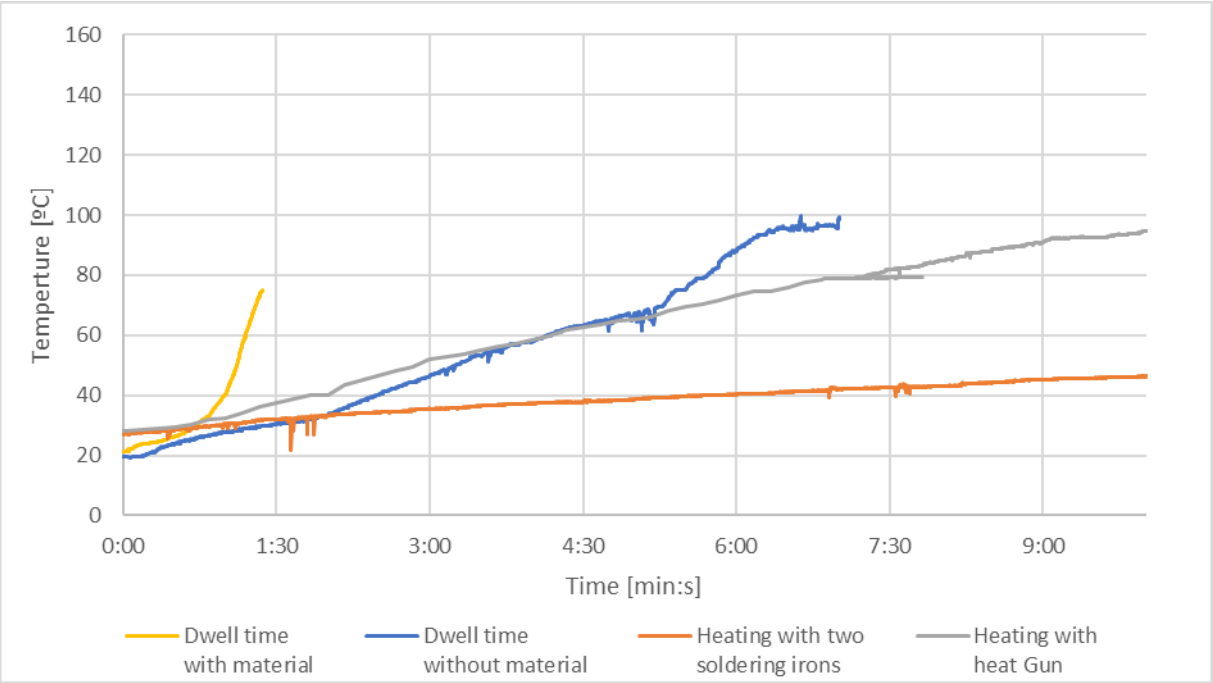

Figure 61 - Temperature measurement for different heating procedures of the welding tool.

Dwelling with the material, PA6 GF30, was the fastest way to heat up the copper sleeve of the tool since the material being welded has a low heat conductivity and the axial force used was higher than when doing the dwelling without the material.

Preheating the shoulder and the sleeve to 150 ºC

In order to make it easier for the machine to weld the composite PA6 30GF without failing, the welding tool was heated before welding and the electric motor of the welding machines was cooled using compressed air.

The static shoulder and the copper sleeve were heated using a heat gun with 2000 W of power.

Welds were performed using the parameter present in Table 15. The tool was preheated to a temperature of around 150 ºC, but at the start of the welding it had cooled down to around 135 ºC. This is due to the time that took to mount the tool in the spindle of the machine.

Table 15 - Welding parameters for hybrid tool preheated to 150 ºC.

Rotating speed [RPM]	Traversing speed [mm/min]	Axial force [N]	Dwell Time [s]	Pre heated temperature [ºC]
2500	30	400	5	150

The welding, Figure 62, presented gaps due to insufficient fixing of the plates. The welded area is where the rotating shoulder was in contact with the material. The sleeve effect was very faint, leaving only superficial marks on the material, an interesting observation is that the width of the sleeve zone is not equal to copper sleeve of the tool, but equal to the width of the steel shoulder, meaning that for this usage the difference in thermal conductivity between steel and copper is not enough to isolate the copper sleeve.

The lack of sleeve effect results in a visible defect on the retreating side of weld. If there was significant sleeve effect, the transition between the welded material and the base material would be smoother.

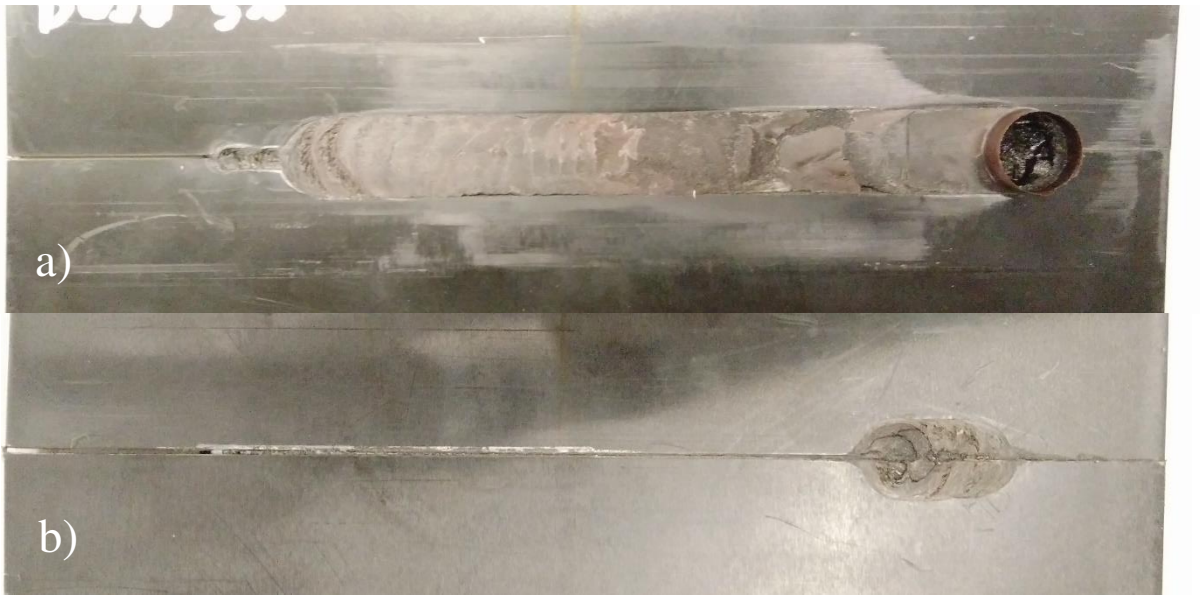

Figure 62 - Weld from hybrid tool preheated to 150 ºC, a) top view, b) bottom view.

In the bottom view of Figure 62 its visible that there's a large stirred zone, that zone is not a defect by the weld, but a previously failed attempt at welding the plates. The root was not smooth and presented poor surface quality. This is due to the formation of a gap between the plates that, during welding, got filled with stirred material forming a distinct region.

The weld in the middle was smooth, but with a nonuniform appearance with very visible markings left by the rotating shoulder. In Figure 63 it's possible to see a defect reassembling a tunnel in the retreating side of the weld, this defect isn't as large as the one produced by the tool without preheating.

Figure 63 - Middle section of weld produced by hybrid tool preheated to 150 ºC

The weld presented a section in which the surface was rougher than the middle section, as seen in Figure 64 , this may be a result of material sticking to the rotating shoulder. The smoothest and most uniform region was at the very end of the weld under the copper sleeve, when the tool was static. A slower traversing speed, a higher axial force and higher tool temperature may help produce welds with better appearance.

Figure 64 - End section of weld produced by hybrid tool preheated to 150 ºC

At the beginning of the weld, made by the tool preheated to 150 ºC, the temperature of the tool was 135 ºC, and the rotation speed of 2000 rpm was not sufficient to maintain this temperature, as it's visible in Figure 65. This led to the presence of rings in the weld where the rotating shoulder contacted the base material. Increasing the rotation speed to 2500 rpm led to an increase in the tool temperature, which achieved a maximum temperature of 182 ºC. The higher temperatures led to a less noticeable onion ring defect, but the surface of the weld presented lack of material in the weld interface of the retreating side.

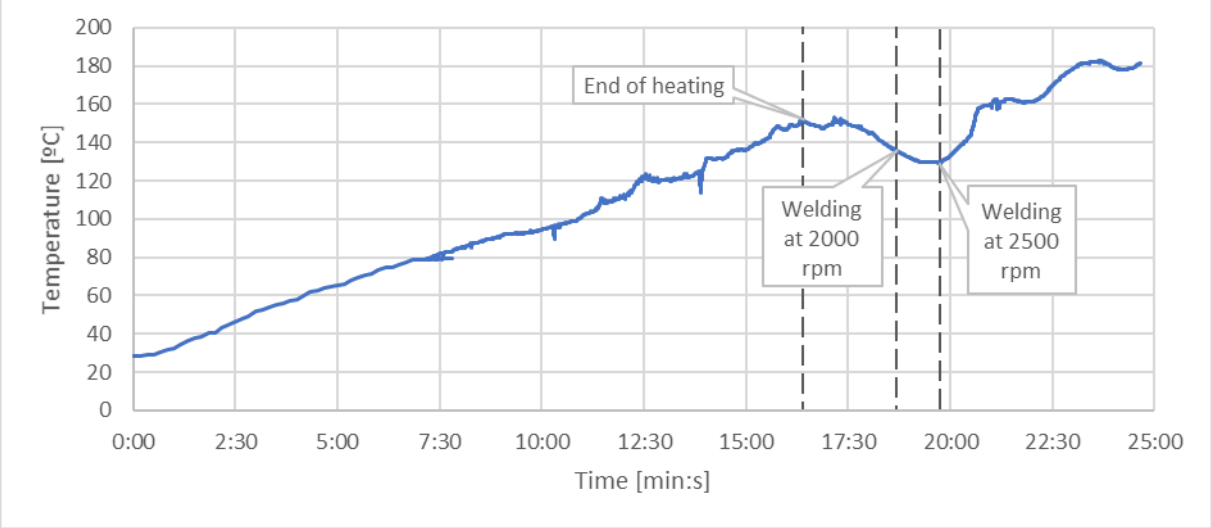

Figure 65 - Temperature of the hybrid tool during heating to 150 ºC and welding.

The forces recorded during welding are displayed in Figure 66. It's visible that there are some abrupt changes in the axial force at the beginning of the weld, this is due the plates movement during the weld. In the middle of the weld the axial force remained around 445 N, which is close to the pre force defined during setup, but in the extremes of the weld the force was higher due to higher rigidity of the backplate in its extremes than in its middle.

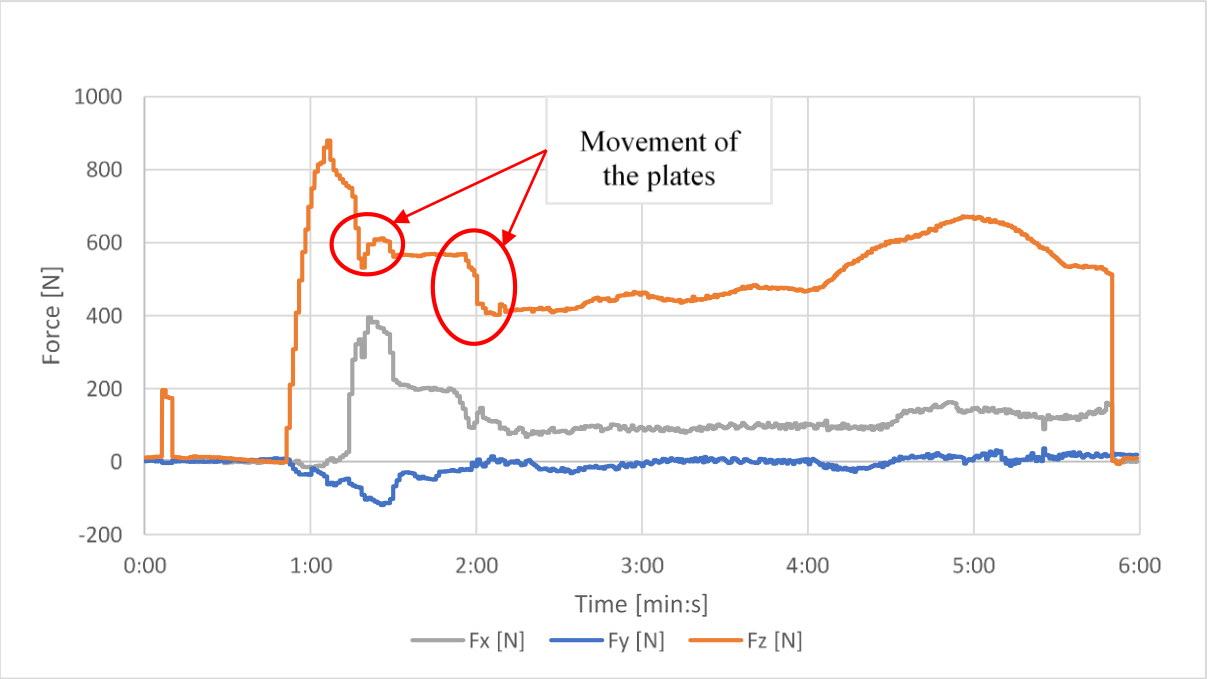

Figure 66 - Force measured during welding using hybrid tool preheated to 150 ºC

Preheating the shoulder and sleeve to 270 ºC with slightly protruding sleeve

In this test, the copper sleeve was protruded around 0.4 mm relative to shoulder. This was made to reinforce the sleeve effect. The tools were heated using a heat gun.

The parameters used for this weld are the ones present in Table 16. The problem with the protruding sleeve is that it makes it harder to setup the pre force. The pre force applied was of 300 N, but during welding this value was closer to 500 N.

Table 16 - Welding parameters for hybrid tool preheated to 270 ºC with protruding sleeve

Rotating speed [RPM]	Traversing speed [mm/min]	Axial force [N]	Dwell Time [s]	Pre heated temperature [ºC]
2000	30	300	15	270

In Figure 67, it is possible to see that copper sleeve had noticeable effect on the weld. In the middle zone, affected by the rotating shoulder, there are some voids. This weld presented a very rough surface with noticeable steps in the interface of the sleeve and the stationary shoulder as well as in the interface of the sleeve and the rotating shoulder. This is due to the difference in heights of these components.

One particular feature of this test was that at the end of the weld the surface was different. The colour was light grey, and the surface was smoother, but it was only superficial.

Figure 67 - Weld from hybrid tool with protruding sleeve preheated to 270 ºC, a) top view, b) bottom view

The bottom of the weld is presented in Figure 67. The root was not properly welded.

The temperature measurements can be seen in Figure 68 . Using the heat gun, the tool took 21 minutes and 13 seconds to heat up to 270 ºC and at the beginning of the weld it had cooled down to around 217 ºC. While welding the tool's temperature stabilized around 215 ºC, which is very close to the 222 ºC melting point of the base material.

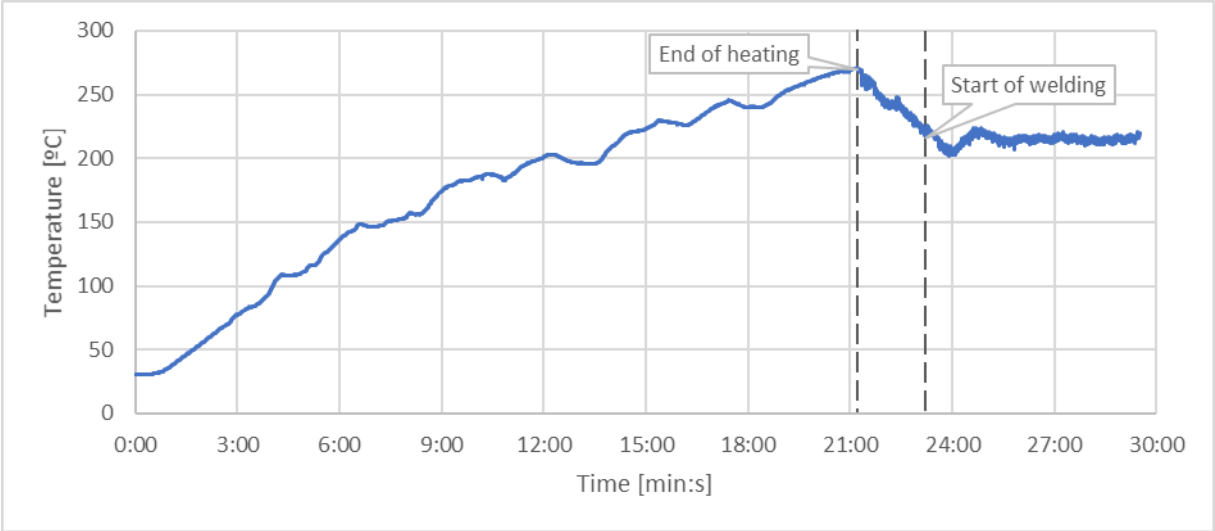

Figure 68 - Temperature of the hybrid tool with protruding sleeve during heating to 270 ºC and welding

The weld had a duration of around 6 minutes and at the around 1 minute and 20 seconds there was some movement between the plates, this is visible in Figure 69. The axial force during the weld was around 512 N, and the force in traversing direction had a maximum of 70 N, which is much lower than welds made without preheating or with preheating at lower temperatures.

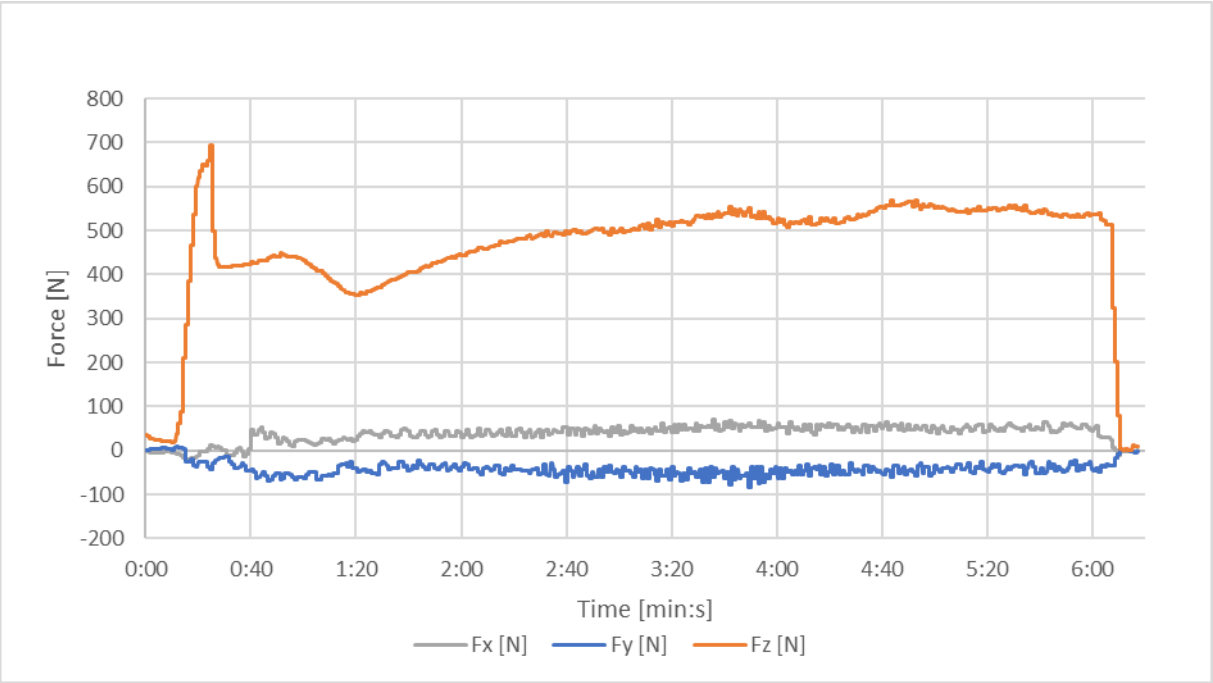

Figure 69 - Forces measured during welding using hybrid tool with protruding sleeve preheated to 270 ºC

Preheating the shoulder and sleeve to 269ºC

In this test, the stationary shoulder and the sleeve were heated to 269 ºC. The sleeve was aligned with the stationary shoulder.

The parameters used are present in Table 17.

Table 17 - Welding parameters for hybrid tool preheated to 269 ºC

Rotating speed [RPM]	Traversing speed [mm/min]	Axial force [N]	Dwell Time [s]	Pre heated temperature [ºC]
2000	20	400	15	269

The surface obtained from this weld was rough like the weld with the protruding sleeve, as it can be seen in Figure 70, but this weld was more uniform and with less voids in the zone of contact of the rotating shoulder. There was a small amount of flash in the edges of the weld, and the sleeve effected zone was not the width of the sleeve, but the width of the static shoulder. The biggest problem with the weld is the surface roughness due to the composite material sticking to the base of the tool, visible in Figure 71.

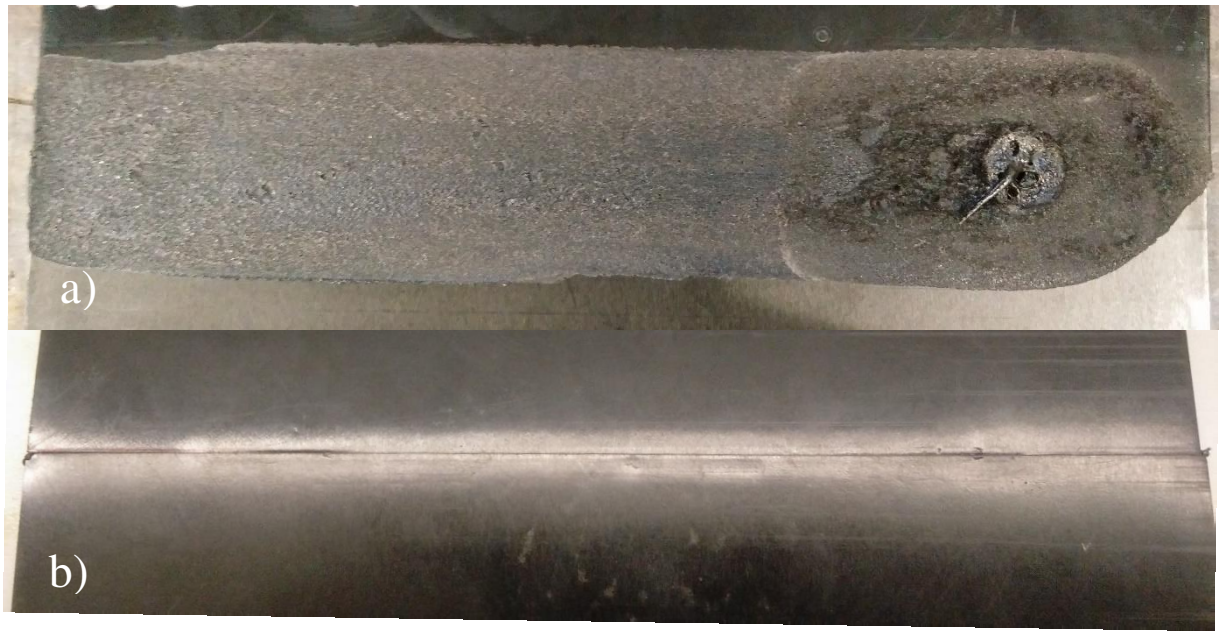

Figure 70 - Weld from hybrid tool preheated to 269 ºC, a) top view, b) bottom view.

Figure 71 - Weld material stuck to the bottom of the welding tool

The root of the weld presented no big gaps and was better than the test with the protruding sleeve, but the plates were not welded in the root. Looking from the bottom, the plates edges are discernible, giving the appearance that the plates are simply pressed together, not welded.

Due to a problem with the text file were the temperatures where being recorded, Figure 72 only presents a few points which were registered by hand, as a result the data does not translate well the tool's temperature behaviour during welding.

The tool was preheated to a temperature of 269 ºC, but at the start of the weld the temperature was of 216 ºC. The weld had a duration of around 9 minutes and the weld temperature was around 206 ºC. It is visible in Figure 72 that at the end of the weld, the temperature was decreasing.

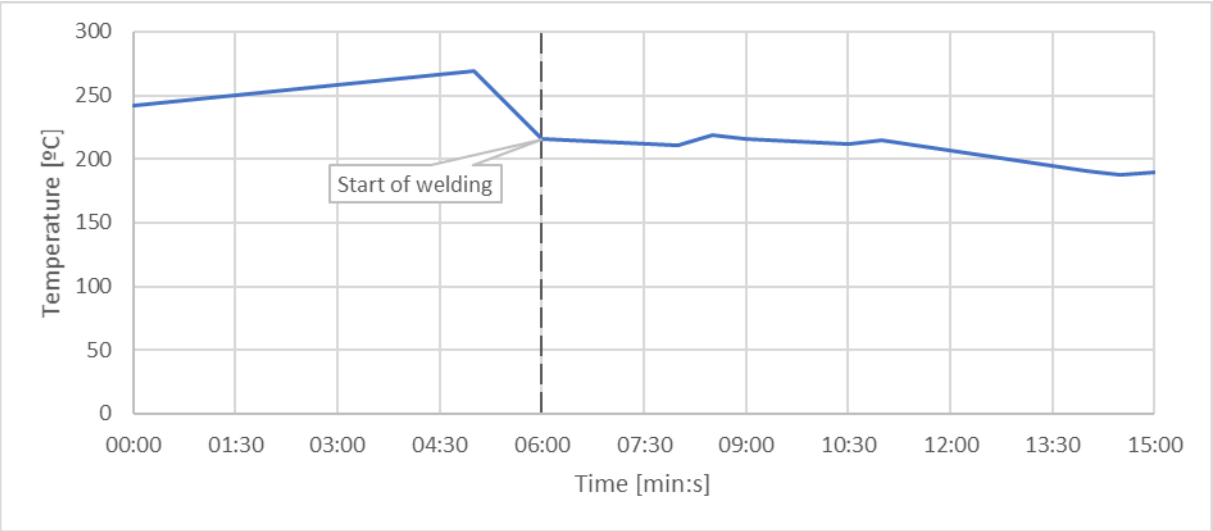

Figure 72 - Temperature of the hybrid tool during welding.

By analysing the forces during welding presented in Figure 73, it's possible to see that there were no abrupt changes in the axial force, which means that the plates didn't move. The axial force was about 580 N during welding, even though the setup was made for 400 N axial force. The axial force increased as the weld progressed, this may be to the cooling of the stationary shoulder. The traversing force was small having a maximum value of 55 N, and with average magnitude of values similar to the lateral force.

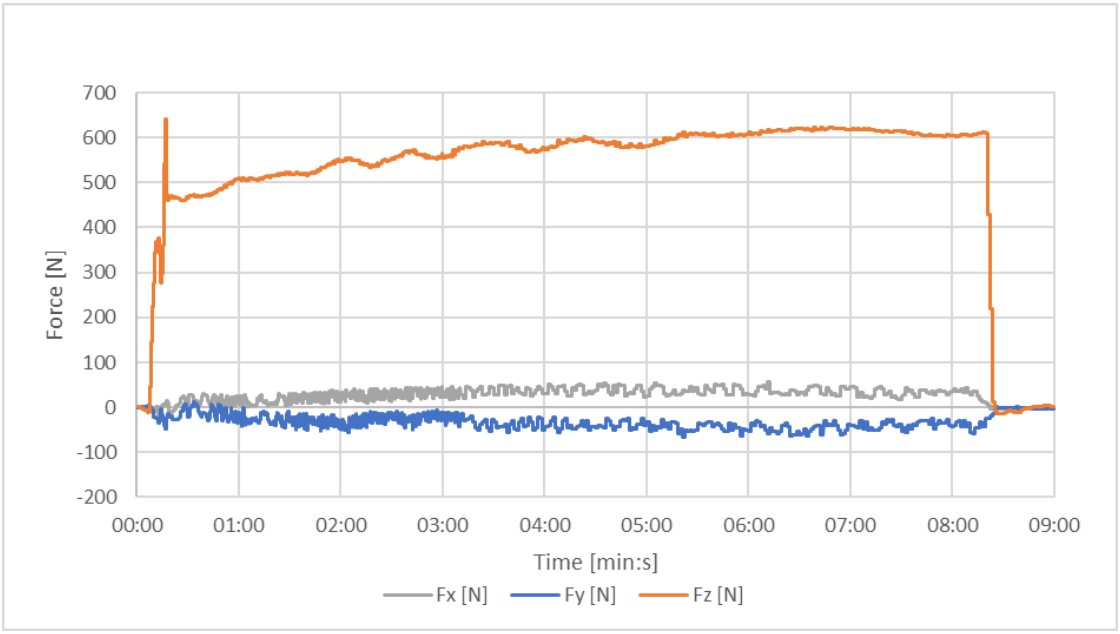

Figure 73 - Forces measured during welding using hybrid tool preheated to 269 ºC

The plate was cut into 5 specimens with dimensions according to ASTM D638 - 14 Type I specimens. The tensile tests were performed with a crosshead speed of 2 mm/min and an extensometer. The results are presented in Table 18.

Table 18 - Ultimate tensile strength obtained from hybrid tool heated to 269ºC

	H1	H2	H3	H4	H5	Average	Standard Deviation
UTS [MPa]	80,8	80,6	69,6	88,2	86,2	81,08	7,23

Specimen H3, which failed from the retreating side of the weld, was the most brittle specimen with a true strain at break of 1.29%. The other specimens were subjected to plastic deformation before breaking. Specimens H5, which broke from the advancing side in the base material had the highest true strain at break with a value of 2.63%. Specimens H4 had the highest true tensile strength with a value of 90.1 MPa but a lower strain at break than specimen H5. Specimens H4 broke in the middle of the weld and on the retreating side of the weld. This is shown in Figure 74.

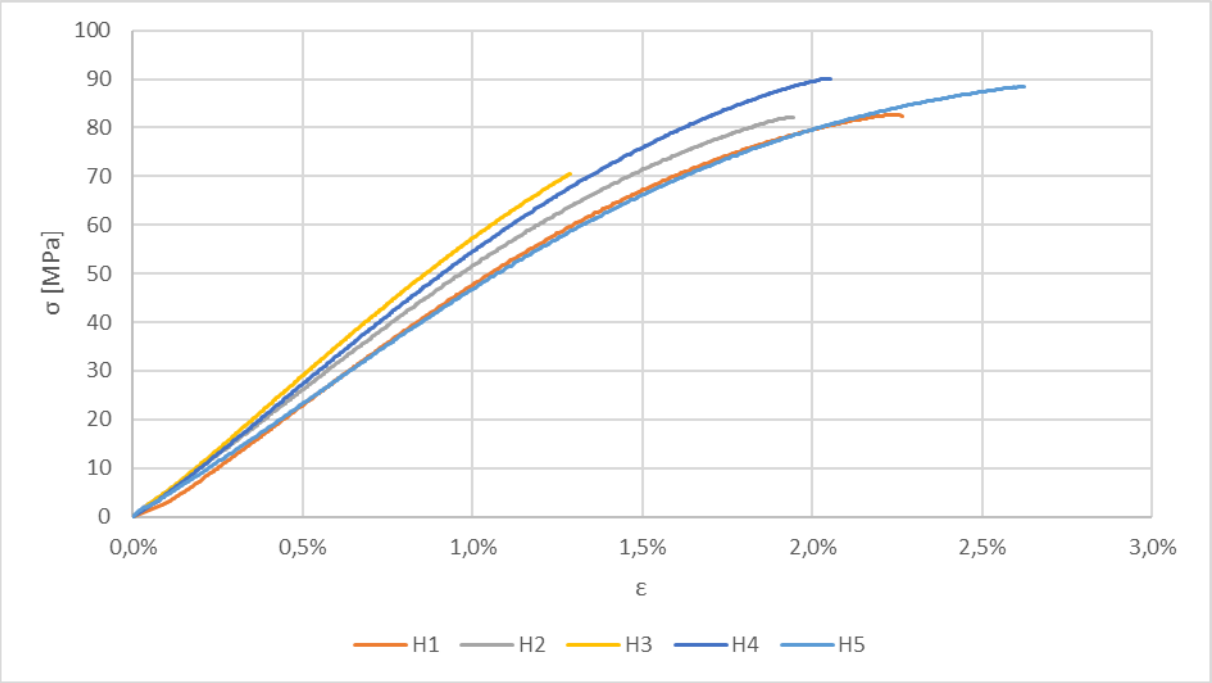

Figure 74 - True stress-strain curves of specimens H1 to H5

Specimen H4 presented the highest tensile strength with a joint efficiency of 58.7%. The weld broke in the middle and the retreating side, visible in Figure 75.

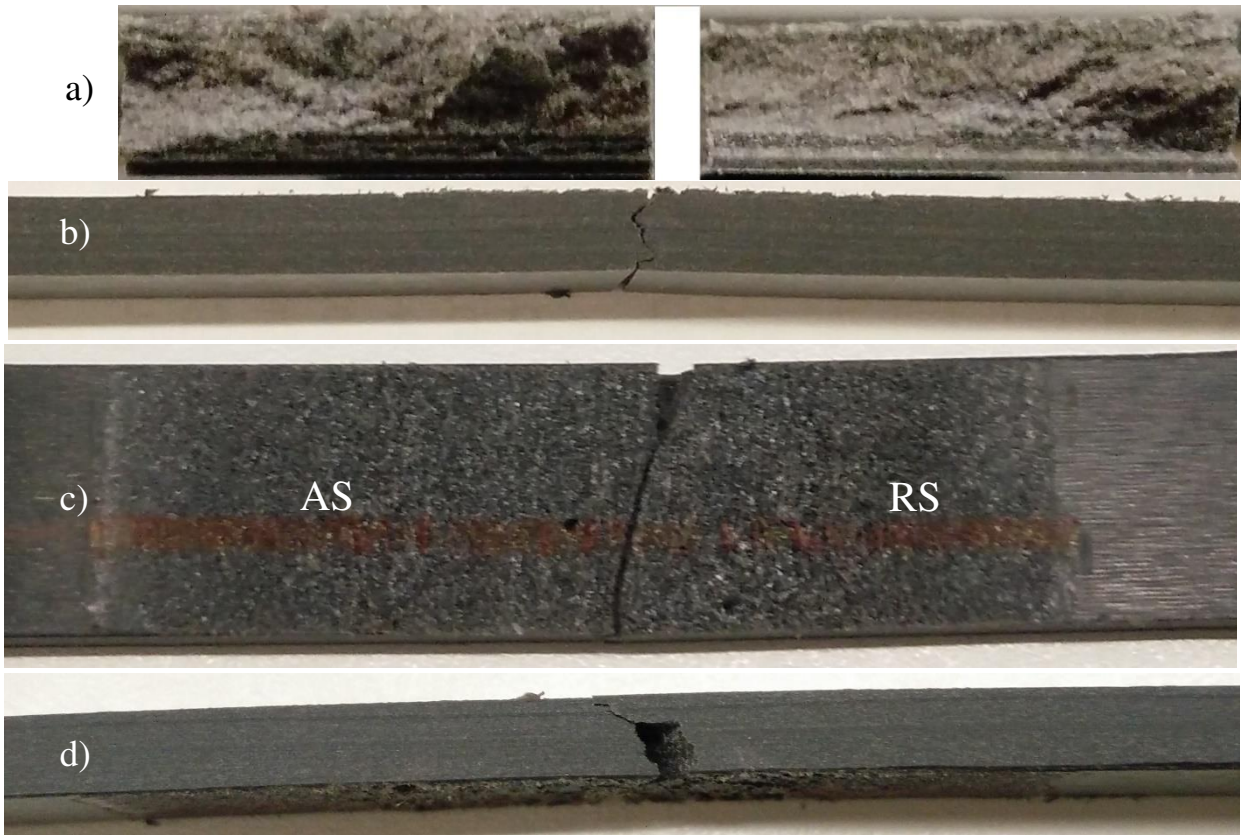

Figure 75 - Specimens H4 a) fractured section, b) front view, c) top view and d) back view

The weld can be improved since specimen H4 presented a very pronounced root defect, Figure 76.

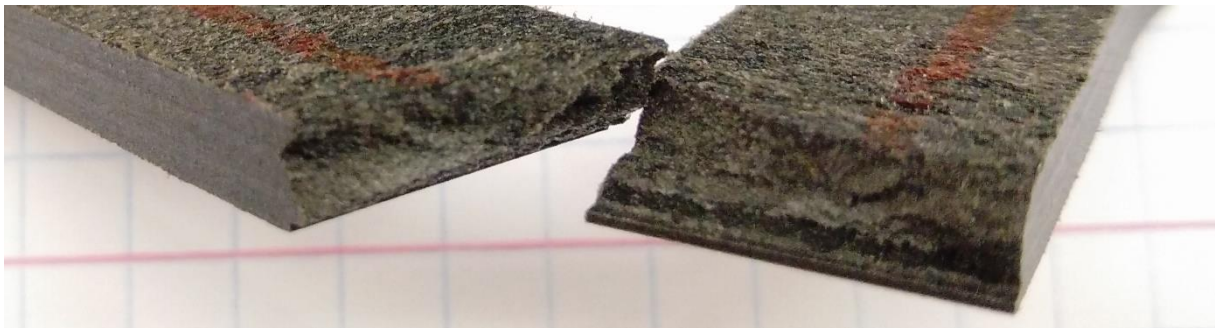

Figure 76 - Root defect of specimen H4.

Specimen H3 had the lowest tensile strength. and broke outside the weld zone on the retreating side. The reason that this specimen does not appear to have root defect is due to the fracture occurring outside the weld line. The fracture may be a result of a surface defect.

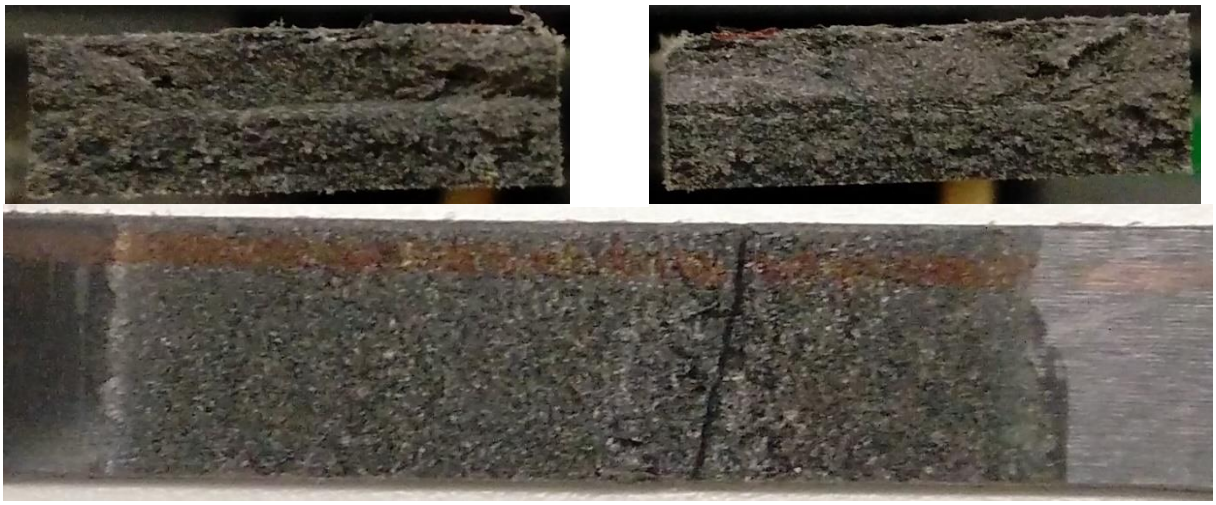

Figure 77 - Broken specimen H3 on the advancing side (left) and on the retreating side (right).

The fractures of all five specimens from the top and bottom can be seen in Figure 78. Specimens H1, H2, H4 have a noticeable root defect and from the bottom view its visible that it broke in the interface between the plates. Specimens H3 and H5 broke outside the weld zone and from the bottom view its visible that the fracture did not occur in the interface between the plates.

Specimen H5 was the only one that fractures in the advancing side, but since it was outside the weld zone it may be a result of a surface defect.

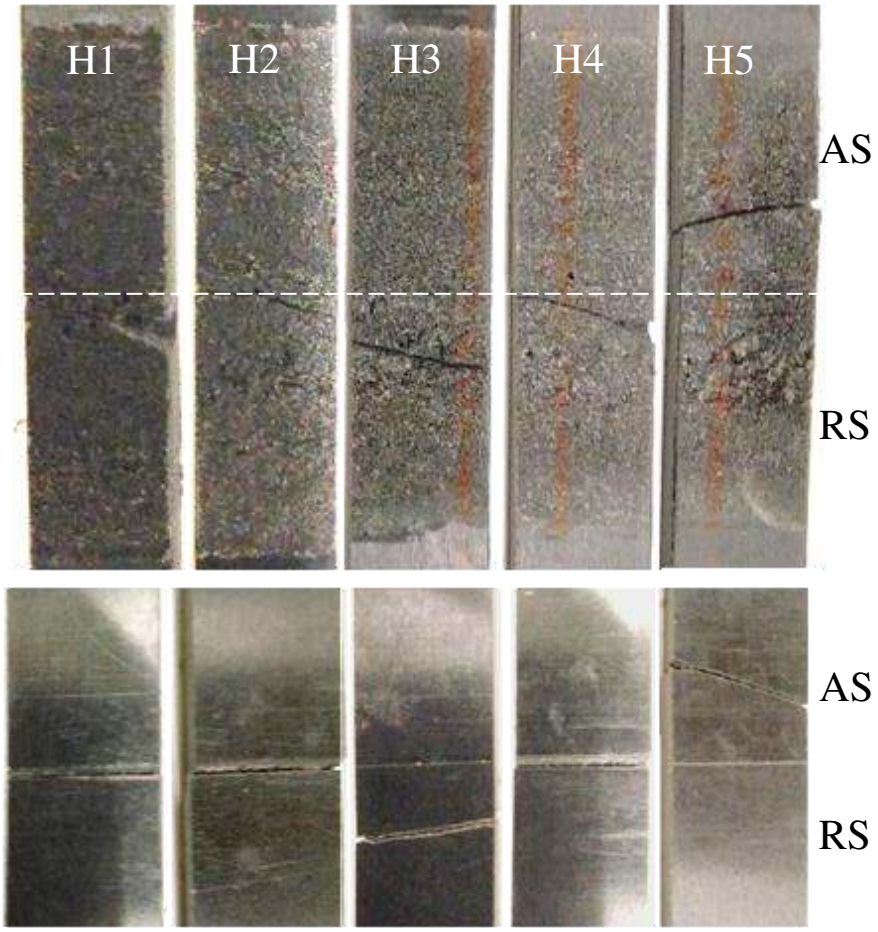

Figure 78 - Fractured specimens H1 to H5 top view (left) and bottom view (right).

5.2 Welding with a PEEK stationary shoulder tool

Using the PEEK stationary shoulder tool designed to weld polymers, the following results were obtained. An advantage of using this combination of tool design and weld material is that it is less demanding for the welding machine and the tool is easier to use, which makes it possible to test a wide range of parameters for optimization.

First attempt welding with PEEK stationary shoulder.

For the first attempt at using this tool to weld the PA6 GF30 composite, the parameters used were the ones present in Table 19.

Table 19 - Welding parameters for PEEK stationary shoulder tool, first attempt

Rotating speed [RPM]	Traversing speed [mm/min]	Axial force [N]	Dwell Time [s]
2800	20	600	30

The weld was very smooth, with no harsh transition or flash between the weld and the base material, as shown in Figure 79, it is also possible to see the sleeve effect in the weld. The surface of the weld presented some voids, this may be due to the wear of the tool. This tool design is much more suitable for welding thermoplastic composites.

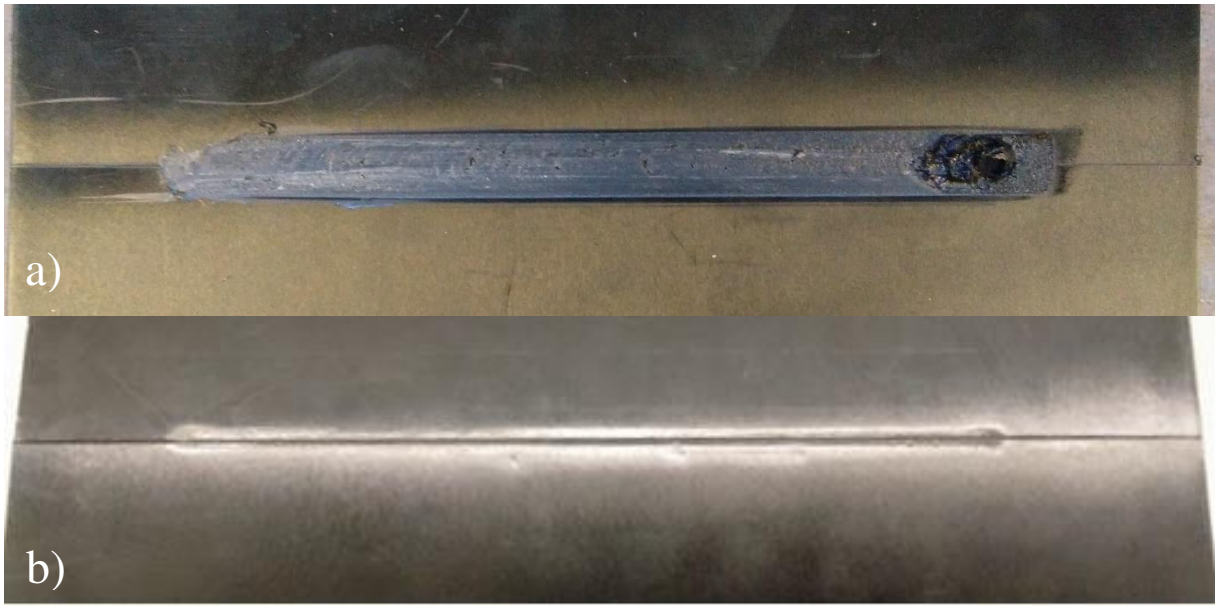

Figure 79 - Weld from PEEK stationary tool first attempt, a) top view, b) bottom view.

The root of the weld was welded and had no gaps. This was one of the better welds in terms of appearance from the top and from the bottom view, although the root of the weld could be smoother

The weld had a duration of approximately 10 minutes and the tool's sleeve was capable to heat up to 212 ºC. The average welding temperature was 201 ºC. Figure 80 shows the temperatures during welding.

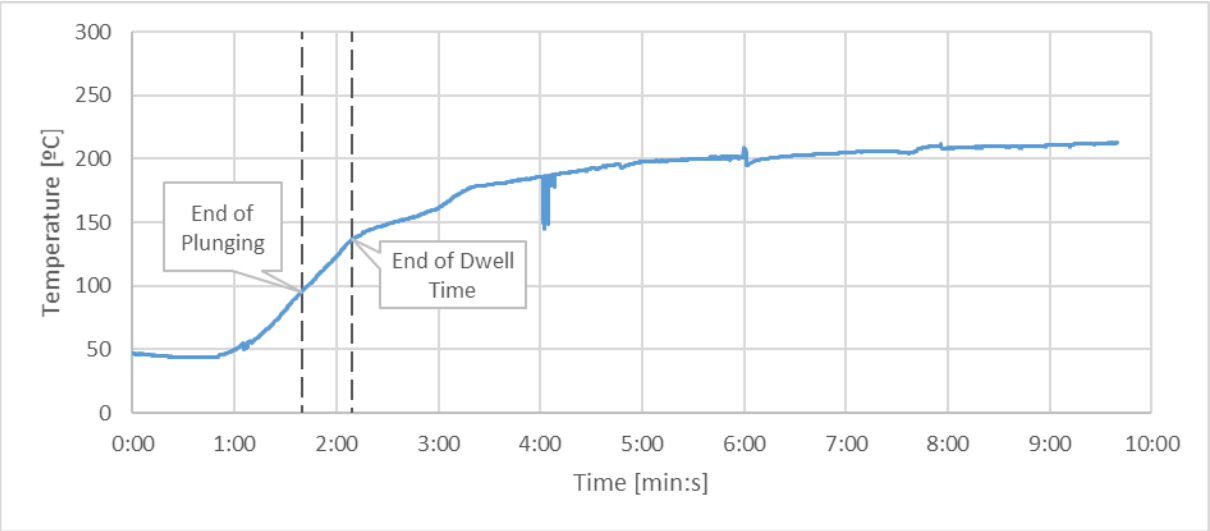

Figure 80 - Temperature of the PEEK stationary shoulder tool during welding

In terms of forces, the setup was made for an axial force of 600 N, but, as shown in Figure 81, the axial force behaviour is erratic. During dwelling and in the beginning of the weld it is visible some spikes in force. Between the 2 and 5 minutes the axial force stabilized around 490 N, but around the 6 minute the axial force spiked and stayed stable around 700 N. This behaviour hasn't been seen before, this may be because of difference of contact pressure along the edge of the plates, difference of fibre concentration of the composite along the weld bead, differences in contact with the side wall or due to the wear of the tool.

The traversing force had a maximum value of 137 N, having an average value of 114 N. This value is not as low as the ones obtained with the heated tool.

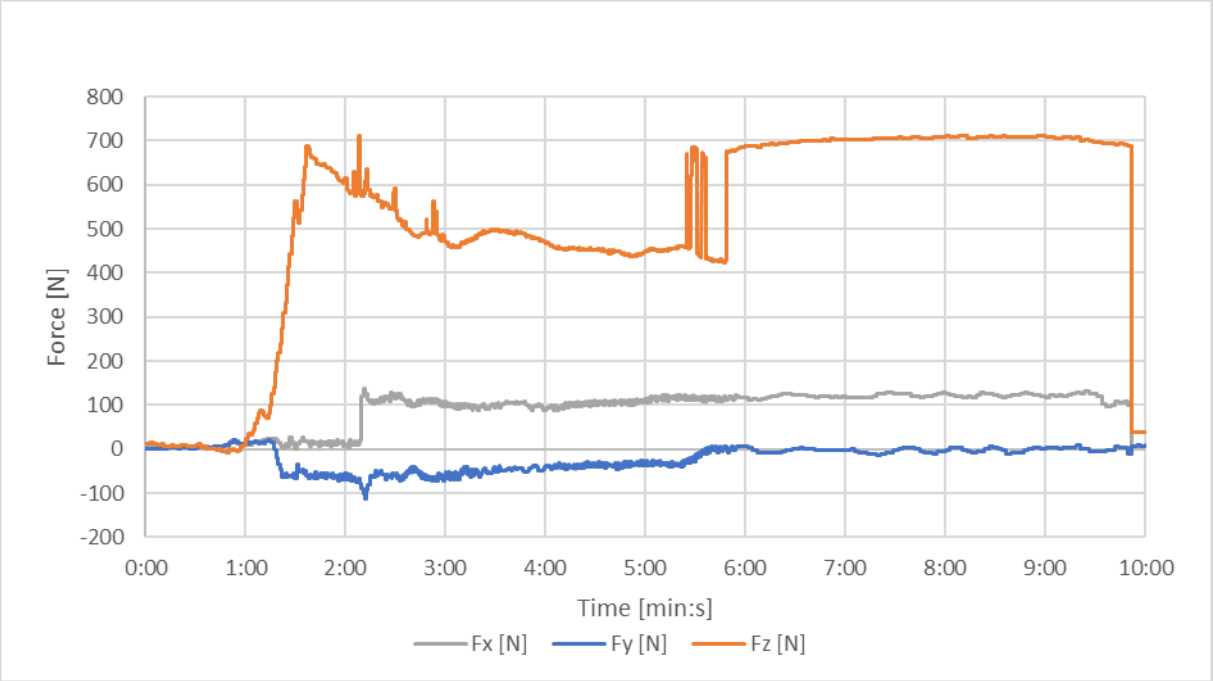

Figure 81 - Forces measured during welding using PEEK stationary tool.

Second attempt welding with PEEK stationary tool

For the second attempt at using this tool to weld the PA6 GF30 composite, the parameters used were the ones present in Table 20. The rotation speed was lowered, but the axial force and dwell time were increased.

Table 20 - Welding parameters for PEEK stationary shoulder tool, second attempt.

Rotating speed [RPM]	Traversing speed [mm/min]	Axial force [N]	Dwell Time [s]
2500	20	800	40

The weld presented a good weld surface, but still with room for improvement. The surface had less voids than the first attempt, but it in the zone stirred by the pin the surface was rougher.

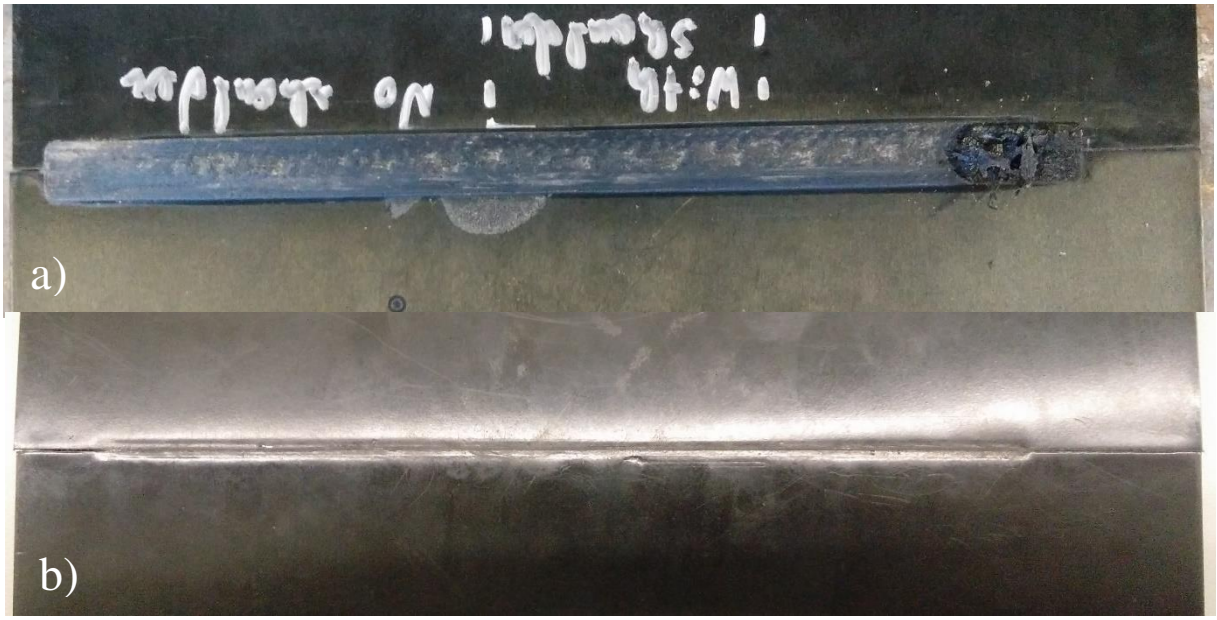

Figure 82 - Weld from PEEK stationary tool second attempt, a) top view, b) bottom view.

The root from this weld was the best, it was welded and the transition between the plates was the smoothest. This is mainly a result from the increase of axial force during welding.

The temperatures during welding can be seen in Figure 83. The maximum temperature measured was of 209 ºC and the average temperature during welding was of 180 ºC.

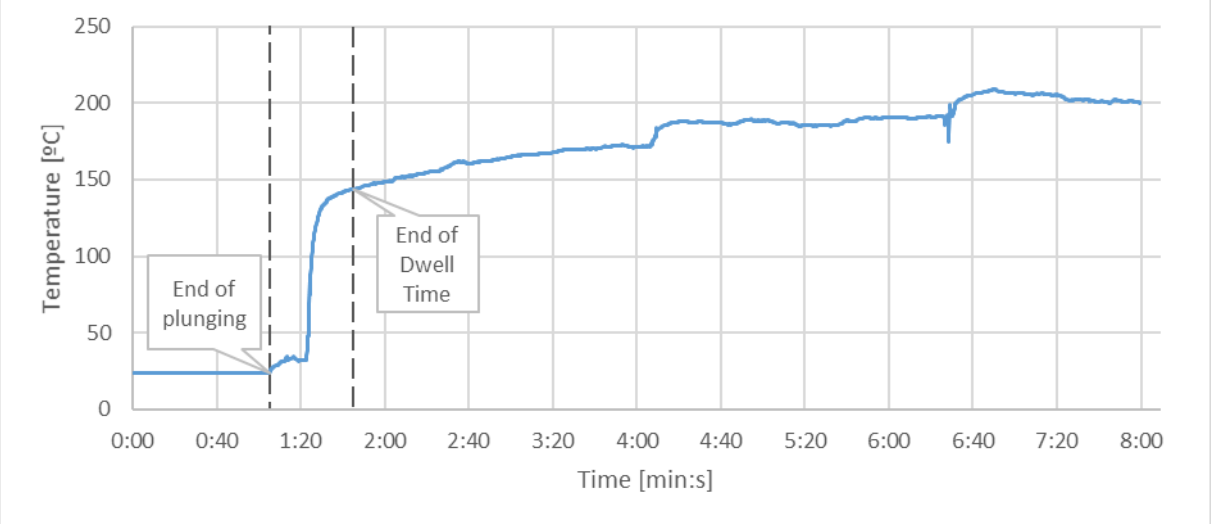

Figure 83 - Temperature of the PEEK stationary shoulder tool during welding, second attempt.

This test exhibited the same erratic behaviour as the first attempt. In this case between the 1:20 and the 2:15 time, the axial force stabilized around 1000 N, between the 2:15 and the 4:10 time, the axial force abruptly fluctuated between 1000 N and 650 N and after the 4:10 mark the axial force stabilized around 1100 N, has can be seen in Figure 84.

The traversing force had a maximum value of 230 N, with an average value during welding of 191 N.

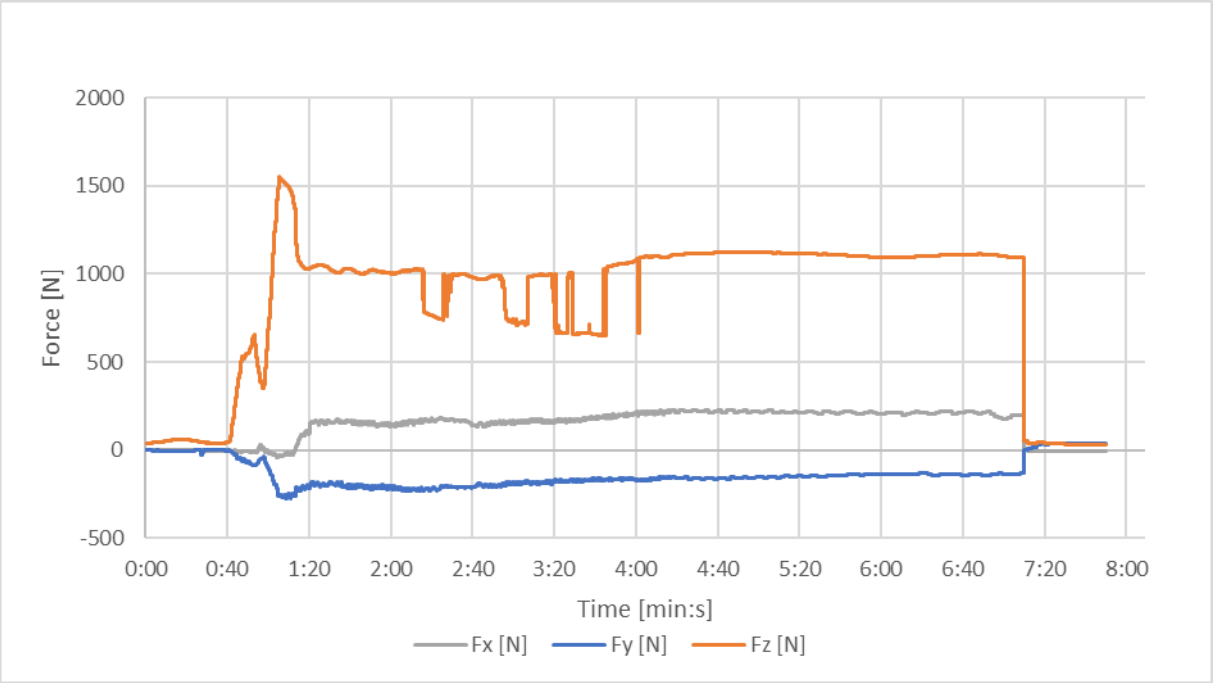

Figure 84 - Forces measured during welding using PEEK stationary tool, second attempt.

5.3 Design of Experiment

The experimental results obtained from the Taguchi design of experiment regarding the ultimate tensile strength and maximum load are shown in Table 21 and Table 22 respectively.

Table 21 - Ultimate tensile strength obtained from tensile tests

	Rotation speed [rpm]	Traversing speed [mm/min]	Axial force [N]	Trial [MPa]				
				1	2	3	4	5
S1	2000	20	800	32,0	43,2	43,7	44,6	50,5
S2	2000	40	1000	58,0	58,5	63,2	63,7	58,2
S3	2800	20	1000	44,0	54,2	54,6	56,1	57,9
S4	2800	40	800	59,5	61,7	60,3	64,1	63,4

Table 22 - Maximum load obtained from tensile tests

	Rotation speed [rpm]	Traversing speed [rpm]	Axial force [rpm]	Trial [N]				
				1	2	3	4	5
S1	2000	20	800	3223	4587	4444	4540	5141
S2	2000	40	1000	6037	6102	6432	6416	5827
S3	2800	20	1000	4469	5409	5439	5582	5746
S4	2800	40	800	5859	6145	6021	6371	6427

The load displacement curves are shown from Figure 85 to Figure 89 . The displacements correspond to the dislocation of the machine actuator. All the fractures were brittle in the retreating side of the weld.

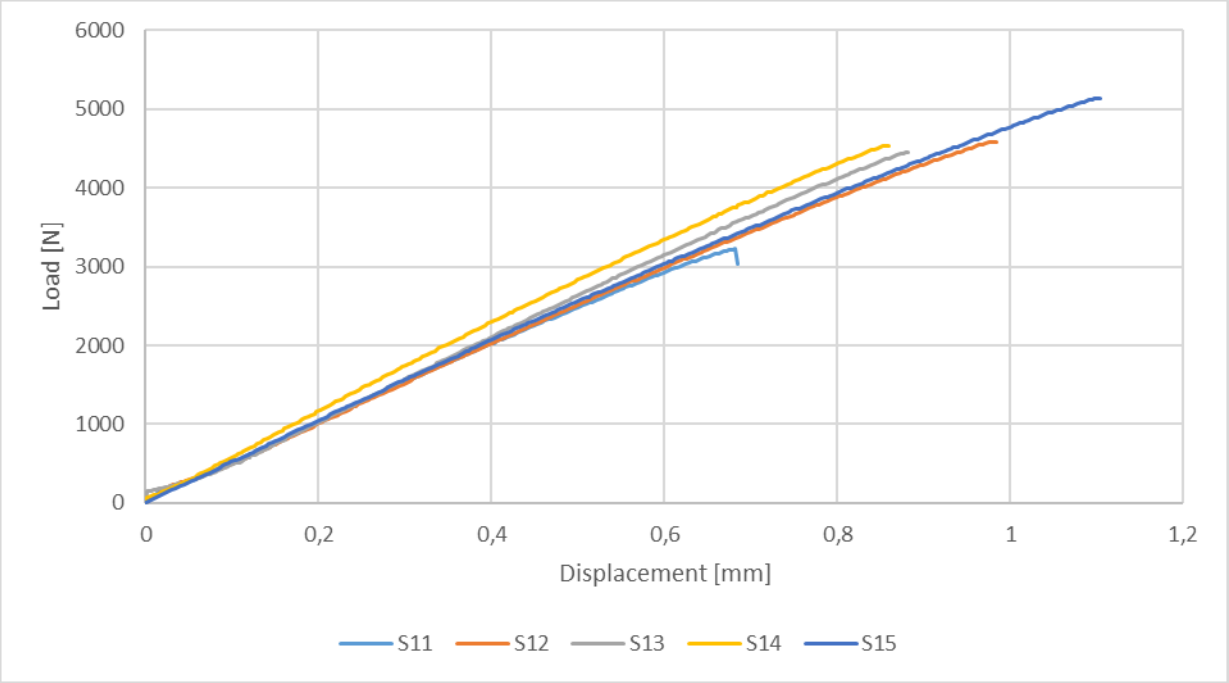

Figure 85 - Load displacement curve for specimens S11 to S15

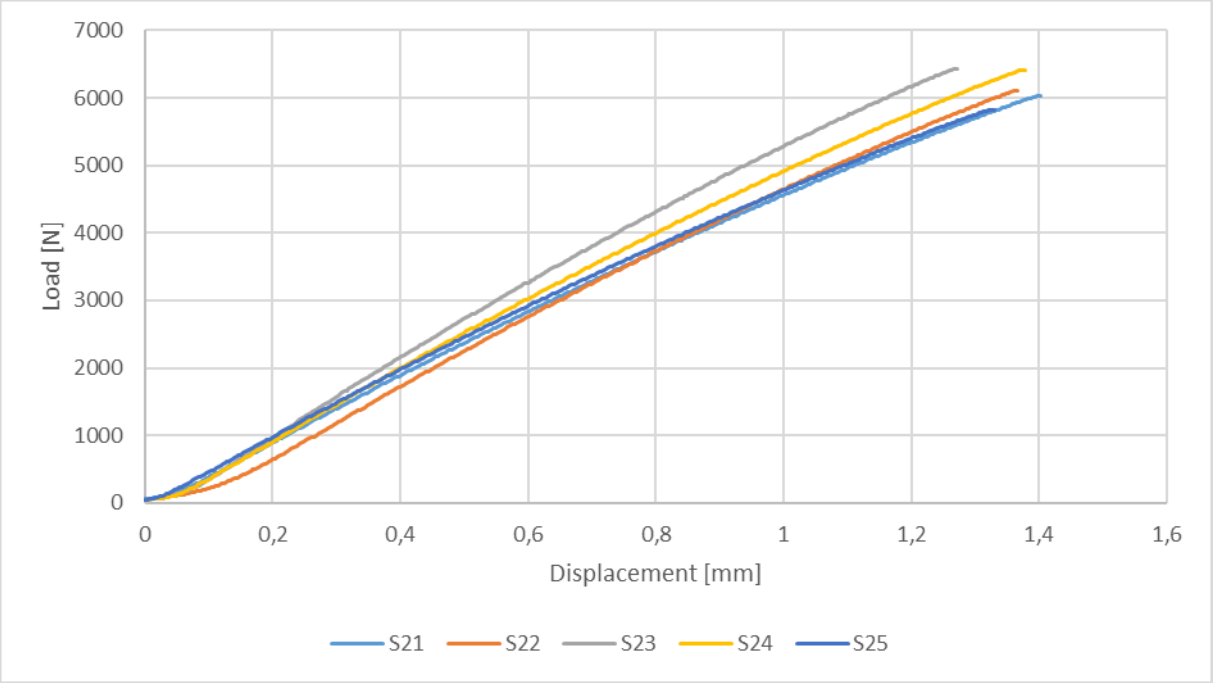

Figure 86 - Load displacement curves for specimens S21 to S25

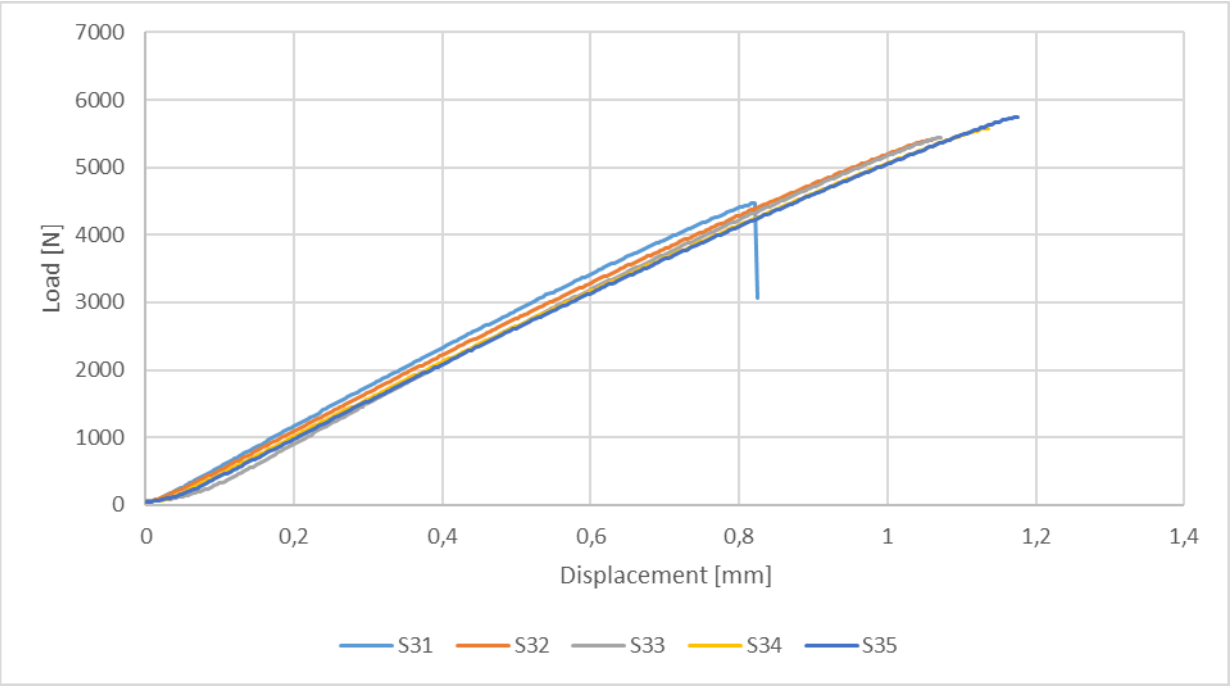

Figure 87 - Load displacement curve for specimens S31 to S35

In Figure 88 it's possible to observe that specimen S43 has a different curve shape. This is due to slippage between the specimens and the grips, because of that the displacements are not accurate for this sample.

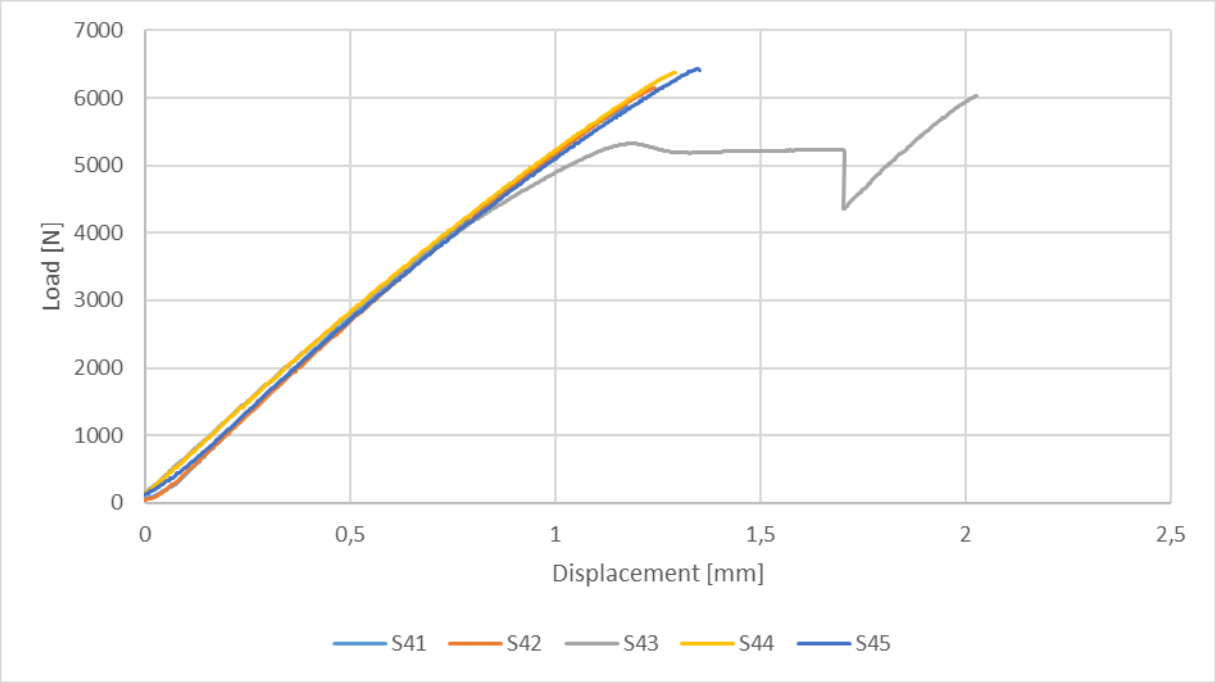

Figure 88 - Load displacement curve for specimens S41 to S45

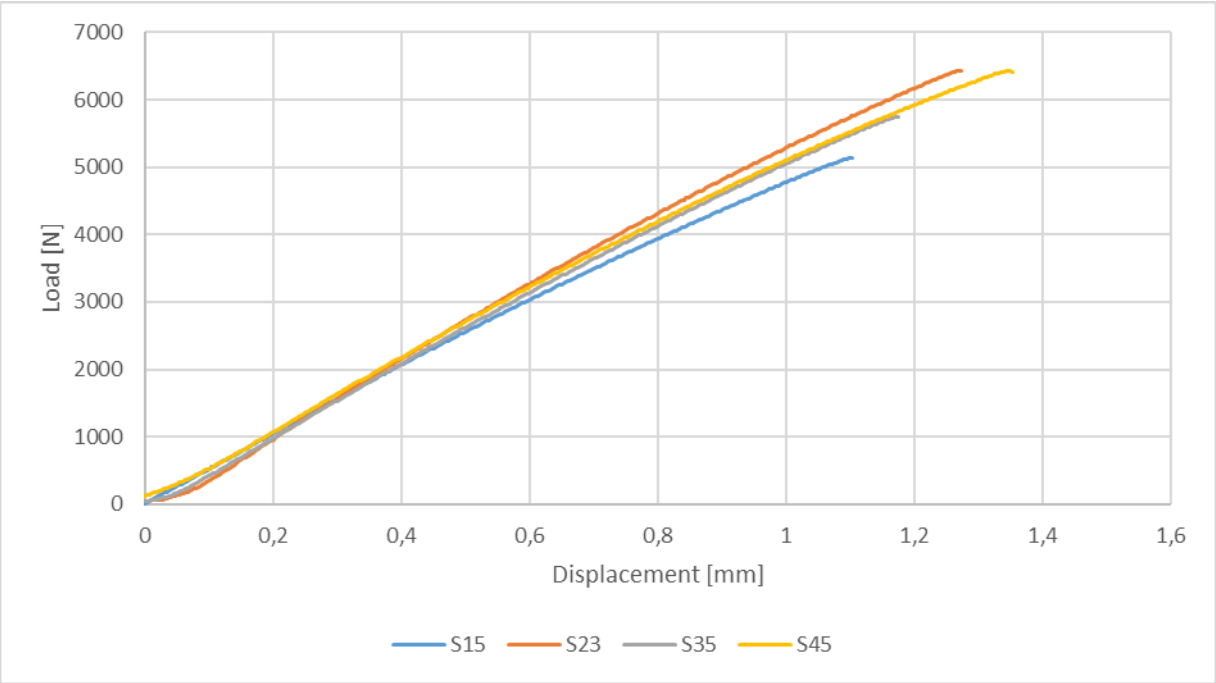

Figure 89 - Load displacement curve for the highest load of each treatment condition

5.3.1 Analyses of results

The analysis of variance is presented in Table 23 and was applied with a significance level of 5%, meaning that parameters with p-values lower than 0.05 have a statistical significance. The signal to noise ratio was calculated using the larger the better formulation with assistance of Minitab software.

Table 23 - Analysis of variance for UTS

Analysis of Variance						
	DF	Adj SS	Adj MS	F-Value	P-Value	contribution percentage
Rotation speed	1	181	180,96	8,35	0,011	12%
Traversing speed	1	840,5	840,49	38,77	0	57%
Axial force	1	102,9	102,94	4,75	0,045	7%
Error	16	346,9	21,68			24%
Total	19	1471,2				

All the parameters were significant to the weld strength, but the most significant one was the traversing speed, as can be seen in Table 23, Figure 90 and Figure 91. The high error is a result of uncontrollable factors, such as tool wear, differences in fixation of the plates and the fact the temperature is not constant during welding. Specimens cut from the beginning of the plate were welded at lower temperatures and specimens cut from the end of the plate were welded at higher temperatures.

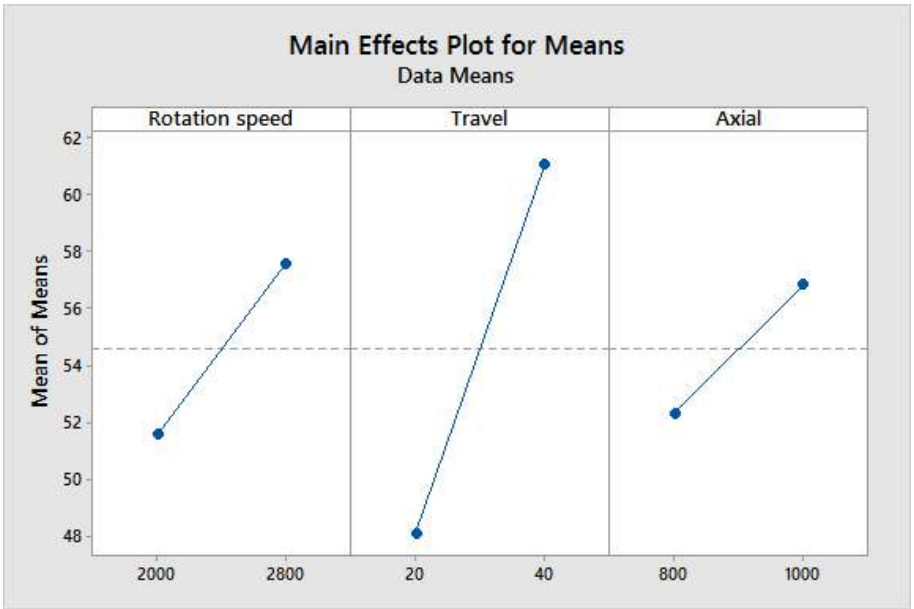

Figure 90 - Main effects plot for Means

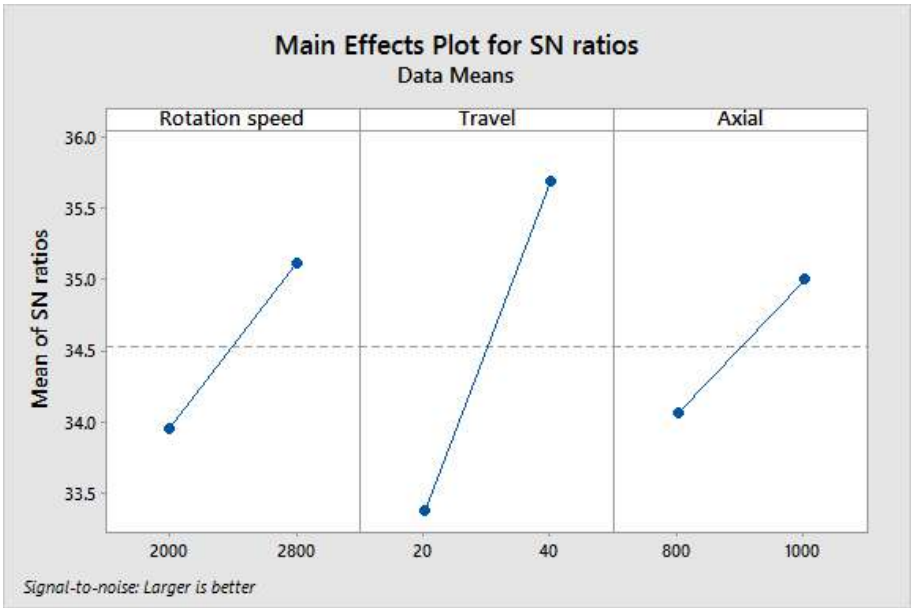

Figure 91 - Main effects plot for SN ratios

The highest load specimen, S23, fractured from the retreating side with a brittle fracture. The weld fracture is shown in Figure 92.

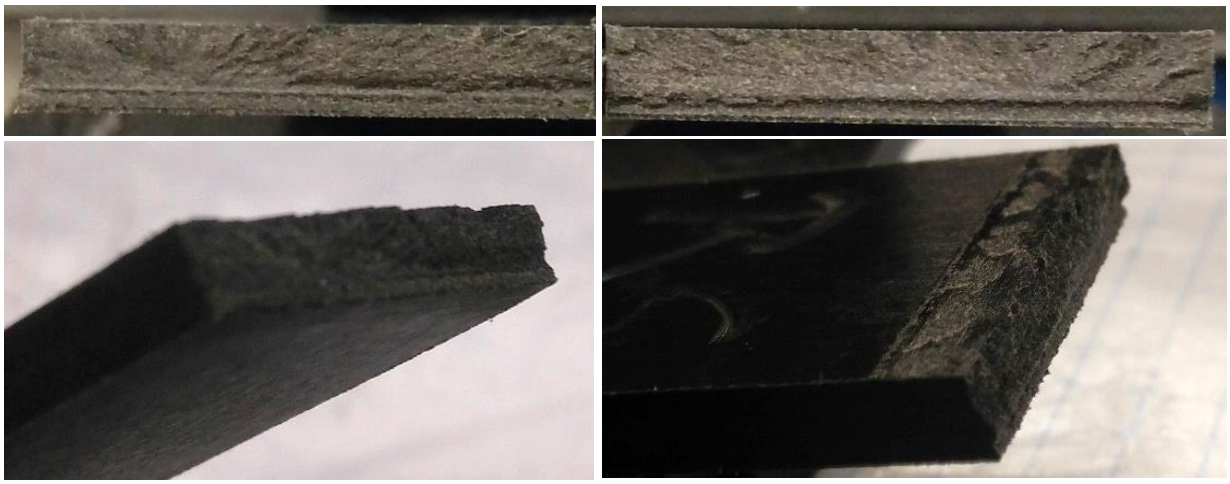

Figure 92 - Fracture of highest load specimen, S23, from the advancing side (left) and the retreating side (right).

The lowest load specimen, fractured on the weld interface of the retreating side and was the only one that in the root the fracture was in the interface where the plates where in contact, meaning the weld did not have enough penetration. The weld fracture is shown in Figure 93.

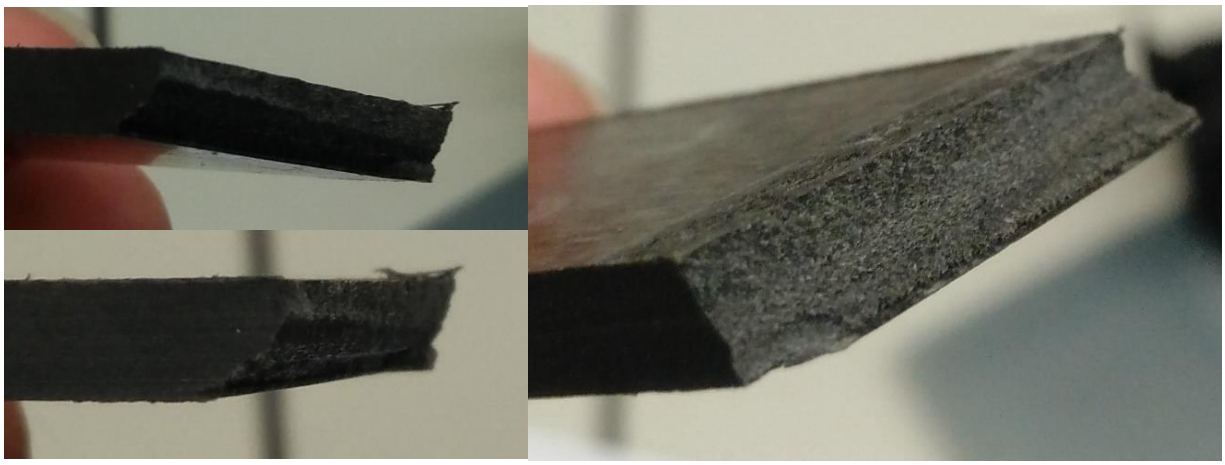

Figure 93 - Fracture of lowest load specimen, S11, from the advancing side (left) and the retreating side (right).

Specimen S11 was the only one that suffered from root defect, meaning that welding temperature was not high enough. The comparison between the fracture on the root side of S11 to every other specimen can be seen in Figure 94.

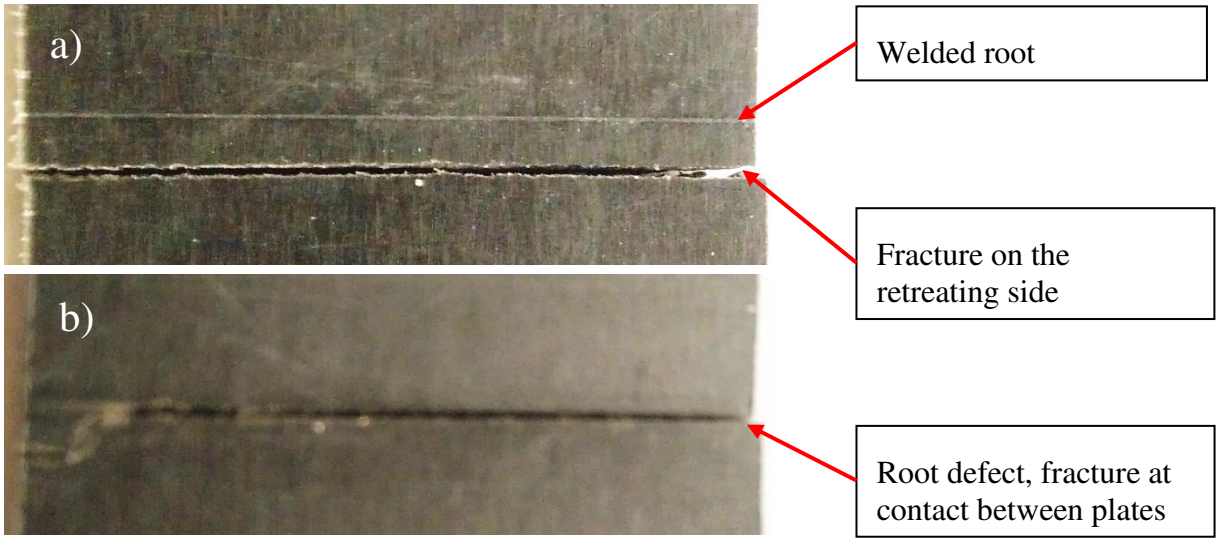

Figure 94 - Comparison of fractures from the root side of a) specimen S21 and b) S11.

The welded specimens' fractures were all brittle, as is shown in Figure 95. The maximum tensile strength was far from the maximum tensile strength of the base material, being the best joint efficiency off only 42.7%.

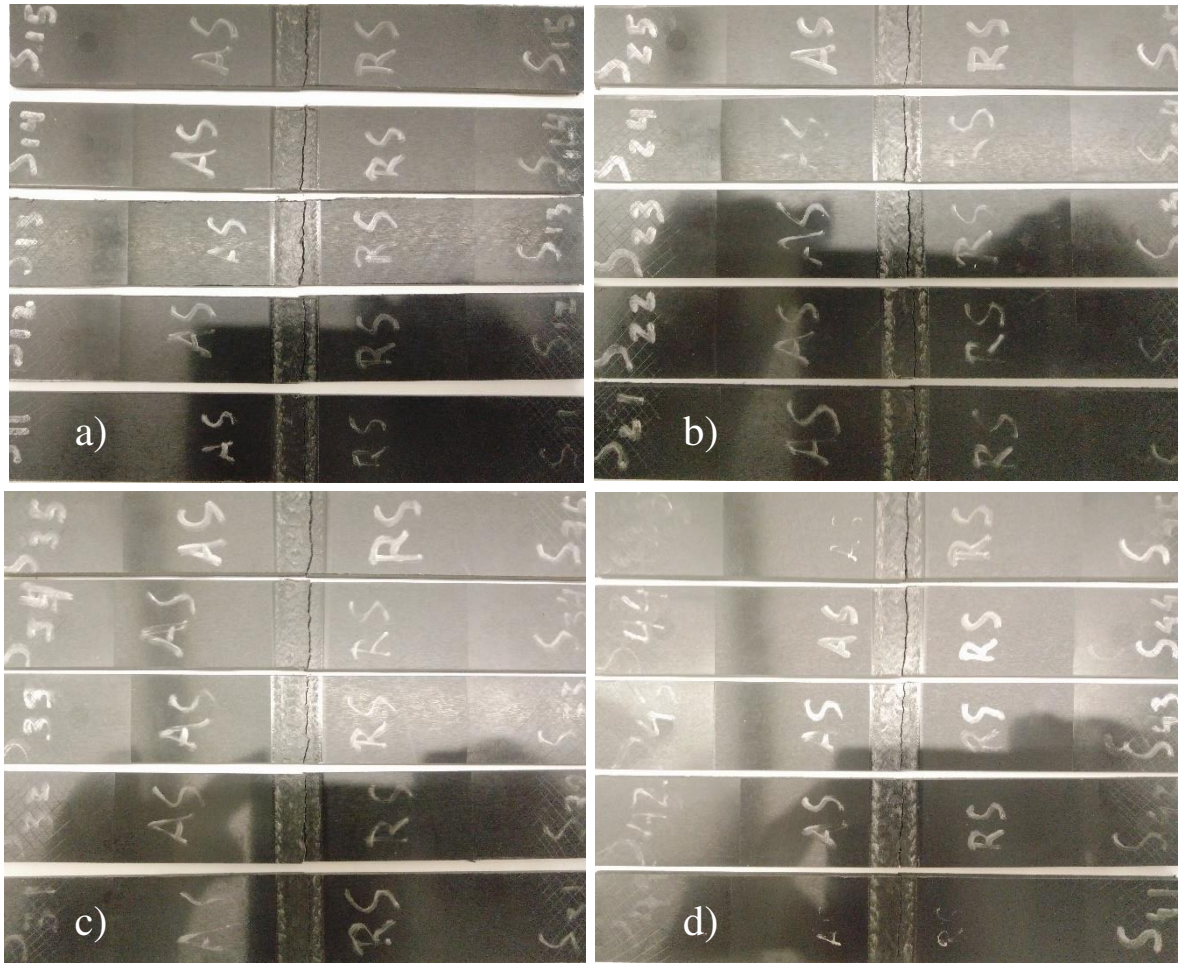

Figure 95 - Fractures of specimens a) S11 to S15, b) S21 to S25, c) S31 to S35 and d) S41 to S45.

All specimens presented a tunnel defect in the bottom region of the weld, Figure 96. This defect is particularly visible in specimens S31 to S35, which had the highest rotation speed, highest axial force and lowest traversing speed, meaning that the heat input was the highest.

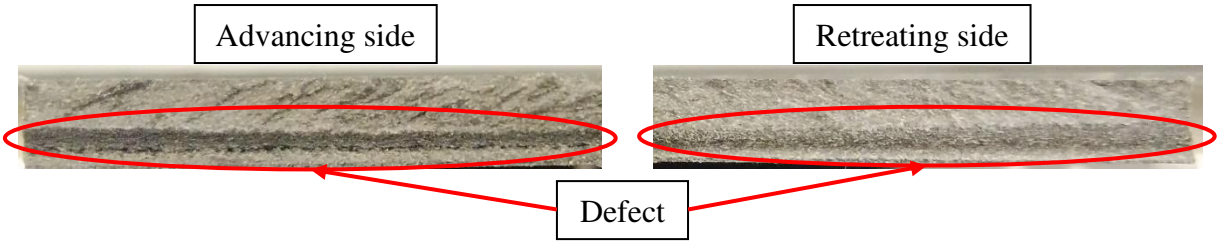

Figure 96 - Tunnel defect of specimen S31

The defect could be a result of the improper mixing in that region. Since all specimens have this defect in the same place, it may be due to the probe design. Using a probe with a bigger pitch thread may help mitigate this effect.

The low tensile strength could be because of the bending of the specimens, Figure 97, which makes the specimens subject to some bending while executing the tensile test, another cause may be the insufficient heat input, since the temperature the tool's sleeve achieves during welding of the specimens didn't surpass the melting temperature of the PA6-GF30. The broken fibres in the weld bead may also be helping in the initiation of cracks in the weld and may cause

the fracture to be brittle. A slower cooling rate of the weld would help with recrystallization and welding in the fibre direction may produce better results.

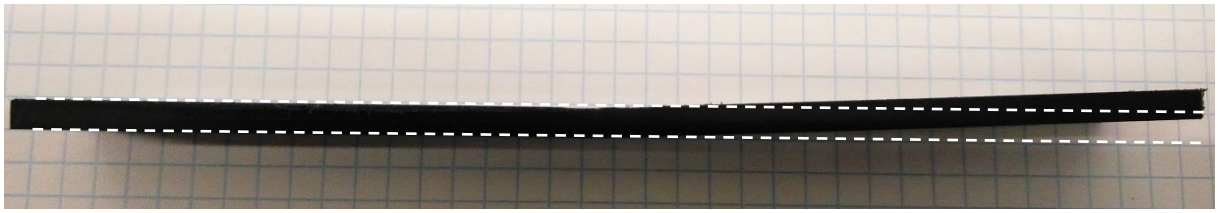

Figure 97 - Bending of specimen

5.3.2 Confirmation test

The parameter combination that should produce the best results are rotation speed of 2800 rpm, traversing speed of 40 mm/min and axial force of 1000 N with a predicted UTS of 66.3 MPa. The predicted UTS was calculated with equation (5.1).

$$\widehat{UTS} = \bar{y} + (\overline{RPM_{2800}} - \bar{y}) + \left(\overline{Travel_{40}} - \bar{y}\right) + (\overline{Force_{1000}} - \bar{y}) \quad (5.1)$$

Where:

$\widehat{UTS}$ is the predicted ultimate strength;
$\bar{y}$ is the average of the tensile strength of all specimens;
$\overline{RPM_{2800}}$ is the average of the tensile strength of all specimens with rotation speed 2800 rpm;
$\overline{Travel_{40}}$ is the average of the tensile strength of all specimens with travel speed 40 mm/min;
$\overline{Force_{1000}}$ is the average of the tensile strength of all specimens with axial force 1000 N.

Five specimens where made with dimensions according to ASTM D 3039/D 3039M - 00, the same as the ones used for the design of experiment. The results from the confirmation test are shown in Table 24.

Table 24 - UTS from confirmation test

	C1	C2	C3	C4	C5	Average	Standard Deviation
UTS [MPa]	44,4	58,3	60,0	63,1	61,4	57,45	7,48

The maximum UTS achieved by the confirmation was 63.1 MPa, which was lower than the predicted value, and lower than the value of 64.1 MPa achieved by specimen S44. The only different parameter between the condition S4 and the confirmation test was the higher axial force.

The confirmation test suffered from a worse fixation and was unable to achieve the 1000 N of axial force, Figure 98. The lower than expected axial force, wear of the tool and less rigid fixation of the plates, may be the reasons for the lower than expected UTS.

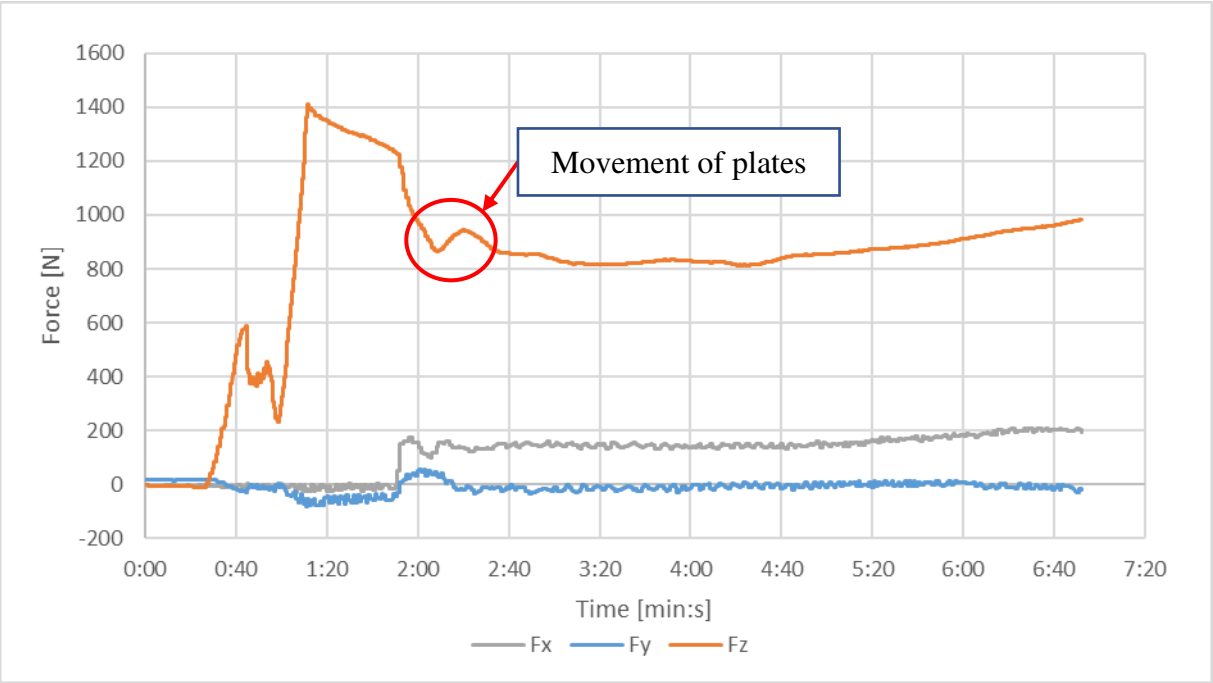

Figure 98 - Force measured during welding of confirmation test.

The average axial force during welding was 877 N with a maximum of 985 N. The traversing force was on average 157 N with a maximum of 210 N.

The appearance of the welds can be seen in Figure 99. The welds are all similar being wider at the top, due to the sleeve effect, and narrower at the bottom.

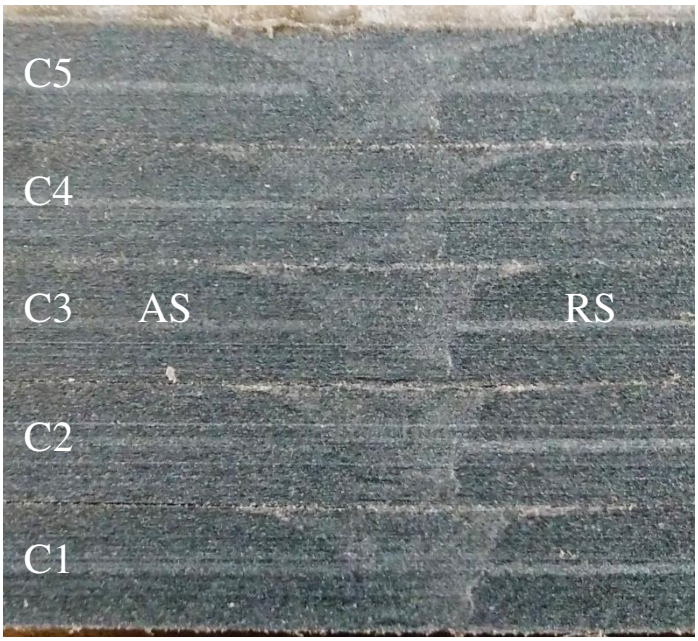

Figure 99 - Side view of welds of the confirmation test

6 Conclusion and future work

The aim of this work was the study and development of friction stir welding for composites. The tool design proved to have significant importance in the quality of the weld as well as the difficulty in welding, since the hybrid tool was more difficult to use than the PEEK tool.

The rotating shoulder tool proved to be inadequate for welding composites because of the production onion ring defect, flash, voids and lack of fill, it was also a demanding tool for the milling machine, because of this no further test were made using this tool design.

The hybrid tool produced better results than the rotating shoulder tool, showing that the static shoulder helps to keep the material in the weld bead. The resulting welds from this tool were smoother with no flash, but still with onion ring defect and some lack of material in the retreating side. This tool design represents an improvement over the rotating tool design.

To make it feasible to weld with the hybrid tool, the static shoulder and copper sleeve were preheated. The preheated tool was less demanding, having lower traversing forces. When preheated to 150 ºC the tool produced a weld with similar appearance to the one obtained without preheating, but with less defects and with a smoother look. When preheated to 270ºC, the weld was more uniform, but the surface was rough due to the material sticking to the bottom of the shoulder and sleeve, also it presented small amounts of flash, some voids, but no lack of material. The preheated hybrid tool produced the highest tensile strength specimen, H4, with a joint efficiency of 58.7%, since the specimen presented root defect there is still space to improve, being possible to obtain higher joint efficiencies with this tool design.

The stationary shoulder tool produced the best appearance welds, was the less demanding tool for the machine without preheating and was the easiest to use. This tool produced a very particular weld with a very smooth appearance. The transition between weld and base material was smooth. It produced no flash or lack of fill but presented some voids in the surface. The tool's most influential parameter was the traversing speed, with a percentage contribution of 57%, and the highest tensile strength specimen was S44 with a joint efficiency of 42.7%. The tool's heat output must increase in order to achieve better results with this material.

6.1 Future work

It would be interesting to analyse the fibre concentration, length and orientation in the base material and compare it to the weld bead, some studies have been made regarding this, but the information is still not plentiful. This would help understand which parameters and tool design are best in order to maintain as much fibre length and fibre concentration in the weld. An analysis of the material microstructure would help understand better the effects of FSW welding parameter.

The tool for welding needs further refinement. The tool´s shoulder, although made of PEEK, which supports high temperatures, after several welds starts to form gaps next to the copper sleeve, these gaps are ways for the composite to escape the weld bead and penetrate the tool. An alternative would be to reduce the amount of PEEK used and simplify its geometry, in order

to make its replacement easier or use a polymeric or ceramic coating on a metallic shoulder. The shoulder material could also be improved, PBI has a higher service temperature and would make a more durable tool, on the other hand, PEEK reinforced with 30% glass fibres present a lower thermal conductivity, helping insulate better the copper sleeve, making it possible to weld at higher temperatures. A metallic shoulder with a ceramic coating may also be a good solution.

In order to produce more heat, the tolerances between the probe and the copper sleeve can be tighter, but this is not a long-lasting solution. An external heat source would help provide a more constant weld temperature and reduce dwell time. A temperature-controlled heating system would reduce variability and, perhaps, make the welding temperature a controllable parameter.

References

[1] D. B. Miracle and S. L. Donaldson, "1. Introduction to Composites," in *ASM Handbook, Volume 21 - Composites*, ed: ASM International, 2001.

[2] M. Biron, "1 - Outline of the Actual Situation of Plastics Compared to Conventional Materials," in *Thermoplastics and Thermoplastic Composites (Second Edition)*, M. Biron, Ed., ed: William Andrew Publishing, 2013, pp. 1-29.

[3] P. K. Mallick, "5 Thermoplastics and thermoplastic-matrix composites for lightweight automotive structures," in *Materials, Design and Manufacturing for Lightweight Vehicles*, ed: Woodhead Publishing, 2010.

[4] GKN Aerospace. (2017, accessed 15 October 2019). *Thermoplastic at the forefront of composite technology*. Available: https://www.gknaerospace.com/en/our-technology/2017/thermoplastics-at-the-forefront-of-composite-technology-2/

[5] "5.4.2.7 Thermoplastic Materials," in *Composite Materials Handbook, Volume 3 - Polymer Matrix Composites - Materials Usage, Design, and Analysis (CMH-17)*, ed: SAE International on behalf of CMH-17, a division of Wichita State University, 2012.

[6] M. Effing, "Expert insights in Europe's booming composites market," *Reinforced Plastics,* vol. 62, pp. 219-223, 2018.

[7] G. Davies, "6.2.5 Friction Stir Welding," in *Materials for Automobile Bodies*, ed: Elsevier, 2012.

[8] P. K. Mallick, "8.3.2 Friction Stir Spot Welding," in *Materials, Design and Manufacturing for Lightweight Vehicles*, ed: Woodhead Publishing, 2010.

[9] S. Eslami, "Friction stir welding of polymers: an innovative technological approach," 2019.

[10] J. Bootle, F. Burzesi, and L. Fiorini, "48. Design Guidelines," in *ASM Handbook, Volume 21 - Composites*, ed: ASM International, 2001.

[11] D. Mishra, S. Sahu, R. Mahto, S. Pal, and K. Pal, "Friction Stir Welding for Joining of Polymers," ed, 2019, pp. 123-162.

[12] R. Cammack, T. K. Attwood, P. N. Campbell, J. H. Parish, A. D. Smith, J. L. Stirling, *et al.*, "polymer," in *Oxford Dictionary of Biochemistry and Molecular Biology (2nd Edition)*, ed: Oxford University Press, 2006, p. 535.

[13] W. D. Callister and D. G. Rethwisch, *Materials science and engineering: an introduction* vol. 7: John wiley & sons New York, 2007.

[14] F. C. Campbell, "10.3.3 Joining Thermoplastic Composites," in *Joining - Understanding the Basics*, ed: ASM International, 2011.

[15] P. K. Mallick, *Fiber-reinforced composites: materials, manufacturing, and design*: CRC press, 2007.

[16] J. F. C. Miranda, "Nova ligação por FSW de materiais poliméricos," Master's thesis, Faculty of Engineering of the University of Porto, 2017.

[17] K. Raza, M. Shamir, M. K. A. Qureshi, A. S. Shaikh, and M. Zain-ul-abdein, "On the friction stir welding, tool design optimization, and strain rate-dependent mechanical properties of HDPE–ceramic composite joints," *Journal of Thermoplastic Composite Materials,* vol. 31, pp. 291-310, Mar. 2017.

[18] Arkema. (19 November 2019). *Elium® resins for composites*. Available: https://www.arkema.com/en/products/product-finder/range-viewer/Elium-resins-for-composites/

[19] M. Biron, "6 - Thermoplastic Composites," in *Thermoplastics and Thermoplastic Composites (Second Edition)*, M. Biron, Ed., ed: William Andrew Publishing, 2013, pp. 769-829.

[20] M. Biron, "5 - Thermoplastic Processing," in *Thermoplastics and Thermoplastic Composites (Second Edition)*, M. Biron, Ed., ed: William Andrew Publishing, 2013, pp. 715-768.

[21] F. C. Campbell, "1.1 Isotropic, Anisotropic, and Orthotropic Materials," in *Structural Composite Materials*, ed: ASM International, 2010.

[22] S. Strand, "Joining plastics - can friction stir welding compete?," in *Proceedings: Electrical Insulation Conference and Electrical Manufacturing and Coil Winding Technology Conference (Cat. No.03CH37480)*, 2003, pp. 321-326.

[23] M. J. Troughton and W. International Institute of, *Handbook of Plastics Joining : A Practical Guide*. Norwich, UNITED STATES: Elsevier Science & Technology Books, 2008.

[24] F. C. Campbell, "9 Adhesive Bonding," in *Joining - Understanding the Basics*, ed: ASM International, 2011.

[25] C. Ageorges, L. Ye, and M. Hou, "Advances in fusion bonding techniques for joining thermoplastic matrix composites: a review," *Composites Part A: Applied Science and Manufacturing,* vol. 32, pp. 839-857, Jun. 2001.

[26] S. D. T. Amancio Filho, M. Beyer, and J. F. Dos Santos, "Method of connecting a metallic bolt to a plastic workpiece," 2009.

[27] S. Amancio, "Friction Riveting: development and analysis of a new joining technique for polymer-metal multi-materials structures," PhD, Hamburg University of Technology, 2007.

[28] F. Gagliardi, R. Conte, C. Ciancio, G. Simeoli, V. Pagliarulo, G. Ambrogio*, et al.*, "Joining of thermoplastic structures by Friction Riveting: A mechanical and a microstructural investigation on pure and glass reinforced polyamide sheets," *Composite Structures,* vol. 204, pp. 268-275, Nov. 2018.

[29] Z. Kiss, T. Temesi, and T. Czigány, "Adherability and weldability of poly(lactic acid) and basalt fibre-reinforced poly(lactic acid)," *Journal of Adhesion Science and Technology,* vol. 32, pp. 173-184, Jan. 2018.

[30] I. Fiebig and V. Schoeppner, "Influence of the initial fiber orientation on the weld strength in welding of glass fiber reinforced thermoplastics," *International Journal of Polymer Science,* 2016.

[31] R. Kumar, R. Singh, I. P. S. Ahuja, R. Penna, and L. Feo, "Weldability of thermoplastic materials for friction stir welding- A state of art review and future applications," *Composites Part B: Engineering,* vol. 137, pp. 1-15, 2018.

[32] S. T. Amancio-Filho and J. F. dos Santos, "Joining of polymers and polymer–metal hybrid structures: Recent developments and trends," *Polymer Engineering & Science,* vol. 49, pp. 1461-1476, Aug. 2009.

[33] A. Yousefpour, M. Hojjati, and J.-P. Immarigeon, "Fusion Bonding/Welding of Thermoplastic Composites," *Journal of Thermoplastic Composite Materials,* vol. 17, pp. 303-341, Jul. 2004.

[34] M. Gehde, M. Giese, and G. W. Ehrenstein, "Welding of thermoplastics reinforced with random glass mat," *Polymer Engineering & Science,* vol. 37, pp. 702-714, Apr. 1997.

[35] V. Kagan, "Optimized Mechanical Performance of Welded and Molded Butt Joints: Part II - Weld and Knit Lines Integrity," *Journal of Reinforced Plastics and Composites,* vol. 22, pp. 867-879, Jul. 2003.

[36] T. J. Ahmed, D. Stavrov, H. E. N. Bersee, and A. Beukers, "Induction welding of thermoplastic composites—an overview," *Composites Part A: Applied Science and Manufacturing,* vol. 37, pp. 1638-1651, Oct. 2006.

[37] D. B. Miracle and S. L. Donaldson, "76. Processing and Joining of Thermoplastic Composites," in *ASM Handbook, Volume 21 - Composites*, ed: ASM International, 2001.

[38] R. S. Mishra and Z. Y. Ma, "Friction stir welding and processing," *Materials Science and Engineering: R: Reports,* vol. 50, pp. 1-78, Aug. 2005.

[39] W. Thomas, E. Nicholas, J. Needham, M. Murch, P. Temple-Smith, and C. Dawes, "Friction stir butt welding. Int Patent App PCT/GB92/02203, and GB Patent App 9125978.8, December 1991," 1995.

[40] S. Eslami, T. Ramos, P. J. Tavares, and P. M. G. P. Moreira, "Shoulder design developments for FSW lap joints of dissimilar polymers," *Journal of Manufacturing Processes,* vol. 20, pp. 15-23, Oct. 2015.

[41] S. Eslami, P. J. Tavares, and P. M. G. P. Moreira, "Friction stir welding tooling for polymers: review and prospects," *The International Journal of Advanced Manufacturing Technology,* vol. 89, pp. 1677-1690, Mar. 2017.

[42] Y. Huang, X. Meng, Y. Xie, L. Wan, Z. Lv, J. Cao*, et al.*, "Friction stir welding/processing of polymers and polymer matrix composites," *Composites Part A: Applied Science and Manufacturing,* vol. 105, pp. 235-257, 2018/02/01/ 2018.

[43] G. Payganeh, N. M. Arab, Y. D. Asl, F. Ghasemi, and M. S. Boroujeni, "Effects of friction stir welding process parameters on appearance and strength of polypropylene composite welds," *International Journal of Physical Sciences,* vol. 6, pp. 4595-4601, 2011.

[44] H. Laieghi, S. Alipour, and A. Mostafapour, "Heat-assisted friction stir welding of polymeric nanocomposite," *Science and Technology of Welding and Joining,* pp. 1-10, 2019.

[45] S. P. Meyer, B. Jaeger, C. Wunderling, and M. F. Zaeh, "Friction stir welding of glass fiber-reinforced polyamide 6: Analysis of the tensile strength and fiber length distribution of friction stir welded PA6-GF30," *IOP Conference Series: Materials Science and Engineering,* vol. 480, p. 012013, Mar. 2019.

[46] F. Simões and D. M. Rodrigues, "Material flow and thermo-mechanical conditions during Friction Stir Welding of polymers: Literature review, experimental results and empirical analysis," *Materials & Design,* vol. 59, pp. 344-351, 2014.

[47] S. R. Strand, "Effects of friction stir welding on polymer microstructure," Master, Department of Mechanical Engineering Brigham Young University, 2004.

[48] P. N. Banjare, P. Sahlot, and A. Arora, "An assisted heating tool design for FSW of thermoplastics," *Journal of Materials Processing Technology,* vol. 239, pp. 83-91, Jan. 2017.

[49] B. Vijendra and A. Sharma, "Induction heated tool assisted friction-stir welding (i-FSW): A novel hybrid process for joining of thermoplastics," *Journal of Manufacturing Processes,* vol. 20, pp. 234-244, Oct. 2015.

[50] H. Ahmadi, N. B. M. Arab, F. A. Ghasemi, and R. E. Farsani, "Influence of Pin Profile on Quality of Friction Stir Lap Welds in Carbon Fiber Reinforced Polypropylene Composite," *International Journal of Mechanics and Applications,* vol. 2, pp. 24-28, 2012.

[51] H. Ahmadi, N. B. Mostafa Arab, and F. A. Ghasemi, "Optimization of process parameters for friction stir lap welding of carbon fibre reinforced thermoplastic composites by Taguchi method," *Journal of Mechanical Science and Technology,* vol. 28, pp. 279-284, 2014/01/01 2014.

[52] S. Kumar, T. Medhi, and B. Saha Roy, "Friction Stir Welding of Thermoplastic Composites," ed, 2019, pp. 221-235.

[53] F. Kordestani, F. Ashenai Ghasemi, and N. Arab, "Effect of Pin Geometry on the Mechanical Strength of Friction-Stir-Welded Polypropylene Composite Plates," *Mechanics of Composite Materials,* vol. 53, pp. 525-532, 2017.

[54] T. Czigány and Z. Kiss, "Friction stir welding of fiber reinforced polymer composites," in *Proceedings of the 18th International Conference on Composite Materials*, 2011, pp. 21-26.

[55] V. Infante and C. Vidal, "5 - Tool and welding design," in *Advances in Friction-Stir Welding and Processing*, M. K. B. Givi and P. Asadi, Eds., ed: Woodhead Publishing, 2014, pp. 199-240.

[56] E. Azarsa and A. Mostafapour, "Experimental investigation on flexural behavior of friction stir welded high density polyethylene sheets," *Journal of Manufacturing Processes,* vol. 16, pp. 149-155, Jan. 2014.

[57] C. Schilling and J. Santos, "Method and device for linking at least two adjoining work pieces by frictional welding," 2005.

[58] J. Gonçalves, J. F. dos Santos, L. B. Canto, and S. T. Amancio-Filho, "Friction spot welding of carbon fiber-reinforced polyamide 66 laminate," *Materials Letters,* vol. 159, pp. 506-509, Nov. 2015.

[59] A. Scialpi, M. J. Troughton, S. Andrews, and L. De Filippis. (2007, accessed 17 September 2019). *In-line reciprocating friction stir welding of plastics*. Available: https://www.twi-global.com/technical-knowledge/published-papers/in-line-reciprocating-friction-stir-welding-of-plastics-may-2007

[60] X. Meng, Y. Huang, Y. Xie, J. Li, M. Guan, L. Wan*, et al.*, "Friction self-riveting welding between polymer matrix composites and metals," *Composites Part A: Applied Science and Manufacturing,* vol. 127, p. 105624, Dec. 2019.

[61] D. Baffari, G. Buffa, D. Campanella, E. Lo Valvo, and L. Fratini, "Experimental and numerical investigation on a new FSW based metal to composite joining technique," *Journal of Manufacturing Processes,* vol. 34, pp. 758-764, Aug. 2018.

[62] Lanxess. (2019, accessed 17 December 2019). *Durethan BKV30H2.0 901510 Data sheet*. Available: https://techcenter.lanxess.com/scp/emea/en/products/type/datasheet.jsp?ref=&gid=9285&pid=47

[63] V. C. H. Wiley, "Polyamides," in *Ullmann's Polymers and Plastics - Products and Processes, 4 Volume Set*, ed: John Wiley & Sons, 2016.

[64] ASTM, "D638-14," in *Standard test method for tensile properties of plastics*, ed, 2014.

[65] S. Eslami, L. Mourão, N. Viriato, P. J. Tavares, and P. M. G. P. Moreira, "Multi-axis force measurements of polymer friction stir welding," *Journal of Materials Processing Technology,* vol. 256, pp. 51-56, Jun. 2018.

[66] S. Eslami, T. Ramos, P. J. Tavares, and P. M. G. P. Moreira, "Effect of Friction Stir Welding Parameters with Newly Developed Tool for Lap Joint of Dissimilar Polymers," *Procedia Engineering,* vol. 114, pp. 199-207, Jan. 2015.

[67] S. Eslami, J. Francisco Miranda, L. Mourão, P. J. Tavares, and P. M. G. P. Moreira, "Polyethylene friction stir welding parameter optimization and temperature characterization," *The International Journal of Advanced Manufacturing Technology,* vol. 99, pp. 127-136, Oct. 2018.

[68] "CES EduPack," 19.1.0 ed. Cambridge, UK: Granta Design Limited, 2019.

[69] P. D. Funkenbusch, *Practical Guide To Designed Experiments: A Unified Modular Approach*: CRC Press, 2004.

[70] K. Y.-B. El-Haik and K. Yang, "Design for Six Sigma, A Roadmap for Product Development," *RR Donnelly, SAD, str,* vol. 21, 2003.

[71] ASTM, "D3039/D3039M–00," in *Standard test method for tensile properties of polymer matrix composite materials*, ed, 2000.